

UNIVERSITÀ DELLA CALABRIA



UNIVERSITA' DELLA CALABRIA

Dipartimento di Ingegneria per l'Ambiente e il Territorio e Ingegneria Chimica

Dottorato di Ricerca in

Scienze e Ingegneria dell'Ambiente, delle Costruzioni e dell'Energia (SIACE)

CICLO

XXXII

GAS PERMEATION THROUGH ZEOLITE MEMBRANES:

MODELLING AND EXPERIMENTAL ANALYSIS

Settore Scientifico Disciplinare ING-IND/25

Coordinatore: Ch.mo Prof. Salvatore Critelli

Firma _____


**CRITELLI
SALVATORE
28.03.2020
21:39:14
UTC**



Supervisor/Tutors: Prof. Giuseppe Barbieri

Firma 

Dr. Ing. Adele P

Firma_ 

Firma oscurata in base alle linee guida del Garante della privacy

Dottorando: Dott. Ing. Pasquale Francesco Zito

Firma  *Firma oscurata in base alle linee guida del Garante della privacy*

Dedicata
a Sara, Antonella
e
ai miei genitori

Ringraziamenti

Alla fine di questa lunga attività di ricerca, mi sembra doveroso ringraziare tutte le persone che mi hanno accompagnato nel percorso.

Ringrazio il Prof. Giuseppe Barbieri e l'Ing. Adele Brunetti per avermi seguito e stimolato nel corso dei tre anni di dottorato.

Vorrei naturalmente ringraziare tutta la mia famiglia, che è sempre al mio fianco, mostrandomi l'affetto necessario ad affrontare al meglio ogni nuova sfida. In particolare mia moglie e mia figlia, che sono la mia ragione di vita. Un grazie speciale è per i miei genitori, che mi hanno dato la possibilità di studiare e raggiungere traguardi importanti, sostenendomi sempre con il loro caloroso affetto. Non posso non citare mia sorella, per il nostro saldo legame sempre intatto nel tempo.

Grazie, infine, ai miei amici, compagni di questi anni e di esperienze indimenticabili.

Abstract

La separazione gassosa è uno stadio fondamentale in numerosi processi industriali, in quanto consente la purificazione e il recupero di componenti ad alto valore (come H₂) e, allo stesso tempo, la riduzione delle emissioni di vari inquinanti atmosferici, quali, ad esempio, la CO₂. Tradizionalmente, essa viene condotta tramite assorbimento e distillazione criogenica, tecniche ben note e consolidate. Tuttavia, entrambe risultano ad alto impatto ambientale, in quanto necessitano dell'impiego di un solvente (assorbimento) o di condizioni operative drastiche (distillazione criogenica). Pertanto, nell'ottica di uno sviluppo più sostenibile, che vada nella direzione della *green chemistry* (ovvero progettare prodotti e processi che evitino o riducano l'utilizzo e la produzione di sostanze dannose per l'ambiente) e segua i principi della *Process Intensification* in termini di minori consumi energetici e volumi di impianto, le membrane rappresentano una valida alternativa ai processi tradizionali.

In questo lavoro di dottorato, sono state studiate le potenzialità delle membrane zeolitiche nel separare correnti gassose contenenti CO₂, gas permanenti (N₂, H₂, CH₄) e vapore, mediante un'indagine modellistica e sperimentale. Il trasporto di materia attraverso i pori zeolitici è stato descritto sviluppando un modello *ad-hoc* che considerasse la competizione tra *surface diffusion* e *gas translation diffusion*. Tale modello, validato per miscele secche ed umide su membrane di vario tipo (SAPO-34, DDR, NaY, 4A), è stato utilizzato per prevedere la separazione multicomponente al variare delle condizioni operative.

La permeazione in miscela è risultata molto diversa rispetto quella in gas singolo. In particolare, la CO₂ ha mostrato un incremento di permeanza in presenza di alcune specie, come l'idrogeno. In questo caso, infatti, essa usufruisce dell'effetto positivo esercitato dall'idrogeno sulla diffusività binaria, che regola la *surface diffusion* in miscela. Al contrario, le specie più debolmente adsorbite (H₂, N₂, CH₄) hanno subito una netta riduzione di flussi e permeanze in miscela, a causa dell'effetto di *hindering* che la CO₂ adsorbita esercita sulla loro diffusione. Ciò si è tradotto in selettività di miscela (per esempio, 22 nel caso di CO₂/N₂ in SAPO-34) significativamente migliori rispetto a quelle valutate con i gas singoli. Si è dimostrato, quindi, come sia importante avere un'analisi

del trasporto in miscela, nell'ottica di una valutazione realistica delle proprietà separative delle membrane, fondamentale in fase di progettazione di unità di separazione.

Le previsioni modellistiche sono state confermate e corroborate da prove sperimentali per correnti a diversa composizione, effettuate su una membrana DDR fornita dal Professore Xuehong Gu, della Nanjing Tech University. Le misure sperimentali hanno confermato elevate selettività in miscela (per esempio, 106 e 17 nel caso di CO_2/CH_4 e CO_2/H_2), diverse da quelle calcolate sulla base di misure a gas singolo. Questi valori di selettività rendono le zeoliti particolarmente adatte per recuperare la CO_2 da correnti di miscele multicomponente.

Per quanto riguarda le miscele umide, si è dimostrato come l'acqua in fase vapore blocchi completamente la diffusione superficiale dei gas permanenti (H_2 , CO e CH_4), i quali permeano solo per *gas translation diffusion*.

Pertanto, la competizione tra *surface diffusion* e *gas translation diffusion*, espressa nel modello proposto, ha consentito di descrivere accuratamente la permeazione in membrane zeolitiche e di prevedere così il comportamento in ampi intervalli di condizioni operative. L'analisi modellistica ha confermato come l'alta affinità di queste membrane verso CO_2 e H_2O le renda particolarmente selettive e, dunque, indicate per ottenere correnti concentrate di permeato e retentato da poter riutilizzare e valorizzare.

Contents

Aim of the thesis	5
Summary.....	5
1. Zeolite membranes: potentialities and applications in gas separation.....	7
1.1 Membranes as “green” alternative to the traditional processes.....	7
1.2 Zeolites: classification and characteristics	9
1.3 Zeolites as thin membranes for gas separation.....	12
2. Mass transport through zeolite membranes	15
2.1 Gas adsorption in zeolites: Langmuir and Sips models	17
2.2 Modelling of mass transport through zeolite membranes	21
2.3 Experimental apparatus for permeation measurements	34
3. Adsorption and diffusion of single components in zeolites.....	36
3.1 Evaluation of adsorption properties	37
3.1.1 SAPO-34 zeolite.....	39
3.1.2 4A zeolite	44
3.2 Evaluation of diffusivity	54
3.2.1 DD3R membrane	55
3.2.2 SAPO-34 membrane	60
3.2.3 4A membrane	63
3.2.4 NaY membrane	67
4. Permeation of gas mixtures through zeolite membranes.....	71
4.1 Dry mixtures: the effect of CO ₂	72
4.1.1 SAPO-34 membrane	72
4.2 Humid mixtures: the effect of water vapor	84
4.2.1 4A membrane	84
5. Experimental analysis.....	94
5.1 Permeation through a DDR membrane	95
5.2 Comparison with the modelling results.....	103
Conclusions	111
Notation.....	114
References.....	117

Publications on international journals during the PhD.....	126
Publications on national journals during the PhD.....	126
Book chapters during the PhD	127
Presentations to international conferences during the PhD.....	127
Presentations to seminars during the PhD.....	127
Teaching activity during the PhD	128

Aim of the thesis

This PhD thesis is focused on the permeation of mixtures containing CO₂, permanent gases (i.e., H₂, CH₄, CO and N₂) and water vapor through zeolite membranes. The goal is to predict the separation performance by means of a mass transport analysis able to correctly describe the behavior of a large number of species and materials under dry and wet conditions. At the same time, an important contribution is given to the debate on the mass transport mechanisms taking place in zeolite pores. A significant part of this work is devoted to the modelling analysis of humid mixtures, to well describe, for the first time at the best of our knowledge, the multicomponent permeation in presence of water vapor. In addition, a particular attention is given to the mutual influence among the diffusing species, which makes the mixture permeation quite different from the single gas behavior (e.g., higher selectivity). Thus, here it is evaluated the importance of knowing the mass transport in mixture, which is a fundamental step in the design of separation units.

Summary

Gas separation is a crucial step in several industrial processes, allowing the purification and recovery of valuable components and, at the same time, avoiding the emissions of some air pollutants. It can be carried out using zeolite membranes, which give the possibility to operate at moderate conditions (i.e., room temperature and pressure) and without using any environmentally harmful solvent. In this work, the potentialities of zeolite membranes in separation of gas mixtures are analyzed by a modelling and experimental study focused on the estimation of the contributions to the overall mass transport.

The five chapters of this PhD thesis report in detail this research activity and a conclusion section summarizes the best achievements.

Chapter 1 is devoted to present zeolites, focusing on the state-of-the-art related to their application as thin membranes for gas separation. The principles and equations governing the mass transport through zeolite pores are discussed in Chapter 2. Chapter 3 contains the details about the estimation of single gas adsorption and diffusion through different materials (i.e., SAPO-34, DD3R, NaY and 4A), which are the necessary input for the

multicomponent mass transport analysis. Chapter 4 is devoted to discuss the main results of the mixture permeation through zeolite membranes at different temperatures, feed pressures and compositions. These results include model validation for mass transport in both dry and, especially, humid conditions. This last point is very important since water vapor is often present in real streams. In addition, this model is the first one, at our knowledge, able to predict the mixture permeation through zeolite membranes in presence of water vapor. In the last chapter (Chapter 5), the experimental results on a laboratory apparatus (described in Chapter 2) are shown, aimed to strengthen the modelling analysis. Both simulated and experimental results confirm the high potentiality of zeolite membranes for separating CO₂ or water vapor from gas streams. The high selectivity of these membranes allows the target to get a permeate stream rich in CO₂ or H₂O to be achieved, in order to have a pure component that can be recovered and valorized. The results of this PhD work are reported in 6 papers, which are published in peer reviewed journals as summarized on page 126.

1. Zeolite membranes: potentialities and applications in gas separation

1.1 Membranes as “green” alternative to the traditional processes

The continuous increment in energy demand, associated to the depletion of fossil fuels reserves and the greater attention to environmental issues, especially in terms of CO₂ emissions, is moving the international community towards the development of greener industrial technology, based on the *Process Intensification* principles. CO₂ capture and valorization, H₂ and biomass utilization instead of fossil fuel are some examples of necessary actions to be taken in order to fight the climate changes.

Membrane technology meets the requirements of *Process Intensification* in terms of better performance, lower energy consumption and volume of equipment with respect to the traditional processes [1]. As typical examples, membranes can successfully separate gas mixtures avoiding the use of solvents or drastic operating conditions as in the case of absorption and cryogenic distillation. A membrane can be represented as a barrier that allows the fast passage of some components from the feed to the permeate side, whereas obstacles the transfer of the remaining components, which constitute the retentate stream (Figure 1).

Membranes are typically divided into four groups: liquid, polymeric, inorganic and mixed matrix [2]. Supported liquid membranes are used for examples in separation of organic compounds [3]. Nevertheless, they present problems of membrane stability that limit the applications. A possible solution to these problems is given by the ionic liquid

membranes, which are organic salts presenting a very low vapor pressure. They are used for CO₂ capture owing to the high CO₂ solubility, showing as the main drawback a high viscosity [4]. However, the main problems that limit the use in large scale are the cost and stability. Polymeric membranes are the most used in the separation field, because of their low cost, ease in processing, tuneability and scalability. The main drawbacks are represented by the low chemical and thermal stability and, especially, the permeability/selectivity trade-off, reported in the Robeson diagram [5]. Differently, inorganic membranes show chemical and thermal stability much higher. Dense (i.e., metallic) and porous structures (e.g., carbon, amorphous silica and zeolite) are part of this category. Dense membranes based on palladium are typically used in membrane reactors (e.g., water gas shift reaction) allowing the hydrogen separation from a multicomponent gas stream, since they show an infinity selectivity towards H₂. Thus, reaction and separation are integrated in the same unit, with the possibility to increase the conversion of several equilibrium limited reactions owing to the continuous removal of some products from the reaction environment. Nevertheless, the two main drawbacks that limit the membrane reactors employ to the industrial level are the high cost and the poisoning or the inhibition exerted by some components like sulfur and carbon monoxide[6,7,8,9,10]. Porous inorganic membranes assure higher flux and chemical stability than the dense structures [2]. **Zeolite membranes** belong to this category and can be used for separation of water/organics by pervaporation and in gas separation, exploiting the preferential adsorption of some components onto the zeolite surface. This allows a high selectivity to be achieved, which is coupled to the high permeability assured by the porosity of their structure. The current problems related to the limited practical use of zeolite membranes are the high fabrication costs and difficult in reproducibility and scale-up. Some efforts to reduce the fabrication costs are made, especially related to the support that may constitute the 70% of the total membrane cost [2]. In some cases, inorganic fillers, such as zeolites, are incorporated in an organic structure giving the so-called mixed matrix membranes. These materials allow to overcome the limitations of organic and inorganic materials and, at the same time, to exploit their advantages.

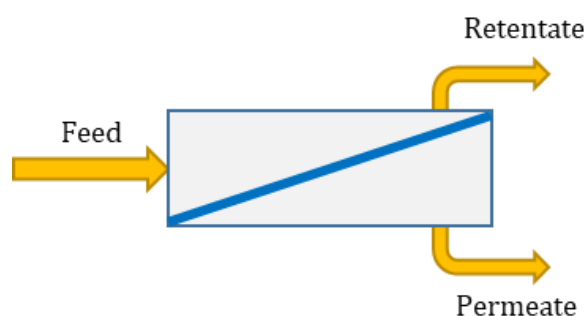


Figure 1. Schematic view of a membrane module.

1.2 Zeolites: classification and characteristics

Zeolites are aluminosilicates having a microporous and crystalline structure. Their framework is characterized by silicon, aluminum and oxygen, by T-O-T bonds in tetrahedral building block TO_4 , to form pores and channels [11,12]. An isolated SiO_4 group has a formal negative charge of -4, but this unit becomes neutral in the zeolite structure, since each oxygen atom is connected to other two T atoms. On the other hand, the AlO_4 group has a negative charge of -1, thus the overall zeolite framework is negatively charged. Hence, exchangeable cations (e.g., Na^+ , K^+ etc.) can be located in the structure to compensate this charge. The chemical formula of a zeolite can be written as $M_{x/n}[(AlO_2)_x(SiO_2)_y]mH_2O$, where M are the cations with valence n that have to neutralize the negative charge owed to Al.

Zeolites are classified with a three letters identification code by the International Zeolite Association IZA. A further classification, which is based on the pore size, distinguishes zeolites into small, medium, large and ultra large structures [11]. The main zeolite structures used as in gas separation are reported in Table 1.

The Si/Al ratio, on which the adsorption capacity strongly depends, can vary from a lower bound of 1 (as in the case of zeolite X) to very high values (ranging from 10 to infinity for ZSM-5 [13]). The ability of material to exchange cations increases with increasing Al content. Moreover, zeolites become more polar and, therefore, improve their capacity to adsorb molecules when the aluminum content in its framework is higher (i.e., Si/Al is lower) [2].

Small structures consist of 6-, 8-, 9-membered rings. Sodalite (SOD), deca-dodecasil 3R (DDR), Linde type A (LTA) and chabazite (CHA) belong to this category [14] (Figure 2 [2]). Sodalite has apertures formed by six-membered ring, with a pore size of about 2.6 Å [14]. DDR presents eight-membered ring openings forming a two dimensional pore framework, with apertures of 3.6 Å x 4.4 Å [14]. The LTA zeolites consist of eight-membered ring structure with a cubic unit cell of 24.6 Å, including 3A, 4A (or NaA) and 5A type. The chemical formula for a single dehydrated NaA cell can be written as $\text{Na}_{12}\text{Si}_{12}\text{Al}_{12}\text{O}_{48}$ [15,16], with a Si/Al ratio of 1. Its pseudo-unit cell consists of eight large cavities (α -cage) of diameter 11.4 Å and eight small cavities (β -cage or sodalite) of 6.6 Å [17,18], with the large ones connected by windows with a diameter of 4.1 Å [19]. Regarding the CHA type, which includes SSZ-13 and SAPO-34, it has a symmetric three-dimensional structure with pore size of 3.8 x 3.8 Å [2, 14]. In particular, SAPO-34 is a silicoaluminophosphate that belongs to the family of zeotype, consisting of SiO_4 , AlO_4 and PO_4 tetrahedra. This different chemical composition leads to a higher polarity of SAPO-34 than that of aluminosilicate, which enhances its hydrophilicity but reduces its hydrothermal stability [2,20].

Medium structures have 10-membered rings pore channels, as in the case of the MFI types (e.g., ZSM-5). Mordenite framework inverted (MFI) possesses an orthorhombic symmetry, with cells having the following dimensions: $a= 20.07$ Å, $b= 19.92$ Å, $c=13.42$ Å [21]. It presents a 3-dimensional pore network, in which sinusoidal (a -direction) and straight channels (b -direction) are intersected to give a pore size of about 5.5 Å [2].

Large pore zeolites have 12-membered rings and a typical example is represented by the faujasite (FAU) structure (Figure 3 [22]). FAU possesses a three-dimensional structure consisting of sodalite units (β -cages), linked together by six-membered double rings d6R to give super-cages having a diameter of 12.5 Å, interconnected by windows of 7.4 Å [14,23-24]. They can be divided into X- and Y-type, having a Si/Al ratio in the range of 1-1.5 and 1.5-3, respectively.

Furthermore, it is possible to synthesize several intermediate structures, as zeolite T, which is an erionite (8-ring structure) and offretite (12-rings structure) intergrowth-type of material, presenting pore size of 3.6 Å x 5.1 Å and 6.7 Å x 6.8 Å [14, 25].

Finally, the ultra large framework consists in 14-, 18- or 20-membered rings (e.g., AET, VFI and CLO types) [14]. These zeolites present very large pore channels and, thus, are not suitable for gas separation.

Zeolites find applications in several fields, such as adsorption, catalysis, ion-exchange, liquid and gas separation. The main achievements in the gas separation field are reported below.

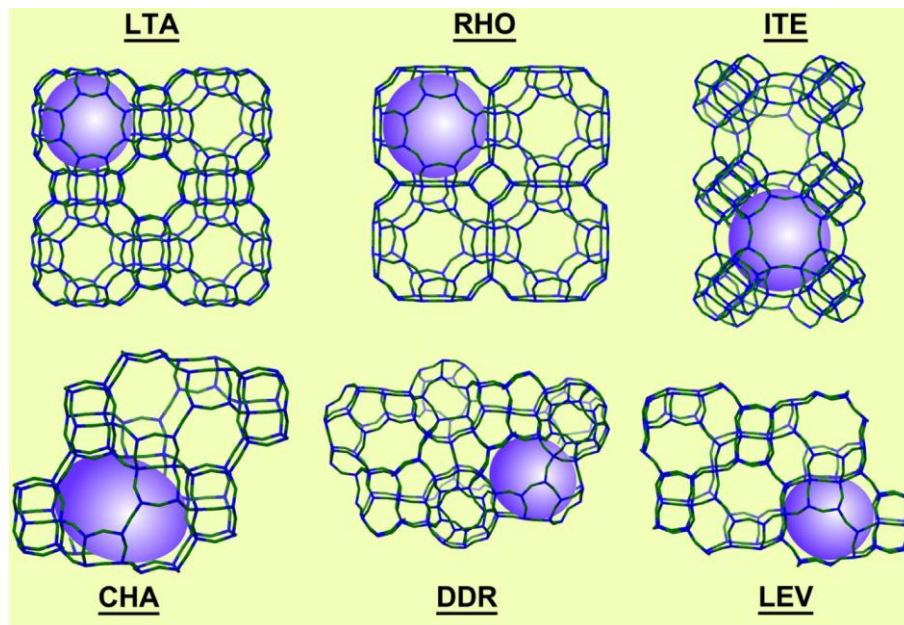


Figure 2. Structure of some 8-membered rings zeolites. Reprinted from Journal of Membrane Science, 499, Nikolay Kosinov, Jorge Gascon, Freek Kapteijn, Emiel J.M. Hensen, Recent developments in zeolite membranes for gas separation, 65-79, Copyright (2016) with permission from Elsevier.

1.3 Zeolites as thin membranes for gas separation

Zeolites can be used as thin layers for separation of CO₂, light gases and hydrocarbons. Typically, a zeolite film is deposited on a porous support to increase the mechanical stability of the membrane. Thus, a zeolite membrane can be considered as a selective zeolitic layer, having a pore size between about 0.28 and 1.3 nm, on a mesoporous/macroporous support (typically α -alumina, silica). Permeation of CO₂ and light gases through the selective zeolite film takes place by surface and gas translation diffusion, as will be discussed in details in Chapter 2. Differently, molecular sieving can also occur in presence of hydrocarbons, which can have a kinetic diameter higher than the pore size of some zeolites. The porous support can provide a further resistance to mass transport, which is associated to the Knudsen diffusion or Poiseuille flow. This resistance does not affect the selectivity in case of permeance much higher than the zeolite permeance (permeance ratio higher than 10) [2]. Several experimental investigations on zeolite membranes are carried out in the literature, concerning in most cases single gas and binary equimolar mixtures. Some selectivity values, which demonstrate the potential of zeolite membranes in gas separation, are reported in Table 1 at the end of this section.

Regarding the small pore structures, sodalite membranes do not find application in gas separation owing to the very low permeance through their pores, which have dimensions accessible only to H₂ and water [2]. Therefore, sodalite is typically used to produce ultra-pure water by seawater desalination [26]. On the other hand, DDR (Figure 2) is very promising for CO₂/CH₄ and CO₂/air separation, providing selectivity values of 500 [27, 28] and above 20 [28], respectively. LTA-type (Figure 2) includes the 3A, 4A (NaA) and 5A. In particular, zeolite 4A is successfully used for H₂/nC₄H₁₀ separation, achieving a selectivity of 106 [29]. Moreover, even if this zeolite find the main applications in pervaporation for dehydration of liquid mixtures [30], it can also provide interesting results in gas separation in presence of water vapor because of its high hydrophilicity. In fact, water vapor is strongly adsorbed on the material and hinders the permeation of the remaining species. Lee *et al.* [31] synthesized a 4A membrane providing a very low H₂ flux in presence of H₂O. They found a separation factor tending to infinity. Zhu *et al.* [30] measured mixture selectivity of 244, 309 and 615 for H₂O/CO, H₂O/H₂ and H₂O/CH₄ at

303 K. CHA type (Figure 2), including SSZ-13 and SAPO-34, is considered one of the best candidates for separating mixtures of flue gas and natural gas [32]. In two works, Li *et al.* [33, 34] obtained CO₂/N₂ and CO₂/CH₄ selectivity values of about 32 and 170, feeding equimolar mixture at room temperature. In CO₂/H₂ separation, Hong *et al.* [35] measured a selectivity towards CO₂ greater than 100 at -20°C, which decreases to about 15 at 25°C. This value is similar to that measured by Mei *et al.* [36] of 17.6.

MFI zeolite is the most studied in the literature, showing interesting results especially for CO₂/N₂ and CO₂/H₂ [2]. In particular, Guo *et al.* [37] measured separation selectivity of 69 and 17, respectively, feeding equimolar mixtures at 20°C.

The intermediate zeolite T is appropriate not only for water/organic liquid mixtures, but also for CO₂/CH₄ and CO₂/N₂ separation, as investigated by Cui *et al.* [25].

Low-silica FAU zeolites (X- and Y-types, Figure 3) have a polar structure that make them highly selective towards CO₂, which is much more adsorbed than permanent gases as H₂ and N₂ [38, 39, 40, 41]. White *et al.* [40] obtained very high CO₂/N₂ selectivity (>550), which is counterbalanced by a too low CO₂ permeance value. The hydrophilic character of FAU zeolites provokes an important CO₂ permeance reduction in humid conditions. Thus, this material loses the capacity of separating CO₂ from N₂ in the moderate temperature range, whereas selectivity increases with respect to the dry condition only above 110°C [41].

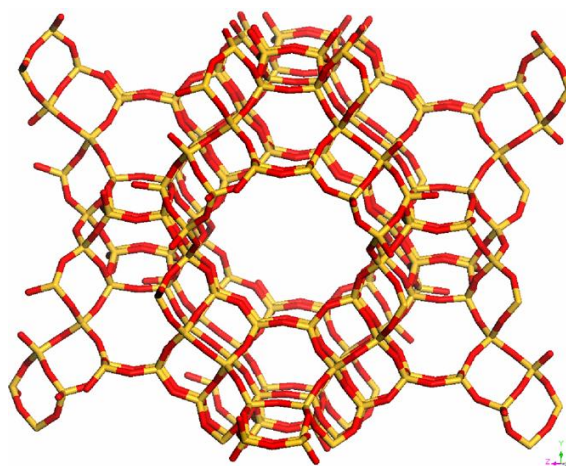


Figure 3. Structure of FAU zeolite. Reprinted from Microporous and Mesoporous Material, 119, A. Ghoufi, L. Gaberova, J. Rouquerol, D. Vincent, P.L. Llewellyn, G. Maurin, Adsorption of CO₂, CH₄ and their binary mixture in Faujasite NaY: A combination of molecular simulations with gravimetry-manometry and microcalorimetry measurements, 117-118, Copyright (2009), with permission from Elsevier.

In the next chapter, the mass transport model used to predict the separation performance and the experimental apparatus for permeation tests are presented and discussed.

Table 1. Structure and mixture selectivity of several zeolite used as membranes for gas separation.

<i>Zeolite type</i>	<i>Material</i>	<i>Structure</i>	<i>Pore size, Å x Å</i>	<i>Selectivity at room temperature</i>
DDR	DD3R	8-ring	3.6 x 4.4	CO ₂ /CH ₄ = 500 [27, 28] CO ₂ /air > 20 [28]
CHA	SAPO-34	8-ring	3.8 x 3.8	CO ₂ /CH ₄ = 170 [34] CO ₂ /N ₂ = 32 [33] CO ₂ /H ₂ = 18 [36]
LTA	4A	8-ring	4.1 x 4.1	H ₂ O/H ₂ = 309 [30] H ₂ O/CH ₄ = 615 [30] H ₂ O/CO = 244[30]
ERI/OFF	T	8-ring/12-ring	3.6 x 5.1 6.7 x 6.8 3.6 x 4.9	CO ₂ /CH ₄ =400 [25] CO ₂ /N ₂ = 107 [25]
MFI	Silicalite	10-ring	5.1 x 5.5 5.3 x 5.6	CO ₂ /N ₂ = 69 [37] CO ₂ /H ₂ = 17 [37]
FAU	NaY	12-ring	7.4 x 7.4	CO ₂ /N ₂ = 100 [38] CO ₂ /H ₂ = 28 [39] H ₂ O/CO ₂ = 270 [41] H ₂ O/N ₂ = 160 [41]

2. Mass transport through zeolite membranes

Most of this chapter is devoted to the modelling of mass transport through zeolite membranes, focusing on the physical principles and mathematical equations governing it. In the last section, the experimental apparatus used for permeation measurements is described.

It is well known that gas permeation through zeolite pores takes place by surface diffusion, which occurs by molecular hopping of the adsorbed components from site-to-site. Nevertheless, some experimental trends of permeance as a function of temperature suggest the presence of different contribution to mass transport, especially when temperature is high enough. About that, different points of view are observed in the literature for describing the experimental evidence (Table 2). Several authors explained their results considering a combination between surface diffusion (at a low temperature) and gas translation diffusion (at a high temperature), whose transition is represented by a minimum in permeance [42, 43 44, 45]. Differently, others authors [46] did not find any minimum in the permeance trend, justifying such an absence with the presence of inter-crystalline gaps in the membrane structure, which enlarge the effective pore in the polycrystalline zeolite layer. Some other authors gave a different interpretation [47,48]. In particular, Van den Bergh *et al.* [47] attributed the reduction of permeance with increasing temperature through a DD3R membrane only to surface diffusion even at high temperatures. Miachon *et al.* [48] made same considerations to model the gas permeation through MFI membranes. These authors supposed inter-crystalline pore openings at high temperatures as a possible explanation for the flux/permeance increment eventually

observed. Specifically, the difference in thermal expansion coefficient between support and zeolite can create defects and cause an increment of flux, since it provokes a mismatch between the expansion of the support and the shrink of zeolite crystals [47]. In addition, they argued that this effect can be reduced synthesizing membrane with smaller crystal size, e.g., in the order of 0.5-1 μm [47]. Nevertheless, this consideration is not always confirmed by other experimental results in the literature. In fact, it is found that even membranes with a small crystal size ($< 1\mu\text{m}$), such as those synthesized by Li *et al.* [42], showed this increment of flux and permeance attributed to gas translation diffusion for some light gases. Concerning the permeation through large-pores zeolite membranes, such as NaY, Hasegawa *et al.* [49] proposed the sum of surface and Knudsen diffusion, which Caravella *et al.* [50] revised in a recent paper in terms of competition between these two mechanisms.

Table 2. Some mass transport mechanisms used in the literature for describing the CO₂ and light gases behavior through zeolite membranes.

Species	Zeolite	Mass transport mechanism	Reference
CO ₂ , light gases	DD3R	Surface diffusion	[47]
CO ₂ , light gases, HC	Silicalite/ZSM-5	Surface + gas translation diffusion in parallel	[45]
Light gases, HC		Surface diffusion	[48]
CO ₂ , light gases		Surface + Knudsen diffusion competing	[51]
CO ₂ , CH ₄	SAPO-34	Surface diffusion	[42]
CO ₂ , light gases	NaY	Surface + Knudsen diffusion in parallel	[49]
CO ₂ , light gases		Surface + Knudsen diffusion competing	[50]

Thus, there is still an open scientific debate on the mass transport occurring through the zeolite pores and one of the goals this research is to give a contribution to this issue. In particular, it is here considered unrealistic the possibility to have only surface diffusion at high temperatures, in particular for weakly adsorbed species like H₂, for which a

relatively low amount of adsorption phase is present even at room temperature. Moreover, if the high temperature provoked the formation of defects and a consequent increment of flux, it would expect a minimum followed by an increasing trend for all the species in a reasonable range of temperature, whereas some species never exhibit this minimum. Thus, it is more plausible, in my opinion, the presence of gas translation paired to surface diffusion in defects-free zeolite membranes, especially for components having a dimension comparable to the pore size. Thus, the competition between surface and gas translation diffusion is here proposed for modelling the mass transport in a wide range of temperature and pressure, considering the four zeolite membranes investigated (i.e., DD3R, SAPO-34, NaY and 4A) defects-free. The reasons and adequacy of this hypothesis are discussed in the sections 3.2.1 – 3.2.4 of chapter 3. The mass transport model is focused on the variations of flux and concentration along the zeolite thickness, whereas the changes on the axial direction on both the feed and permeate sides are neglected, since a laboratory membrane module typically has a length of few centimeters and operates in the condition of very low stage-cut (i.e. permeate flow much lower than feed flow). Thus, this hypothesis can be considered reasonable.

Previously, a brief description regarding the fundamentals of pure component adsorption process is presented, since adsorption represents the crucial step of gas permeation by surface diffusion. Specifically, the attention is focused on the most common theory used for describing adsorption, the Langmuir's model, which allows a simple prediction of the monolayer coverage on an ideal surface. However, not all the species follow the Langmuir adsorption law and, therefore, a different model taking into account the system heterogeneity originated from the adsorbent or adsorbate must be adopted. Hence, the Sips model is additionally proposed for evaluating the non-ideal adsorption.

2.1 Gas adsorption in zeolites: Langmuir and Sips models

Adsorption is a process used to capture and separate gas or liquid from a multicomponent mixture, which exploits the physical or chemical interaction between molecules in a fluid phase (adsorbate) and a solid (adsorbent). In particular, it describes

the tendency of these molecules to adhere to a solid surface. It can be distinguished in two types depending on the nature of the surface forces: physical and chemical adsorption. Physical adsorption takes place when the solid-gas interaction is weak, since typically involves van der Waals forces and low adsorption energy. Furthermore, molecules can be adsorbed in excess with respect to those in contact with the surface, originating a multilayer coverage. On the other hand, chemisorption involves chemical bonds between adsorbent and adsorbate and a higher enthalpy of adsorption. In this case, molecules occupy only certain adsorption sites on the surface, forming a monolayer of adsorbed phase.

Langmuir proposed the first theory of adsorption in 1918, based on the assumptions of ideal surface and the monolayer formation. Specifically, Langmuir model considers the following hypotheses [52]:

- Surface is energetically homogeneous, that is adsorption energy constant and does not depend on coverage
- Atoms or molecules are adsorbed at a definite site (i.e., adsorption localized)
- Absence of interactions among the adsorbed species on adjacent sites
- Each adsorption site can accommodate only one atom or molecule (i.e., monolayer coverage)

The Langmuir equation is obtained considering the rate of adsorption of molecules from the bulk phase to the solid surface equal to that of desorption from surface to the bulk phase. The rate of adsorption (Eq. 1) can be considered proportional to the applied pressure in the gas phase P and the surface fraction available for adsorption $(1 - \theta)$:

$$r_{adsorption} = k_{adsorption} P (1 - \theta) \quad (1)$$

On the contrary, rate of desorption (Eq. 2) is related to the dimensionless amount adsorbed θ :

$$r_{desorption} = k_{desorption} \theta \quad (2)$$

At equilibrium, the rates of adsorption and desorption are equal (Eq. 3) and the affinity constant b is defined as the ratio of the kinetic constants for the two processes, measuring the attraction strength of an adsorbate molecule on the surface [52].

$$k_{adsorption} P (1 - \theta) = k_{desorption} \theta \implies b = \frac{k_{adsorption}}{k_{desorption}} = \frac{\theta}{P (1 - \theta)} \quad (3)$$

The affinity constant can be correlated to the Langmuir heat of adsorption by the pre-exponential factor b_0 (Eq. 4), which can be estimated from the experimental isotherms:

$$b = b_0 e^{\frac{Q_{Adsorption}}{RT}} = \frac{b_0}{\sqrt{T}} e^{\frac{Q_{Adsorption}}{RT}} \quad (4)$$

Thus, the Langmuir equation (Eq. 5) describing the fractional loading θ as a function of the applied pressure P is shown below:

$$\theta = \frac{bP}{1 + bP} \quad (5)$$

The adsorption coverage can be also expressed as the ratio of the molecular loading C_μ over the saturation loading $C_{\mu s}$, which is the maximum amount adsorbed on the surface. Thus, Langmuir equation can be also expressed in terms of molecular loading (Eq. 6):

$$C_\mu = C_{\mu s} \frac{(bP)}{1 + (bP)} \quad (6)$$

In case of a multicomponent mixture, Langmuir equation for the component i assumes the following expression (Eq. 7):

$$\theta_i = \frac{(b_i P_i)}{1 + \sum_{j=1}^{n_{species}} (b_j P_j)} \quad (7)$$

Sips model (Eqs. 8-12) differs from the Langmuir one since takes into account the species-species and species-surface interactions, which are included in an additional parameter n , giving a measure of the system heterogeneity [52].

$$C_{\mu,i} = C_{\mu s,i} \frac{(b_i P_i)^{\frac{1}{n_i}}}{1 + \sum_{j=1}^{n_{species}} (b_j P_j)^{\frac{1}{n_j}}} \quad (8)$$

$$\theta_i = \frac{(b_i P)^{\frac{1}{n_i}}}{1 + \sum_{j=1}^{n_{\text{species}}} (b_j P_j)^{\frac{1}{n_j}}} \quad (9)$$

$$b_i = b_{i,\infty} e^{\frac{Q_{\text{Adsorption}}}{RT}} \quad (10)$$

$$b_{i,\infty} = b_{i,0} e^{\frac{Q_{\text{Adsorption}}}{RT_{0,i}}} \quad (11)$$

$$\frac{1}{n_i} = \frac{1}{n_{i,0}} + a \left(1 - \frac{T_{0,i}}{T} \right) \quad (12)$$

Therefore, Sips equation is reduced to the Langmuir form when n is equal to 1. In both the adsorption models, saturation loading of the considered component $C_{\mu s, i}$ is a crucial property, providing the maximum amount adsorbed on the zeolite surface. It should be independent of temperature being related to the active sites available to adsorb a specific component. However, this capacity can be reduced by the high temperature that changes the surface-molecules and molecules-molecules interactions, limiting the possibility to be adsorbed. Specifically, Do [52] proposed an exponential decrease with temperature (Eq. 13), in which χ is an empirical parameter and T_0 the reference temperature, which is the lowest temperature at which an adsorption isotherm for the considered species was measured:

$$C_{\mu s, i} = C_{\mu s, 0, i} e^{\chi_i \left(1 - \frac{T}{T_{0, i}} \right)} \quad (13)$$

Saturation loading at the reference temperature ($C_{\mu s, 0}$), empirical parameter χ , heat of adsorption and affinity constant can be evaluated using the adsorption isotherms of the considered species, as will be described in Chapter 3.

2.2 Modelling of mass transport through zeolite membranes

Permeation through zeolite membranes is typically attributed to **surface diffusion** at a low temperature, which takes place by adsorption onto the zeolite surface and molecular hopping of the adsorbed molecules from site-to-site [45]. The generalized **Maxwell-Stefan** equations were extended by Krishna [53, 54, 55] for describing surface diffusion in zeolite pores. Specifically, the driving force for diffusion of the single component I is represented by the chemical potential gradient $\nabla\mu_I$, which is balanced by the friction between the component and the zeolite matrix:

$$-\nabla\mu_1 = \frac{RT}{D_{SD,1zeolite}} \theta_{zeolite} u_1 \quad (14)$$

Where $D_{SD,1zeolite}$ is the Maxwell-Stefan diffusivity related to surface diffusion, μ_I the chemical potential of the adsorbed species I and u_I its velocity. Krishna [54] proposed to use a different definition of the Maxwell-Stefan diffusivity $D_{SD,I}$, expressed as the ratio of $D_{SD,1zeolite}$ over the zeolite coverage $\theta_{zeolite}$:

$$-\nabla\mu_1 = \frac{RT}{D_{SD,1}} u_1 \quad (15)$$

In terms of molar flux:

$$N_{SD,1} = \rho C_{\mu 1} u_1 \implies u_1 = \frac{N_{SD,1}}{\rho C_{\mu 1}} \quad (16)$$

Thus, by replacing the expression of the velocity (Eq. 16) in Eq. 15, molar flux can be related to the chemical potential gradient (Eq. 17):

$$N_{SD,1} = -\rho C_{\mu 1} D_{SD,1} \frac{1}{RT} \nabla\mu_1 \quad (17)$$

The chemical potential can be related to that in standard state and to the fugacity of the component (Eq. 18):

$$\mu_1 = \mu_1^0 + RT \ln(f_1) \quad (18)$$

For systems operating at low pressure conditions, pressure can replace fugacity and chemical potential gradient can be correlated to the adsorption coverage as follows:

$$\frac{1}{RT} \nabla \mu_1 = \frac{1}{\theta_1} \Gamma \nabla \theta_1 \quad (19)$$

Where Γ is the thermodynamic correction factor, representing the deviation from the ideal behavior. Specifically, $\Gamma = 1$ for the ideal condition, whereas for the non-ideal one is a function of the mixture composition [56]. In case of Langmuir adsorption model, thermodynamic factor is described by Eq. 20 [45]:

$$\Gamma = \frac{\partial \ln P}{\partial \ln \theta} = \frac{1}{1 - \theta_1} \quad (20)$$

Thus, the expression for molar flux (Eq. 17) can be written in terms of saturation loading (Eq. 21), defined as the ratio of the molecular loading $C_{\mu l}$ over the coverage θ_1 :

$$N_{SD,1} = -\rho C_{\mu s1} D_{SD,1} \Gamma \nabla \theta_1 \quad (21)$$

Being in single gas condition, the subscript that identify the component l can be removed and Eq. 21 can be written as (Eq.22):

$$N_{SD} = -\rho C_{\mu s} D_{SD} \Gamma \nabla \theta \quad (22)$$

Where the Maxwell-Stefan surface diffusivity D_{SD} can be independent or dependent on coverage. Malek *et al.* [57] summarized the results of many groups regarding the dependence of CH₄ diffusivity on loading in MFI. The former condition is the so-called weak confinement scenario (Eq. 23), whereas the most common dependence on coverage is the linear reduction of diffusivity (i.e., strong confinement scenario) given by Eq. 24. However, Reed and Ehrlich [58] proposed a different expression for diffusivity, based on the intermolecular repulsions, which can reduce the energy barrier for diffusion.

$$D_{SD} = D_{SD}^0 e^{-\frac{E_{SD}}{RT}} \quad (23)$$

$$D_{SD} = D_{SD}^0 e^{-\frac{E_{SD}}{RT}} (1 - \theta) \quad (24)$$

Considering the single gas permeation through an infinitesimal zeolite thickness dz , molar flux (Eqs. 25-26) can be expressed as follows in case of weak confinement scenario (i.e., Eq. 23 for diffusivity) and flat geometry (Figure 4):

$$N_{SD} = -\rho C_{\mu s} D_{SD} \frac{1}{1-\theta} \frac{d\theta}{dz} \quad \Rightarrow \quad \int_0^{\delta_{zeolite}} dz = -\frac{\rho C_{\mu s} D_{SD}^0 e^{-\frac{E_{SD}}{RT}}}{N_{SD}} \int_{\theta_{feed}}^{\theta_{\delta_{zeolite}}} \frac{d\theta}{1-\theta} \quad (25)$$

$$N_{SD} = \frac{\rho C_{\mu s} D_{SD}^0 e^{-\frac{E_{SD}}{RT}}}{\delta_{zeolite}} \ln \left(\frac{1-\theta_{\delta_{zeolite}}}{1-\theta_{feed}} \right) \quad (26)$$

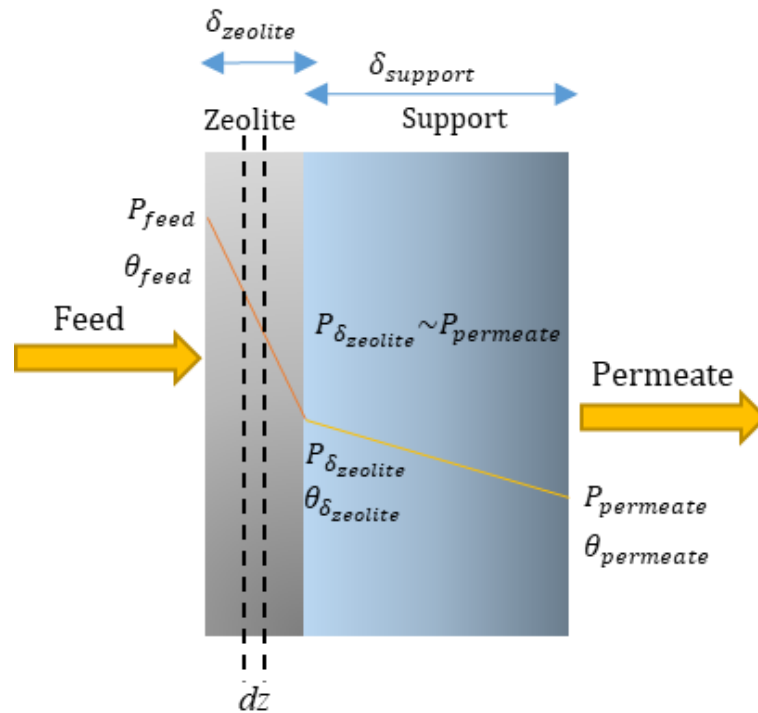


Figure 4. Schematic view of permeating flux through a supported zeolite membrane.

In the case of strong confinement scenario (i.e., Eq. 24 for diffusivity):

$$N_{SD} = -\rho C_{\mu s} D_{SD} \frac{1}{1-\theta} \frac{d\theta}{dz} \quad \Rightarrow \quad \int_0^{\delta_{zeolite}} dz = -\frac{\rho C_{\mu s} D_{SD}^0 e^{-\frac{E_{SD}}{RT}}}{N_{SD}} \int_{\theta_{feed}}^{\theta_{zeolite}} d\theta \quad (27)$$

By integrating:

$$N_{SD} = \frac{\rho C_{\mu s} D_{SD}^0 e^{-\frac{E_{SD}}{RT}}}{\delta_{zeolite}} (\theta_{feed} - \theta_{zeolite}) \quad (28)$$

Support typically provides a further resistance, which is much lower than that of zeolite layer and associated to Knudsen diffusion. If it is assumed a negligible support resistance to mass transport, flux through the membrane thickness for weak (Eq. 29) and strong confinement scenario (Eq. 30) becomes:

$$N_{SD} = \frac{\rho C_{\mu s} D_{SD}^0 e^{-\frac{E_{SD}}{RT}}}{\delta_{zeolite}} \ln \left(\frac{1-\theta_{permeate}}{1-\theta_{feed}} \right) \quad (29)$$

$$N_{SD} = \frac{\rho C_{\mu s} D_{SD}^0 e^{-\frac{E_{SD}}{RT}}}{\delta_{zeolite}} (\theta_{feed} - \theta_{permeate}) \quad (30)$$

A qualitative trend of surface diffusion flux or permeance (being the ratio of flux over the pressure difference) as a function of temperature reveals the presence of a maximum (Figure 5). In fact, temperature affects the flux favoring diffusivity but reducing coverage. Therefore, the increasing trend in the low temperature region is owed to the prevailing increment of diffusivity. On the other hand, the flux drop observed at the right of this maximum is attributed to the opposite condition: the reduction of coverage is more important than the increment of diffusivity.

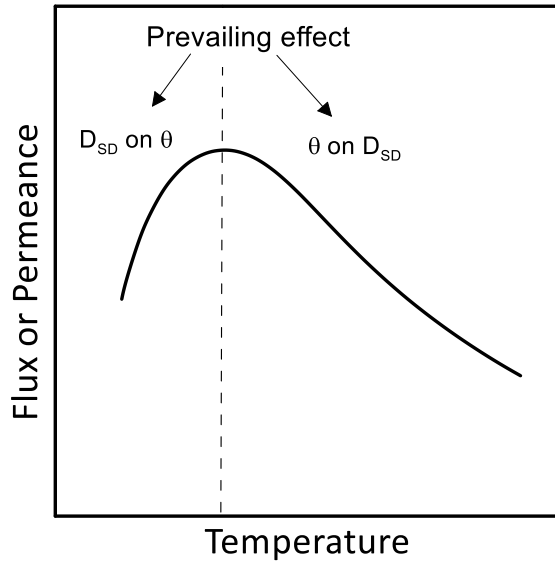


Figure 5. Qualitative trend of surface diffusion flux or permeance as a function of temperature.

However, at sufficiently high temperatures, surface diffusion tends to disappear, since an adsorbed phase is not present anymore onto the inner zeolite surface. In this conditions, Xiao and Wei [59] suggested a mechanism based on permeation in the gas phase, in which molecules maintain their gaseous character passing from site to site by overcoming an energy barrier imposed by the presence of the channel. In particular, the movement of the molecules in the gas phase is restricted since the molecular size approaches the pore size. Hence, a molecule inside a zeolite pore might not complete escape from the potential field of the pore surface: an interaction exists between the gas molecule and pore surface and it can be characterized by an energy barrier. The expression of this so-called **gas translation diffusion** (Eq. 31) is similar to the Knudsen's law with an additional activated term. In fact, gas translation shifts to Knudsen diffusion in the case of pore size much higher than molecular dimension.

$$N_{\text{GTD}} = -\frac{1}{\zeta} \lambda \frac{1}{RT} \sqrt{\frac{8RT}{\pi M}} e^{-\frac{E_{\text{GT}}}{RT}} \nabla P \quad (31)$$

Where λ is the diffusional length ζ and the coordination number. The gas translation contribution along the membrane thickness can be expressed as follows:

$$N_{GTD} = -\frac{1}{\zeta} \lambda \frac{1}{RT} \sqrt{\frac{8RT}{\pi M}} e^{-\frac{E_{GT}}{RT}} \frac{dP}{dz} \Rightarrow \int_0^\delta dz = -\frac{1}{N_{GTD}} \frac{\varepsilon}{\tau \zeta} \lambda \frac{1}{RT} \sqrt{\frac{8RT}{\pi M}} e^{-\frac{E_{GT}}{RT}} \int_{P_{feed}}^{P_{permeate}} dP \quad (32)$$

$$N_{GTD} = \frac{1}{\zeta} \lambda \frac{1}{\delta_{zeolite} RT} \sqrt{\frac{8RT}{\pi M}} e^{-\frac{E_{GT}}{RT}} (P_{feed} - P_{permeate}) \quad (33)$$

Flux by gas translation diffusion (Figure 6) presents a strong increment in the moderate temperature region, which is determined by the exponential term of Eq.33, whereas Knudsen flux decreases with the reverse of the temperature square root. On the contrary, gas translation tends to the Knudsen value for high temperature and very low activation energy E_{GT} , since the exponential term tends to 1 in these conditions. Thus, the temperature dependence of flux related to the two mechanisms is quite different only at a low temperature, becoming similar with increasing temperature.

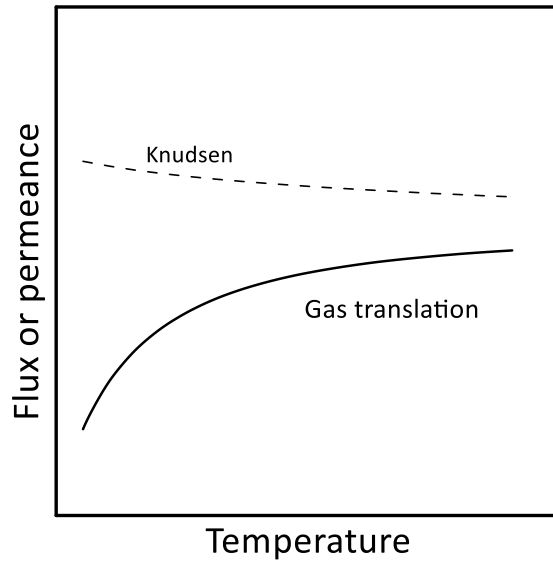


Figure 6. Qualitative trend of gas translation diffusion flux or permeance as a function of temperature.

The single gas overall flux and permeance through a zeolite layer of porosity ε and tortuosity τ are, therefore, the sum of surface and gas translation diffusion (Eqs. 34-35), by neglecting the resistance exerted by the support:

$$N = \frac{\varepsilon}{\tau} \left[\frac{\rho C_{\mu s} D_{SD}^0 e^{-\frac{E_{SD}}{RT}}}{\delta_{zeolite}} \frac{b(P_{feed} - P_{permeate})}{(1+bP_{feed}) + (1+bP_{permeate})} + \frac{\lambda}{\delta_{zeolite} RT \zeta} \sqrt{\frac{8RT}{\pi M}} e^{-\frac{E_{GT}}{RT}} (P_{feed} - P_{permeate}) \right] \quad (34)$$

$$\text{Permeance} = \frac{\varepsilon}{\tau} \left[\frac{\rho C_{\mu s} D_{SD}^0 e^{-\frac{E_{SD}}{RT}}}{\delta_{zeolite}} \frac{b}{(1+bP_{feed}) + (1+bP_{permeate})} + \frac{\lambda}{\delta_{zeolite} RT \zeta} \sqrt{\frac{8RT}{\pi M}} e^{-\frac{E_{GT}}{RT}} \right] \quad (35)$$

In case of tubular membranes (Figure 7), permeating flux is not constant along the radial direction r (Eq. 36):

$$\frac{d(rN)}{dr} = 0 \quad \Rightarrow \quad \frac{dN}{dr} = -\frac{N}{r} \quad (36)$$

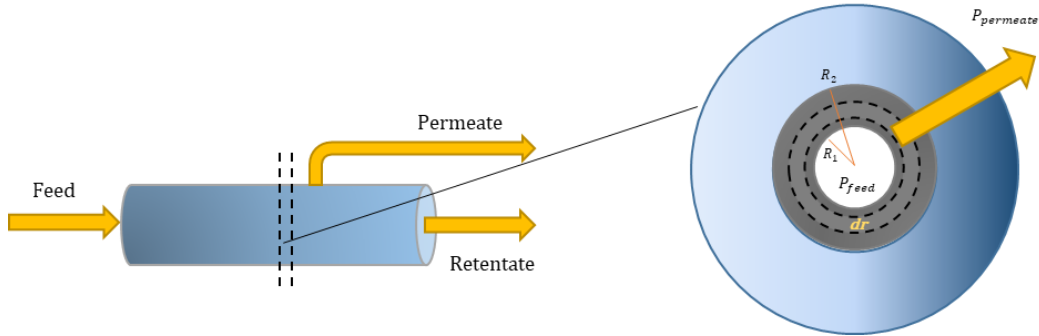


Figure 7. Schematic view of permeating flux through a tubular zeolite supported membrane.

As aforementioned, surface and gas translation fluxes can be obtained neglecting the support resistance. This hypothesis can be adopted only in case of high support-zeolite permeance ratio [2]. When this ratio is higher than 10, membrane selectivity approaches the intrinsic zeolite one. As a practical example, the CO_2 permeance through a DD3R membrane is estimated considering and neglecting the support presence [60]. It is found

that an effective further resistance owed to support is present only at a low temperature, where the zeolite permeance is high because of the strong adsorption (Figure 8). Differently, no differences were observed above 400 K, since the zeolite permeance decreases much more than the support one and, thus, the permeance ratio is high.

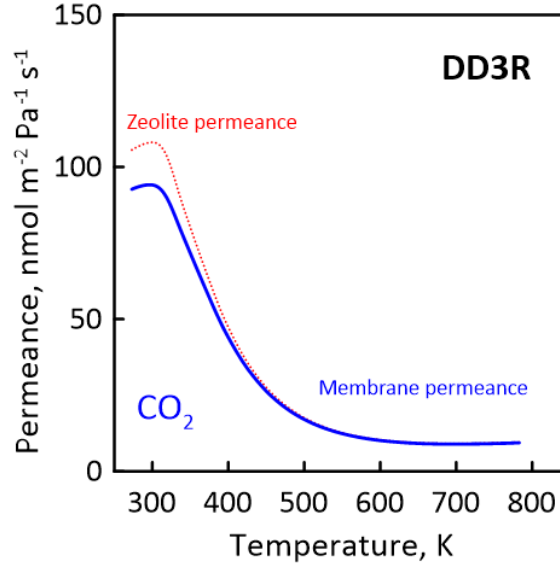


Figure 8. CO₂ permeance through a DD3R membrane including the porous support (blue solid line) and without it (red dashed line). Reprinted from Journal of Membrane Science, 564, P. F. Zito, A. Caravella, A. Brunetti, E. Drioli, G. Barbieri, Discrimination among gas translation, surface and Knudsen diffusion in permeation through zeolite membranes, 166-173. Copyright (2018) Elsevier.

All the previous equations are valid for a single component permeating through a zeolite membrane. In case of a **multicomponent mixture**, Maxwell-Stefan equation for surface diffusion is written considering the balance between the driving force attributed to the chemical potential gradient $\nabla\mu_i$ of the component i and its friction with the other species present in the mixture [53, 54, 55, 61, 62, 63]:

$$-\rho\theta_i \frac{\nabla\mu_i}{RT} = \sum_{j=1}^{n_{\text{species}}} \frac{C_{\mu,j}N_{SD,i} - C_{\mu,i}N_{SD,j}}{C_{\mu,s,j}C_{\mu,s,i}D_{SD,ij}} + \frac{N_{SD,i}}{C_{\mu,s,i}D_{SD,i}} = -\rho \sum_{j=1}^{n_{\text{species}}} \Gamma_{ij} \nabla\theta_j \quad (37)$$

It can be observed the presence of the binary diffusivity $D_{SD,ij}$, representing the interaction between components i and j , which depends on the mixture composition and the single gas diffusivity. In fact, it is comprised between D_i (for $\theta_i=1$ and $\theta_j=0$) and D_j

(for $\theta_i=0$ and $\theta_j=1$). The binary exchange diffusivity can be evaluated using the Vignes correlation [53, 56, 64]:

$$D_{SD,ij} = D_{SD,i}^{\frac{\theta_i}{\theta_i+\theta_j}} D_{SD,j}^{\frac{\theta_j}{\theta_i+\theta_j}} \quad (38)$$

An alternative expression is obtained introducing the self-exchange diffusivity of each component [65] (Eq.39):

$$C_{\mu S,j} D_{SD,ij} = (C_{\mu S,j} D_{SD,ii})^{\frac{C_{\mu,i}}{C_{\mu,i}+C_{\mu,j}}} (C_{\mu S,i} D_{SD,jj})^{\frac{C_{\mu,j}}{C_{\mu,i}+C_{\mu,j}}} = C_{\mu S,i} D_{SD,ij} \quad (39)$$

Γ is expressed as:

$$\Gamma_{ij} = \frac{C_{\mu S,j}}{C_{\mu S,i}} \frac{C_{\mu,i}}{p_i} \frac{\partial p_i}{\partial C_{\mu,j}} \quad (40)$$

Eq.41 provides the fluxes in matrix form:

$$(N_{SD}) = \rho [C_{\mu S}] [B^{-1}] [\Gamma] (\nabla \theta) \quad (41)$$

Where the elements of the matrix B are:

$$B_{ii} = \frac{1}{D_{SD,i}} + \sum_{j=1}^{n_{\text{species}}} \frac{\theta_j}{D_{SD,ij}} \quad (42)$$

$$B_{ij} = -\frac{\theta_i}{D_{SD,ij}} \quad (43)$$

The Maxwell-Stefan surface diffusivity $D_{SD,i}$ for mixtures can assume the two following expressions (Eqs. 44-45):

$$D_{SD,i} = D_{SD,i}^0 e^{-\frac{E_{SD,i}}{RT}} \quad (44)$$

$$D_{SD,i} = D_{SD,i}^0 e^{-\frac{E_{SD,i}}{RT}} \left(1 - \sum_{j=1}^{n_{species}} \theta_j\right) \quad (45)$$

Considering the case of a binary gas mixture, Eq. (41) becomes [61]:

$$\begin{pmatrix} N_{SD,1} \\ N_{SD,2} \end{pmatrix} = -\rho \begin{bmatrix} C_{\mu S,1} & 0 \\ 0 & C_{\mu S,2} \end{bmatrix} \begin{bmatrix} D_{SD,1} & 0 \\ 0 & D_{SD,2} \end{bmatrix} \begin{bmatrix} 1 + \theta_1 \frac{D_{SD,2}}{D_{SD,12}} & \theta_1 \frac{D_{SD,2}}{D_{SD,12}} \\ \theta_2 \frac{D_{SD,1}}{D_{SD,12}} & 1 + \theta_2 \frac{D_{SD,1}}{D_{SD,12}} \end{bmatrix} \frac{1}{\theta_2 \frac{D_{SD,1}}{D_{SD,12}} + \theta_1 \frac{D_{SD,2}}{D_{SD,12}} + 1} \begin{bmatrix} \Gamma_{11} & \Gamma_{12} \\ \Gamma_{21} & \Gamma_{22} \end{bmatrix} \begin{pmatrix} \nabla \theta_1 \\ \nabla \theta_2 \end{pmatrix} \quad (46)$$

Thus, the surface diffusion fluxes of component 1 and 2 are:

$$N_{SD,1} = -\rho \frac{C_{\mu S,1} D_{SD,1} \left\{ \left[\Gamma_{11} + \theta_1 \frac{D_{SD,2}}{D_{SD,12}} (\Gamma_{11} + \Gamma_{21}) \right] \nabla \theta_1 + \left[\Gamma_{12} + \theta_1 \frac{D_{SD,2}}{D_{SD,12}} (\Gamma_{12} + \Gamma_{22}) \right] \nabla \theta_2 \right\}}{\theta_2 \frac{D_{SD,1}}{D_{SD,12}} + \theta_1 \frac{D_{SD,2}}{D_{SD,12}} + 1} \quad (47)$$

$$N_{SD,2} = -\rho \frac{C_{\mu S,2} D_{SD,2} \left\{ \left[\Gamma_{22} + \theta_2 \frac{D_{SD,1}}{D_{SD,12}} (\Gamma_{22} + \Gamma_{12}) \right] \nabla \theta_2 + \left[\Gamma_{2,1} + \theta_2 \frac{D_{SD,1}}{D_{SD,12}} (\Gamma_{21} + \Gamma_{11}) \right] \nabla \theta_1 \right\}}{\theta_2 \frac{D_{SD,1}}{D_{SD,12}} + \theta_1 \frac{D_{SD,2}}{D_{SD,12}} + 1} \quad (48)$$

Thus, flux of a generic component in mixture changes compared to that in single gas owing to the competitive adsorption, which provokes a reduction of its coverage. Considering the case of a binary mixture consisting in a strongly and weakly adsorbed species, coverage of the latter drastically drops since the strongly adsorbed component occupies the available sites for adsorption (Figure 9). Thus, surface diffusion of weakly adsorbed components is much lower in mixture.

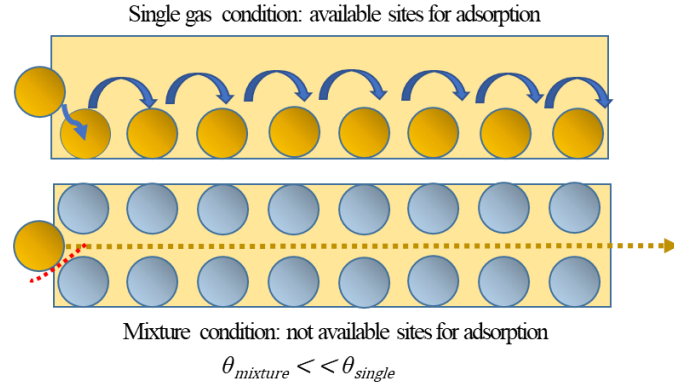


Figure 9. Schematic view of the coverage reduction of a weakly adsorbed species (yellow spheres) in presence of a strongly adsorbed species (blue spheres) inside the zeolite pores.

Gas translation diffusion flux of the generic component *ith* in the mixture has a similar expression as in single gas:

$$N_{GTD,i} = -\frac{\varepsilon}{\tau} \frac{1}{\zeta} \lambda \frac{1}{RT} \sqrt{\frac{8RT}{\pi M_i}} e^{-\frac{E_{GT,i}}{RT}} \nabla P_i \quad (49)$$

For a binary mixture:

$$N_{GTD,1} = -\frac{\varepsilon}{\tau} \frac{1}{\zeta} \lambda \frac{1}{RT} \sqrt{\frac{8RT}{\pi M_1}} e^{-\frac{E_{GT,1}}{RT}} \nabla P_1 \quad (50)$$

$$N_{GTD,2} = -\frac{\varepsilon}{\tau} \frac{1}{\zeta} \lambda \frac{1}{RT} \sqrt{\frac{8RT}{\pi M_2}} e^{-\frac{E_{GT,2}}{RT}} \nabla P_2 \quad (51)$$

In the model proposed in this PhD, surface and gas translation diffusion are considered to compete in permeation through the zeolite pores, starting from a recent model that paired surface and Knudsen diffusion [50-51]. Here, gas translation and surface diffusion of the weakly adsorbed species are hindered by the presence of an adsorbed phase and, therefore, by surface diffusion of a strongly adsorbed species. This **hindering effect** is expressed in terms of a change of coverage, effective porosity and tortuosity (pore diameter is replaced by the diffusional length). In particular, effective porosity and

tortuosity are considered to be functions of molecular loading C_μ , as reported in the modelling approach of Caravella *et al.* [50] for the competition between surface and Knudsen diffusion.

The effective porosity decreases because of the presence of an adsorbed phase, which reduces the free volume available for diffusion (Figure 10). Considering the permeation of a weakly adsorbed component as H_2 (gold spheres of Figure 10), the effective porosity in single gas coincides with the nominal value of the zeolite ε_0 . Differently, an increasing amount of a strong adsorbed component (blue spheres) on the active sites makes smaller this available volume.

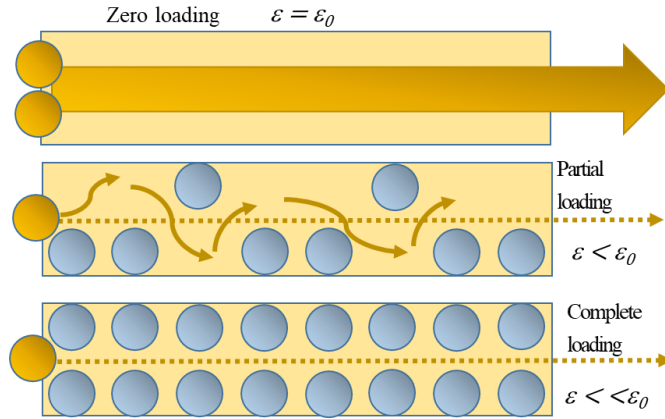


Figure 10. Schematic view of the effective porosity reduction in presence of an adsorbed phase inside the zeolite pores.

In the expression of effective porosity (Eq. 52), the adsorbed molecules are assumed as spheres having a diameter equal to their kinetic diameter d_k [50]. However, the effective volume occupied by the adsorbed molecules is considered equivalent to that of the corresponding cube, since additional volume is not accessible by the bulk molecules (i.e., between the lower part of the sphere and the zeolite surface and at the upper part of the sphere):

$$\varepsilon(C_\mu) = \varepsilon_0 - \rho(1 - \varepsilon_0) N_{Av} \sum_{i=1}^{n_{\text{species}}} d_{k,i}^3 C_{\mu,i} \quad (52)$$

Differently, the effective tortuosity is increased by adsorption, since the actual path followed by the species is supposed longer than the nominal pore length owing to the presence of an adsorbed phase (Figure 11). However, when the complete surface coverage is reached, the actual path returns to the zero-loading tortuosity τ_0 , since the channel assumes the same shape of the zero-loading channel again [50].

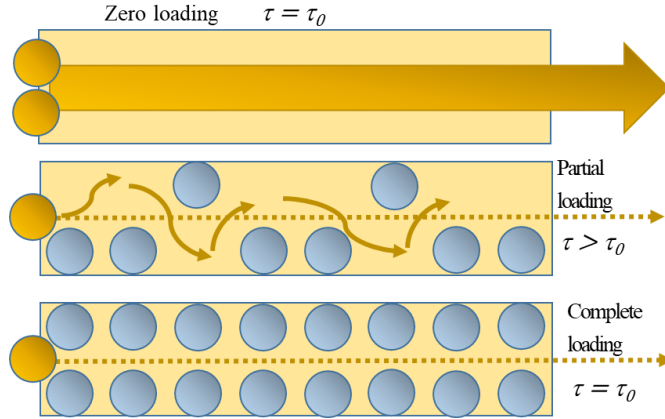


Figure 11. Schematic view of the effective tortuosity increment in presence of an adsorbed phase inside the zeolite pores.

Therefore, the expression of effective tortuosity takes into account the limits of zero loading and full coverage:

$$\lim_{\sigma \rightarrow 0} \tau = \tau_0 \quad \lim_{\sigma \rightarrow 1} \tau = \tau_0 \quad (53)$$

where τ_0 is the nominal tortuosity of material, σ is the covered surface fraction, providing the surface fraction occupied by the adsorbed molecules (Eq. 54):

$$\sigma(C_\mu) = \frac{\frac{\pi}{4} N_{Av} \sum_{i=1}^{n_{species}} d_{k,i}^2 C_{\mu,i}}{S_{g,0}} \quad (54)$$

In Eq. 54, $S_{g,0}$ is the specific surface area at zero loading, defined as follows:

$$S_{g,0} = \frac{4\varepsilon_0}{\rho(1-\varepsilon_0)d_{pore,0}} \quad (55)$$

In addition, there is no effect of adsorption on effective tortuosity if pore size is much larger than kinetic diameter of the permeating species. By defining γ as the ratio of the kinetic diameter over the pore one (Eq. 56), the following limit must be respected (Eq. 57):

$$\gamma = \frac{\frac{1}{n_{species}} \sum_{i=1}^{n_{species}} d_{k,i}}{d_{pore,0}} \quad (56)$$

$$\lim_{\gamma \rightarrow 0} \tau = \tau_0 \quad (57)$$

Thus, Caravella *et al.* [50] proposed the following expression for the effective tortuosity:

$$\tau(C_{\mu}) = \tau_0 + \frac{\gamma \sigma(1-\sigma)}{\varepsilon \gamma} \quad (58)$$

Since the adsorbed amount strongly depends on temperature and pressure, effective porosity and tortuosity are also function of these two variables. In particular, porosity increases with increasing temperature and decreasing pressure, whereas tortuosity follows the opposite trend. These dependences are owed to the increment and reduction of coverage with pressure and temperature. Therefore, gas translation contribution results lower in mixture than in single gas especially at a low temperature and high pressure, since the high adsorption changes the effective porosity and tortuosity compared to the nominal values. These variations of surface and gas translation contributions in mixture are showed and discussed in Chapter 4.

2.3 Experimental apparatus for permeation measurements

Permeation of gas mixtures and single gas through a DDR membrane is experimentally measured using a suitable apparatus (Figure 12). The inlet gas stream (mixture or single) is fed to the membrane by means of mass flow controllers, to tune the desired flow rate and mixture composition. The tubular stainless-steel module, which contains the zeolite membrane, is placed in a furnace to properly control the temperature during the

experiments. No sweep gas is used on permeate side. Back-pressure regulators are on retentate and permeate sides to control the operating pressures, whereas retentate and permeate flow rates are measured by two bubble-soap flow meters. A gas chromatograph (Agilent 7890N) with two parallel analytical lines measures the composition of the retentate and permeate streams at the same time. Each line is equipped with two columns: an HP-Plot-5A (to separate permanent gases such as H₂, N₂, and CO) and an HP-Poraplot Q (for other species). Before permeation measurements, membrane module is heated up to 120°C under argon flow at 2 bar of driving force to remove humidity traces that may be present.

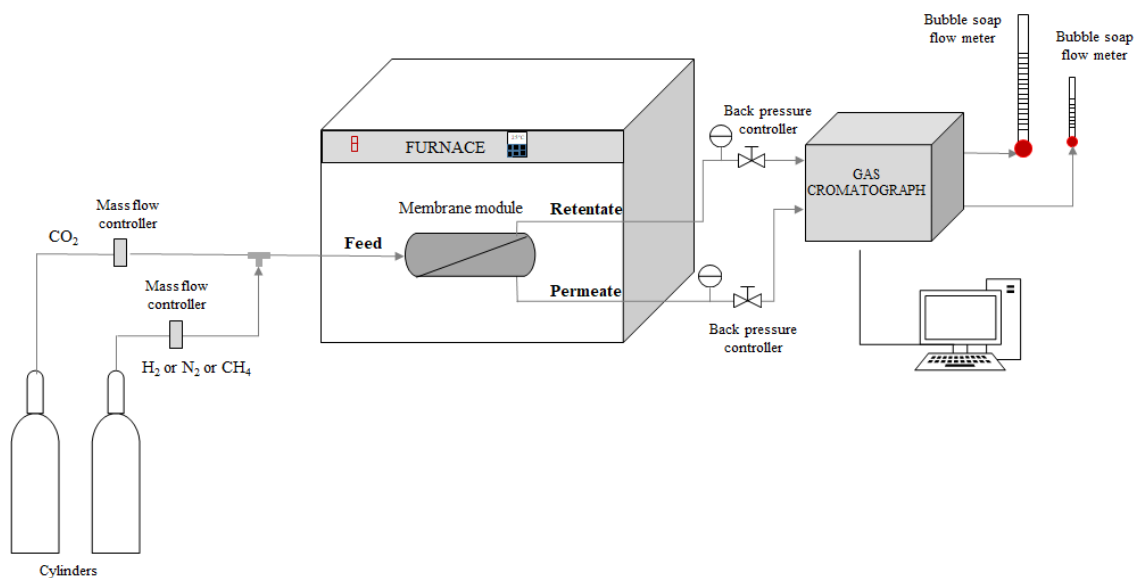


Figure 12. Experimental apparatus for permeation measurements.

3. Adsorption and diffusion of single components in zeolites

This chapter is devoted to the analysis of the single gas behavior, evaluating the adsorption and diffusion of H₂, CH₄, CO₂, CO, N₂ and H₂O through different zeolites (i.e., SAPO-34, DD3R, NaY and 4A). In fact, adsorption properties and single gas diffusivity represent necessary inputs for predicting surface and gas translation contributions to permeation.

Adsorption is estimated using pure-component experimental isotherms taken from the literature by means of a multivariate regression analysis based on the Levenberg-Marquardt algorithm. Langmuir and Sips models are chosen for describing the experimental behavior. Concerning NaY and DD3R, the adsorption properties are already available in two works previous to this PhD [66,67]. Diffusion through zeolite membranes is described using the Maxwell-Stefan approach for surface diffusion, which is matched to gas translation. This analysis needs the evaluation of the activation energy of both the contributions and, moreover, the surface diffusion pre-exponential factor. These properties are obtained using the experimental permeances as a function of temperature in single gas, selecting the low and high temperature values for estimating surface and gas translation contributions, respectively. Table 3 summarizes the origin of the various experimental data used for the evaluation of adsorption and diffusivity by simulations. Simulations of adsorption isotherms, single component and mixture permeation (Chapter 4) are carried out using Matlab.

Table 3. An overview of the literature experimental data used for the evaluation of adsorption and diffusion.

Zeolite	Simulated Adsorption properties	Experimental data	Simulated Diffusivity	Experimental data
4A	This PhD	30, 75, 81-92	This PhD	30
SAPO-34	This PhD	34, 42, 78, 79, 80	This PhD	42
NaY	Previous to this PhD [66]		This PhD	49
DD3R	Previous to this PhD [67]		This PhD	93

The adsorption properties and diffusivity values obtained in this chapter allow a rigorous mass transport analysis and the prediction of separation performance under operating conditions wider than those experimentally investigated.

The results of this chapter are based on four published paper in international journals [60, 68, 69, 70].

3.1 Evaluation of adsorption properties

Generally, the experimental adsorption isotherms are expressed in excess of loading, which therefore should be converted in absolute loading before being used. The conversion can be done using the following expression [71]:

$$m_{adsorbed} = m_{excess} + \rho_{bulk} V_{adsorbed} \quad (59)$$

In this expression, $m_{adsorbed}$ and m_{excess} are the absolute and the excess amount adsorbed respectively, whereas ρ_{bulk} and $V_{adsorbed}$ the density and the volume of the gas and adsorbed phase. By substituting the definition of volume adsorbed (i.e., $\frac{m_{adsorbed}}{\rho_{adsorbed}}$) in Eq. (59), the following final expression is obtained in terms of absolute amount expressed in moles:

$$n_{adsorbed} = \frac{\frac{1000 m_{excess}}{M}}{1 - \frac{\rho_{bulk}}{\rho_{adsorbed}}} \quad (60)$$

In Eq. (60), the density of adsorbed phase can be assumed equal to that at the triple point [72] or to that of the liquid phase, which is 0.0708 g cm^{-3} for hydrogen [73].

Another way to calculate the absolute amount adsorbed consists in assuming the adsorbed phase volume equal to the pore volume [74] (e.g., 0.3 mL g^{-1} for 4A [75]). This approach can be used when the species adsorption on the external surface is ignored [76]. In this condition, the following equation can be used:

$$n_{absolute} = n_{excess} + \frac{PV}{RT} \quad (61)$$

As reported by Krishna [77], the difference between absolute and excess of loading increases with increasing pore volume and pressure. Furthermore, this discrepancy becomes more relevant in case of weakly-adsorbing species, like hydrogen, at high pressure, whereas it is smaller for strongly adsorbed ones, like CO_2 . Therefore, here it is carried out a comparison between the hydrogen adsorption isotherms expressed in excess and absolute loading at the lowest (40 K) and highest (298 K) temperatures among those available (Figure 13) considering the case of zeolite 4A. This comparison allows to verify the possibility to consider the experimental values without making any conversion. Specifically, the blue and red lines indicate the trends of the absolute loading respectively evaluated with Eqs. (60) and (61), whereas the black dashed lines represent the trends of the excess of loading. As expected, it can be observed that all the curves are quite similar at low pressure, whereas they diverge only at high pressure. The negligible difference observed can be explained considering that pore volume of 4A (0.3 mL g^{-1} [75]) is quite small compared to those of the other materials investigated by Krishna [77] (i.e., MOFs CuBTC, MIL-101 and Zn(bdc)dabco], which have a specific pore volumes of 0.75, 1.38 and 0.67 mL g^{-1} .

Hence, it can be assumed valid the hypothesis to use the excess of loading also for the other species and zeolites.

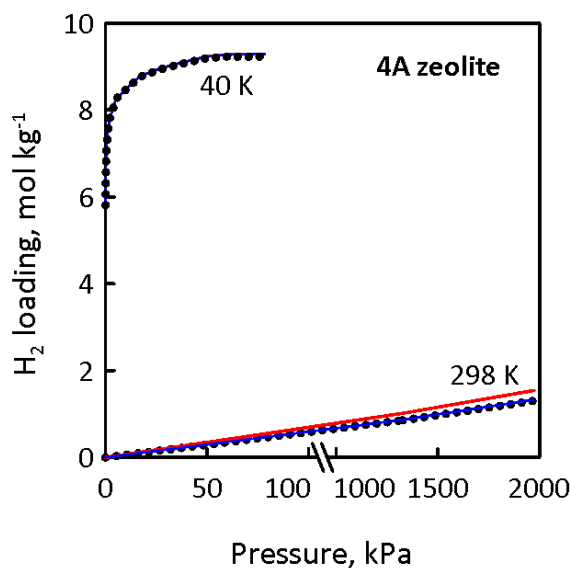


Figure 13. Absolute and excess of loading for H₂ compared at 40 K and 298 K. Absolute loading evaluated with Eq (60) (blue lines), absolute loading evaluated with Eq. (61) (red lines), trend of excess of loading (black dashed lines). Reprinted from *Microporous and Mesoporous Materials*, 249, P.F. Zito, A. Caravella, A. Brunetti, E. Drioli, G. Barbieri, Light gases saturation loading dependence on temperature in LTA 4A zeolite, 67-77. Copyright (2017) Elsevier.

3.1.1 SAPO-34 zeolite

Langmuir model is used for the estimation of adsorption parameters of CO₂, CH₄, N₂ and H₂ through a SAPO-34 zeolite (CHA structure as shown in Figure 2), using several experimental adsorption isotherms available in the literature. The experimental data are preliminary compared in order to verify the consistency of isotherms taken from different authors [34, 42, 78-80]. Table 4 shows the temperature and pressure range concerning the experimental isotherms used for the estimation.

Figures 14-17 show the adsorption isotherms, representing the molecular loading of each species as a function of pressure. The model curves (solid lines) are used for describing the experimental values (symbols) and, moreover, for the prediction of the behavior of each species at high pressure (i.e., up to 2000 kPa). It can be observed a very good agreement between Langmuir model and the experimental isotherms for all the species in both the low (left side of each figure) and high-pressure range (right side of each figure). The high values of the correlation coefficient R^2 (0.9945, 0.9949, 0.9955

and 0.9918 for CO₂, H₂, CH₄ and N₂, respectively) confirm the good matching between model and the experimental values.

Table 4. An overview of the operating conditions ranges concerning the published experimental adsorption isotherms used for SAPO-34 zeolite. Reprinted from Journal of Membrane Science, 595, P.F. Zito, A. Brunetti, A. Caravella, E. Drioli, G. Barbieri, Mutual influence in permeation of CO₂-containing mixtures through a SAPO-34 membrane, 117534, Copyright (2020) Elsevier.

Species	T _{minimum} / °C	T _{maximum} / °C	P _{maximum} / kPa	References	Number of isotherms
H ₂	-196	60	980	78, 79	3
CH ₄	-20	200	120	34, 42, 80	9
CO ₂	-20	200	990	34, 42, 79	9
N ₂	20	150	120	34, 42	5

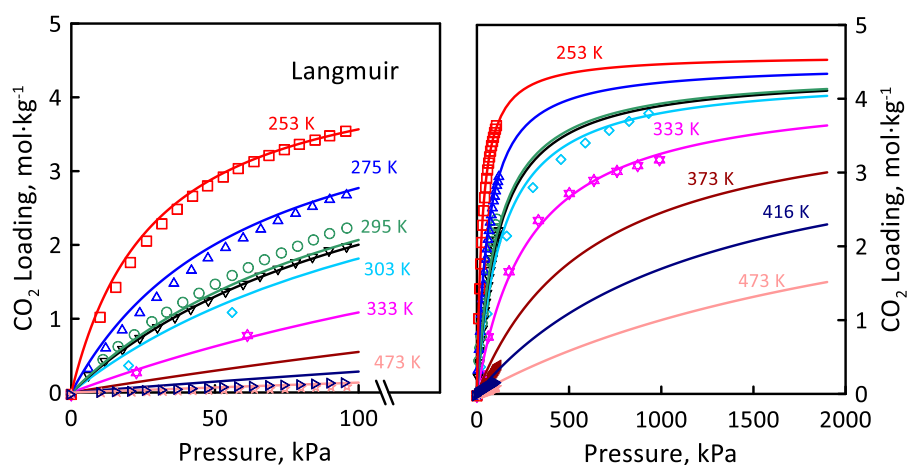


Figure 14. CO₂ adsorption isotherms at, (□, red line) 253 K, (Δ, blue line) 275 K, (○, green line) 295 K, (∇, black line) 297 K, (◇, sky blue line) 303 K, (☆, magenta line) 333 K, (◁, ruby red line) 373 K, (▷, dark blue line) 416 K, (☆, pink line) 473 K on SAPO-34. Symbols: experimental values of [34, 42, 79]; solid lines: model results (non-linear regression of experimental data).

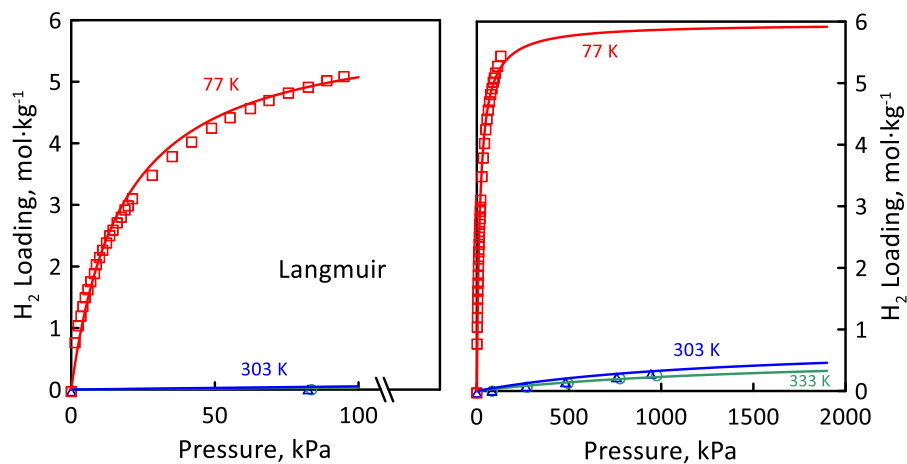


Figure 15. H₂ adsorption isotherms at, (□, red line) 77 K, (Δ, blue line) 303 K, (○, green line) 333 K on SAPO-34. Symbols: experimental values of [78, 79]; solid lines: model results (non-linear regression of experimental data).

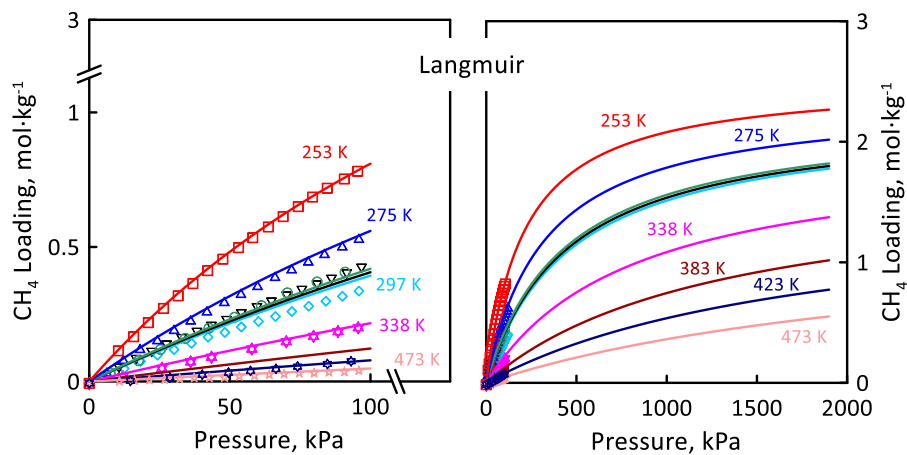


Figure 16. CH₄ adsorption isotherms at, (□, red line) 253 K, (Δ, blue line) 275 K, (○, green line) 293 K, (∇, black line) 295 K, (◇, sky blue line) 297 K, (☆, magenta line) 338 K, (◁, ruby red line) 383 K, (▷, dark blue line) 423 K, (☆, pink line) 473 K on SAPO-34. Symbols: experimental values of [34, 42, 80]; solid lines: model results (non-linear regression of experimental data).

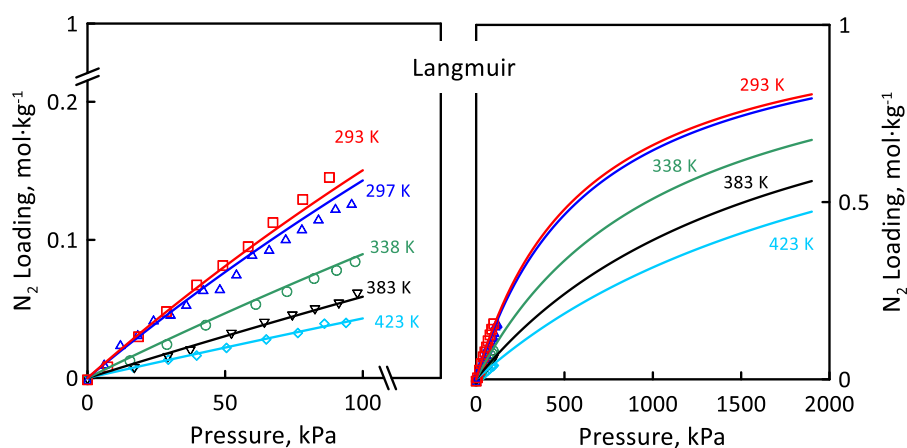


Figure 17. N₂ adsorption isotherms at, (□, red line) 293 K, (Δ, blue line) 297 K, (○, green line) 338 K, (∇, black line) 383 K, (◇, sky blue line) 423 K on SAPO-34. Symbols: experimental values of [34, 42]; solid lines: model results (non-linear regression of experimental data).

The four parameters of the Langmuir model and their respective confidence intervals are presented in Figure 18. The saturation loadings at the reference temperature $C_{\mu s0}$ cannot be directly compared each other, since the T_0 of the species is different. In fact, H₂ presents the highest $C_{\mu s0}$ because its reference temperature is the lowest (i.e., 77 K). The affinity constants b_0 cannot be compared too, being also related to T_0 value. On the other hand, the here estimated heats of adsorption provide an indication of the adsorption strength of each species. It can be observed that, as expected, the more strongly adsorbed species is CO₂ (about 19 kJ mol⁻¹), followed by CH₄ (about 10 kJ mol⁻¹), N₂ (about 9 kJ mol⁻¹) and H₂ (about 3 kJ mol⁻¹). The values of the empirical parameter χ , from which the temperature dependence of saturation loading is obtained (Eq. 62), reveal that CH₄ and H₂ present a more important reduction of the adsorption coverage than CO₂ when temperature increases, since their χ values are higher. Particular is the case of nitrogen, for which a temperature independent loading is estimated ($\chi = 0$). This behavior could be attributed to the narrow temperature range of the experimental adsorption isotherms for N₂ (293 - 423 K), in which the gap in saturation loadings is too small to be appreciated.

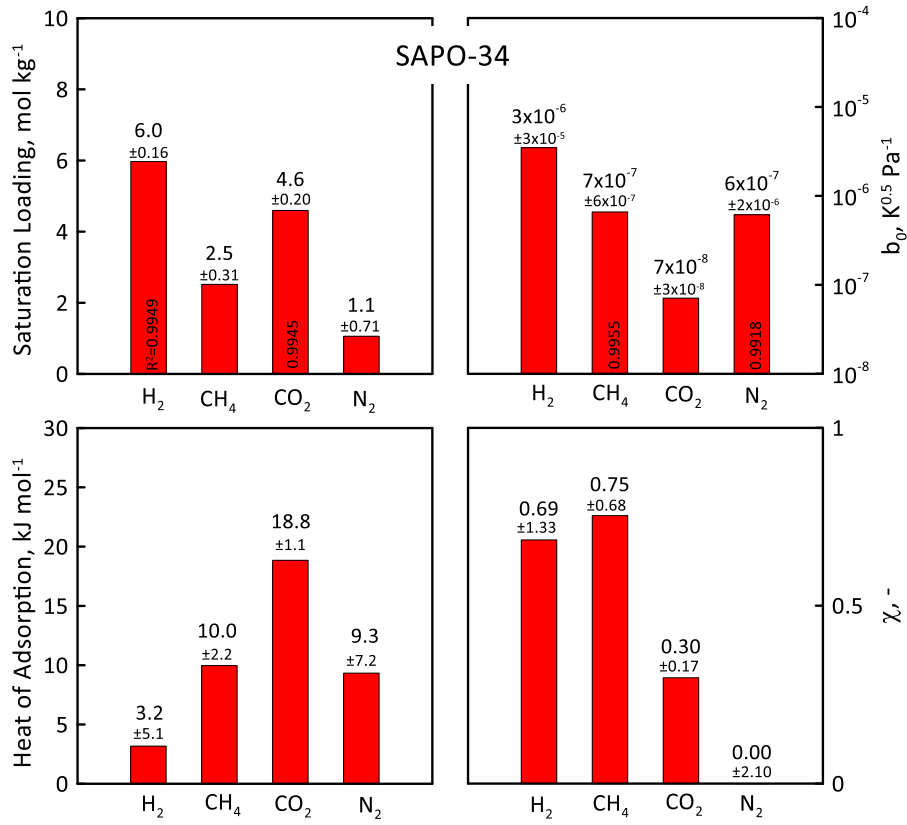


Figure 18. Calculated optimal values of the Langmuir model parameters for the considered species on SAPO-34. Saturation loading at the reference temperature $C_{\mu s0}$, affinity constant b_0 , heat of adsorption, empirical parameter χ_x .

The maximum of adsorption loading of each species on SAPO-34 surface is estimated at the same temperature of 298 K by Eq. 62 (Figure 19), allowing a direct comparison of the adsorption of each species.

$$C_{\mu s,i} = C_{\mu s0,i} e^{\chi_i \left(1 - \frac{298}{T_{0,i}}\right)} \quad (62)$$

It is found a CO₂ saturation loading much higher than that of the other species, being 2, 4 and 5.5 times higher than that of CH₄, N₂ and H₂ respectively. The order of saturation loadings is the same of that of heats of adsorption, which confirms that CO₂ and H₂ are the most and least strongly adsorbed species, respectively.

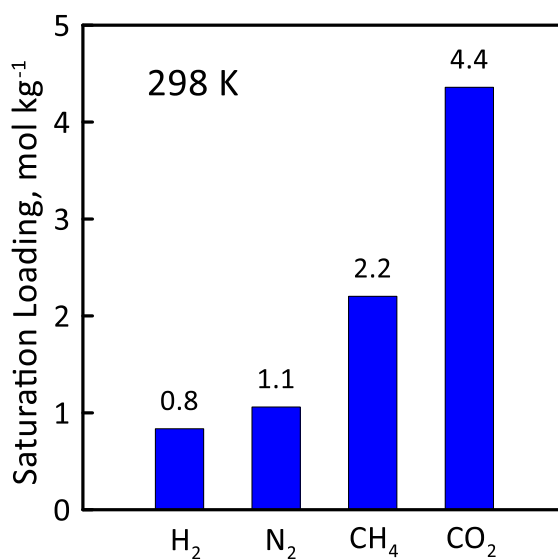


Figure 19. Saturation loading of H₂, N₂, CH₄ and CO₂ on SAPO-34 at 298 K.

3.1.2 4A zeolite

As done for SAPO-34 in the previous section, the temperature and pressure ranges related to the experimental adsorption isotherms of H₂, CH₄, CO₂, CO, N₂ and H₂O on 4A zeolite (LTA structure as shown in Figure 2) available in the open literature are collected in Table 5 [68, 70]. It can be observed that the temperature and pressure ranges covered by the experimental data are wide, as well as the number of isotherms used for each species is high.

Table 5. An overview of the operating conditions ranges concerning the published experimental adsorption isotherms used for LTA 4A zeolite [68, 70].

Species	T _{minimum} , K	T _{maximum} K	P _{maximum} . kPa	References	Isotherms
H ₂	40	298	1970	75, 81, 82	8
CH ₄	195	308	830	83, 84, 85, 86, 87	10
CO ₂	195	373	930	86, 87, 88, 89, 90, 91	13
CO	193	373	120	30, 87, 89	8
N ₂	195	283	550	84, 85, 87, 89	10
H ₂ O	273	438	10.5	30, 92	6

Figures 20-24 show the matching among the experimental isotherms (symbols) and the adsorption models (continuous lines) for the considered species using Langmuir and Sips models. The Sips model is also used for 4A since the adsorption of some species (i.e., H₂, CO₂ and H₂O) is not well described by the Langmuir one. The left-side of each figure presents the results up to 100 kPa, in order to better appreciate the agreement between models and experimental values under low-pressure. On the other hand, the right side shows the behaviour up to 2000 kPa, in order to check the ability of the models to describe the experimental trends even at higher pressures.

The first consideration to make is that H₂ and CO₂ follow a non-ideal adsorption on zeolites (Figures 20-21). In fact, hydrogen and carbon dioxide adsorption isotherms result much better described by the Sips model, as confirmed by the higher correlation coefficient R². Specifically, values of 0.9527 and 0.9951 are estimated for H₂, whereas 0.9601 and 0.9817 for CO₂ using Langmuir and Sips. In particular, the Langmuir equation results less appropriate than the Sips one in the low temperature region (i.e., 40-120 K for H₂, 213-273 K for CO₂) corresponding to the strong adsorption condition.

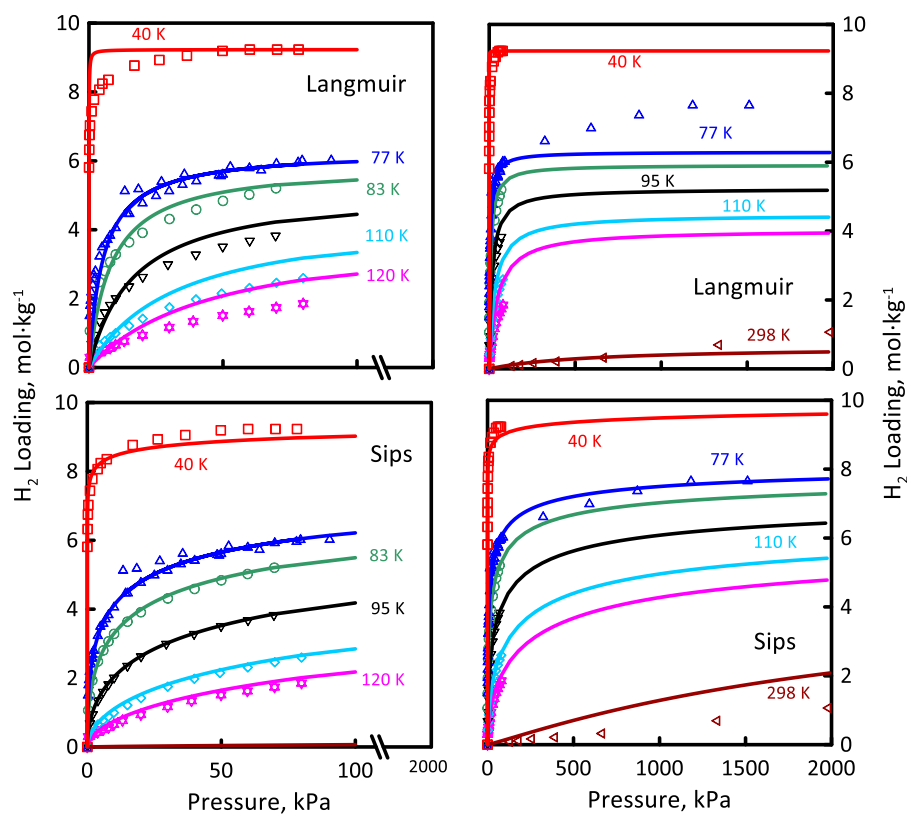


Figure 20. H₂ adsorption isotherms at, (□, red line) 40 K, (Δ, blue line) 77 K, (○, green line) 83 K, (∇, black line) 95 K, (◇, sky blue line) 110 K, (☆, magenta line) 120 K, (◁, ruby red line) 298 K on 4A. Symbols: experimental values of [75, 81, 82]; solid lines: model results (non-linear regression of experimental data). Reprinted from *Microporous and Mesoporous Materials*, 249, P.F. Zito, A. Caravella, A. Brunetti, E. Drioli, G. Barbieri, Light gases saturation loading dependence on temperature in LTA 4A zeolite, 67-77. Copyright (2017) Elsevier.

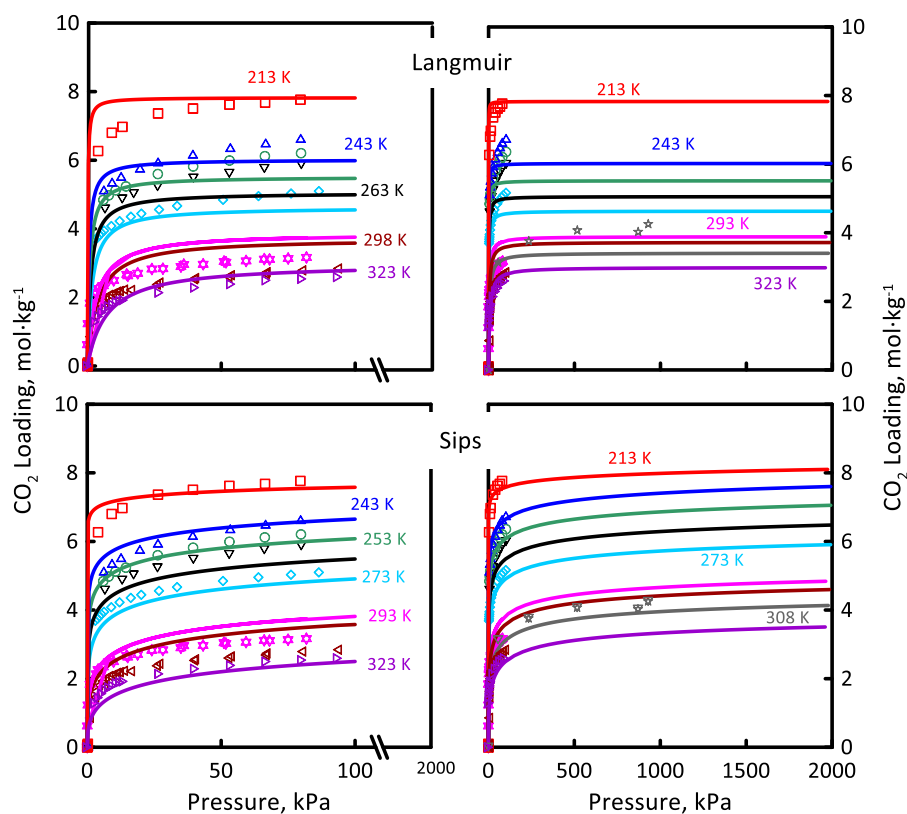


Figure 21. CO₂ adsorption isotherms at, (□, red line) 213 K, (Δ, blue line) 243 K, (○, green line) 253 K, (∇, black line) 263 K, (◇, sky blue line) 273 K, (☆, magenta line) 293 K, (◁, ruby red line) 298 K, (☆, grey line) 308 K, (▷, purple line) 323 K on 4A. Symbols: experimental values of [86-91]; solid lines: model results (non-linear regression of experimental data). Reprinted from *Microporous and Mesoporous Materials*, 249, P.F. Zito, A. Caravella, A. Brunetti, E. Drioli, G. Barbieri, Light gases saturation loading dependence on temperature in LTA 4A zeolite, 67-77. Copyright (2017) Elsevier.

On the other hand, not significant differences between Langmuir and Sips are found for CH₄, CO and N₂ (Figures 22-24); this states that the adsorption of these components is ideal.

Concerning water vapor (Figure 25), the experimental adsorption isotherms are available in a very low-pressure range in order to avoid the condensation. Thus, the model prediction has to consider the limit imposed by vapor pressure. Langmuir equation (left side) could not be used for water vapor, especially between 273 and 374 K, being not able to reproduce the experimental measurements. On the contrary, Sips model (right side) well describes the experimental values of loading in the whole temperature and pressure

ranges taken into account. A further proof is given by the correlation coefficient R^2 , which are 0.9486 and 0.9903 for Langmuir and Sips, respectively.

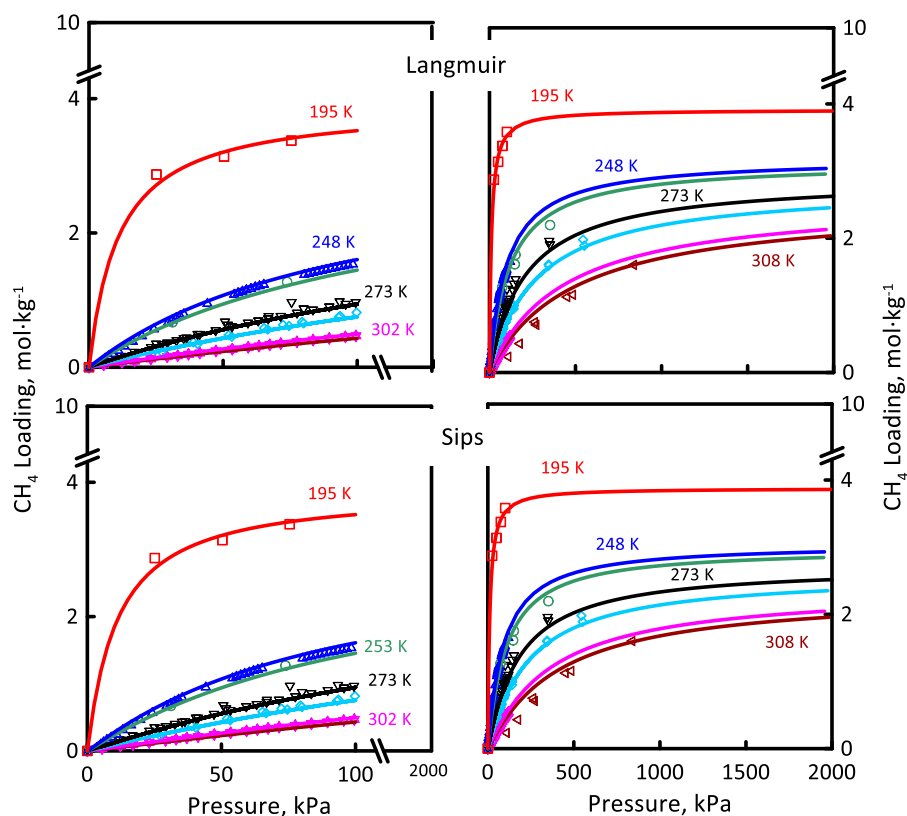


Figure 22. CH_4 adsorption isotherms at, (\square , red line) 195 K, (Δ , blue line) 248 K, (\circ , green line) 253 K, (∇ , black line) 273 K, (\diamond , sky blue line) 283 K, (\star , magenta line) 302 K, (\triangleleft , ruby red line) 308 K on 4A. Symbols: experimental values of [83-87]; solid lines: model results (non-linear regression of experimental data). Reprinted from *Microporous and Mesoporous Materials*, 249, P.F. Zito, A. Caravella, A. Brunetti, E. Drioli, G. Barbieri, Light gases saturation loading dependence on temperature in LTA 4A zeolite, 67-77. Copyright (2017) Elsevier.

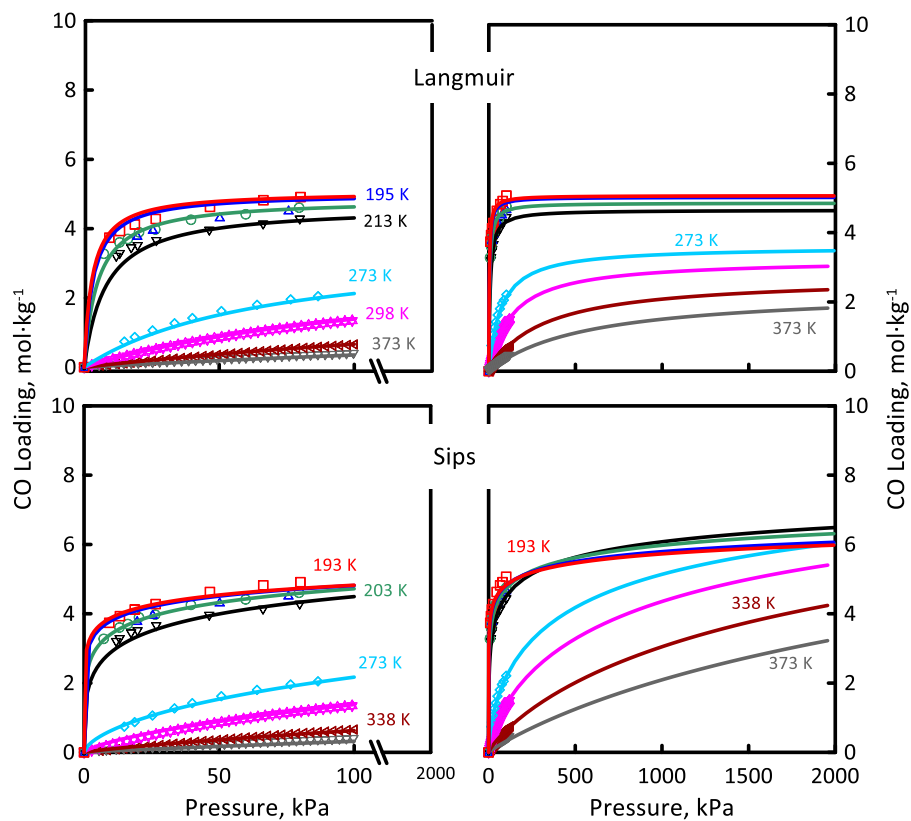


Figure 23. CO adsorption isotherms at, (\square , red line) 193 K, (Δ , blue line) 195 K, (\circ , green line) 203 K, (∇ , black line) 213 K, (\diamond , sky blue line) 273 K, (\star , magenta line) 298 K, (\triangleleft , ruby red line) 338 K, (\triangleright , grey line) 373 K on 4A. Symbols: experimental values of [30, 87, 89]; solid lines: model results (non-linear regression of experimental data). Reprinted from *Microporous and Mesoporous Materials*, 249, P.F. Zito, A. Caravella, A. Brunetti, E. Drioli, G. Barbieri, Light gases saturation loading dependence on temperature in LTA 4A zeolite, 67-77. Copyright (2017) Elsevier.

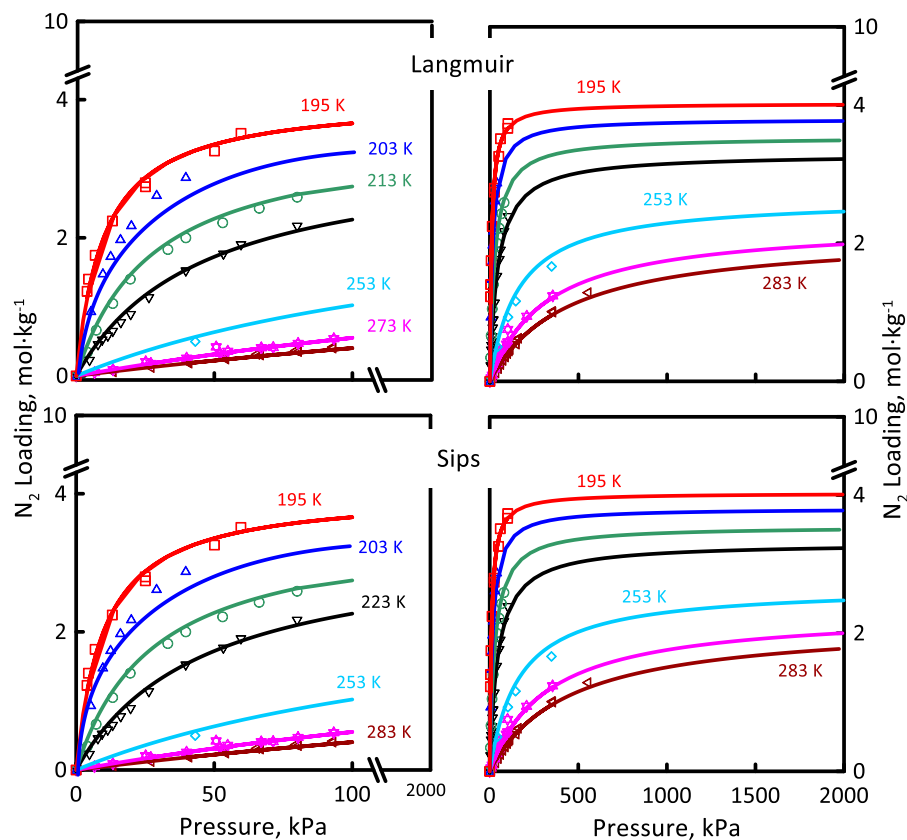


Figure 24. N_2 adsorption isotherms at, (\square , red line) 195 K, (Δ , blue line) 203 K, (\circ , green line) 213 K, (∇ , black line) 223 K, (\diamond , sky blue line) 253 K, (\ast , magenta line) 273 K, (\blacktriangleleft , ruby red line) 283 K on 4A. Symbols: experimental values of [84, 85, 87, 89]; solid lines: model results (non-linear regression of experimental data). Reprinted from *Microporous and Mesoporous Materials*, 249, P.F. Zito, A. Caravella, A. Brunetti, E. Drioli, G. Barbieri, Light gases saturation loading dependence on temperature in LTA 4A zeolite, 67-77. Copyright (2017) Elsevier.

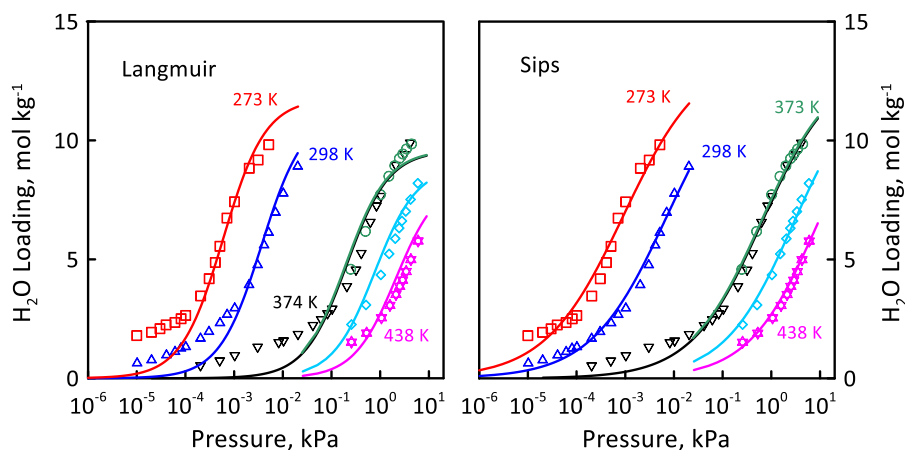


Figure 25. H₂O adsorption isotherms at, (□, red line) 273 K, (Δ, blue line) 298 K, (○, green line) 373 K, (∇, black line) 374 K, (◇, sky blue line) 408 K, (☆, magenta line) 438 K on 4A. Symbols: experimental values of [30, 92]; solid lines: model results (non-linear regression of experimental data). Right side of figure reprinted from Journal of Membrane Science, 574, P.F. Zito, A. Brunetti, A. Caravella, E. Drioli, G. Barbieri, Water vapor permeation and its influence on gases through a zeolite-4A membrane, 154-163. Copyright (2019) Elsevier.

Figure 26 shows the optimal values of the Langmuir model adsorption parameters for H₂, CH₄, CO₂, CO and N₂. It can be observed that the confidence intervals are quite narrow, stating that the calculated optimal values can be considered accurate. The agreement between model and experimental values is attested by the correlation coefficient R^2 . The highest values of R^2 are obtained for CH₄, CO and N₂, whereas the Langmuir model is found not to work very well for H₂ and CO₂, as mentioned above. The values of heat of adsorption confirm that CO₂ is the most strongly-adsorbing species followed by CH₄, N₂ and CO, which present a similar adsorption capacity. Differently, H₂ the weakly-adsorbed one, among those investigated. All species show a significant temperature dependence of saturation loading, as confirmed by the χ values significantly different from zero.

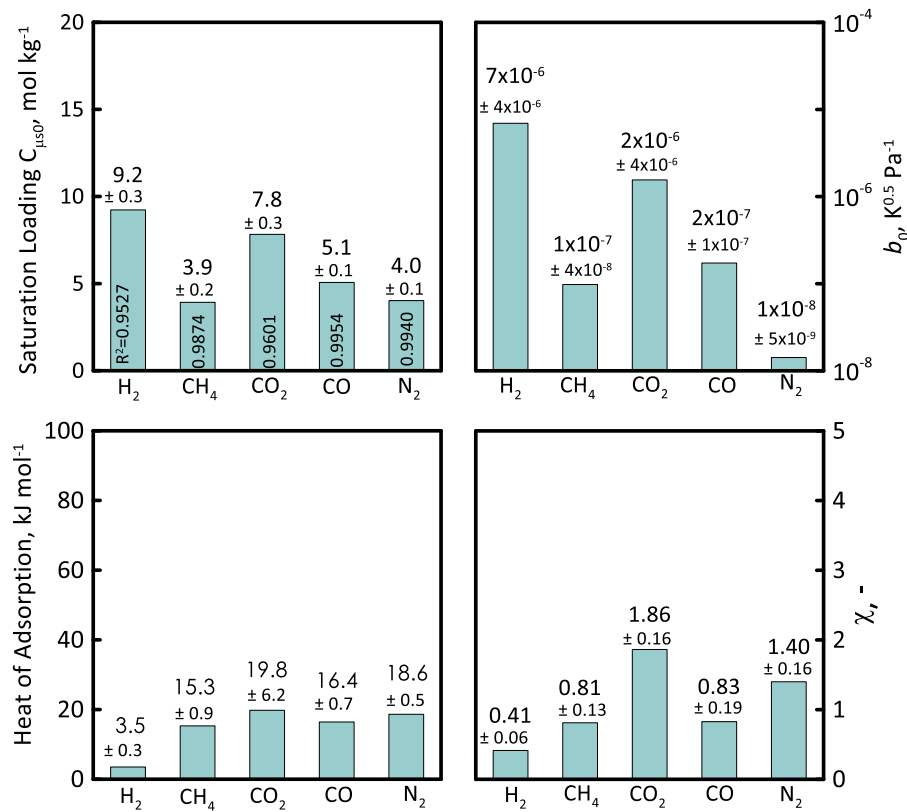


Figure 26. . Calculated optimal values of the Langmuir model parameters for the considered species on 4A. Saturation loading $C_{\mu s0}$, parameter b_0 , heat of adsorption, empirical parameter. Reprinted from Microporous and Mesoporous Materials, 249, P.F. Zito, A. Caravella, A. Brunetti, E. Drioli, G. Barbieri, Light gases saturation loading dependence on temperature in LTA 4A zeolite, 67-77. Copyright (2017) Elsevier.

Figure 27 shows the adsorption properties obtained with the Sips model. Also in this case, the confidence intervals are pretty narrow, this indicating a good accuracy of optimal values. Moreover, R^2 is close to the unity for all the species, including CO₂, H₂ and, thus, the Sips equation well describes the experimental adsorption isotherms. Sips model provides higher saturation loading than the Langmuir one for H₂, CO₂ and CO, whereas the same value is obtained for CH₄ and N₂. Heat of adsorption are quite similar, except for CO₂ and H₂, for which Sips values are much higher. The parameters n_0 and α give an indication of the deviation from the ideal behaviour represented by Langmuir model (i.e., $n_0=1$ and $\alpha=0$). It can be observed that CH₄ and N₂ present values of n_0 and α equal to 1 and 0 respectively, stating that Sips equation is reduced to the Langmuir one.

Furthermore, in case of CO, Sips model predicts a saturation loading that is temperature-independent, as attested by the χ value equal to zero. This is the reason why all the isotherms tend to the same value of loading at high pressure (Figure 23).

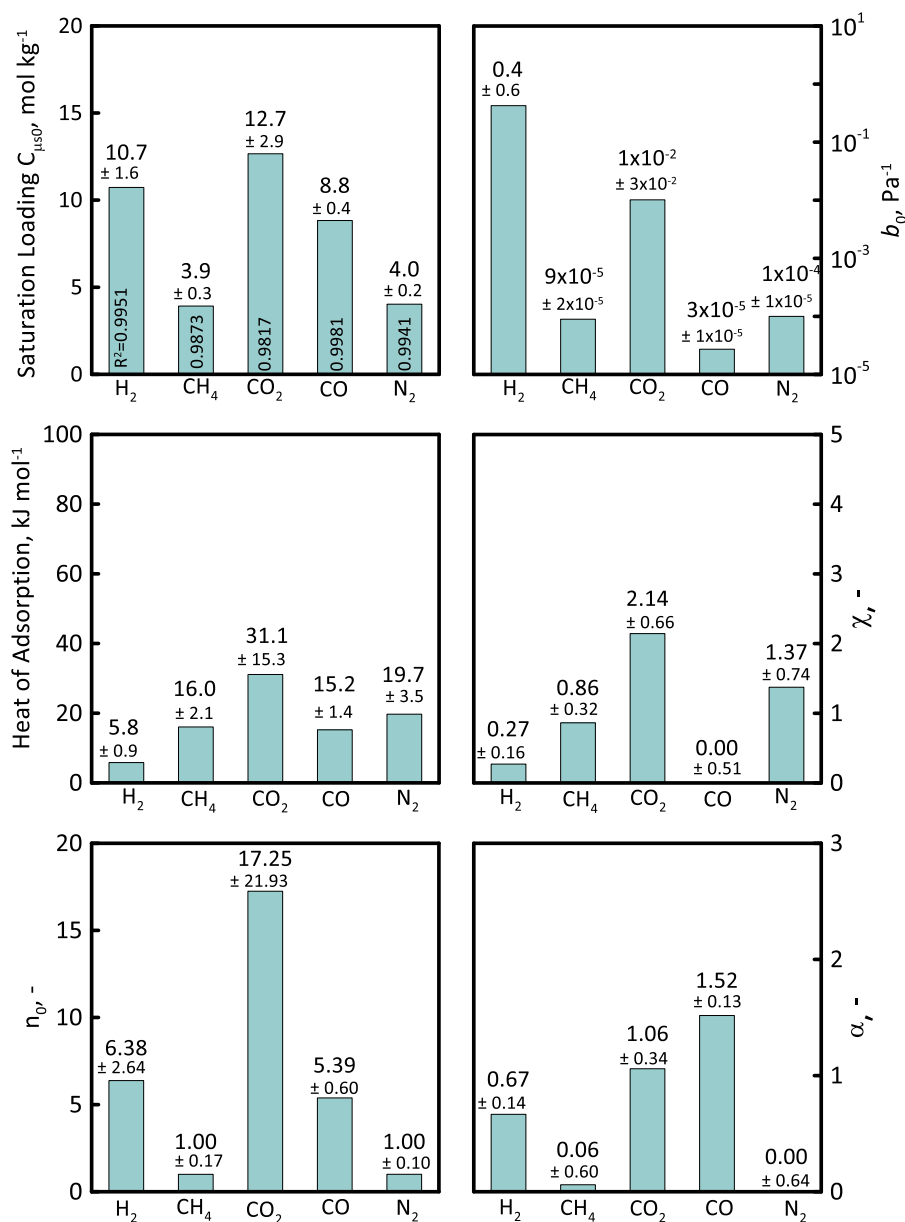


Figure 27. Calculated optimal values of the Sips model parameters for the considered species on 4A. Saturation loading $C_{\mu s0}$, Sips affinity constant at infinite temperature b , heat of adsorption, empirical parameter χ , empirical exponent n_0 , empirical parameter α . Reprinted from Microporous and Mesoporous Materials, 249, P.F. Zito, A. Caravella, A. Brunetti, E. Drioli, G. Barbieri, Light gases saturation loading dependence on temperature in LTA 4A zeolite, 67-77. Copyright (2017) Elsevier.

Water vapor parameters are discussed separately, since H₂O has quite different characteristics than the other investigated species. In fact, it is much more adsorbed than the other species and condenses at a much lower pressure. The Sips and Langmuir properties of water vapor (Table 6) confirm this behavior. In fact, heat of adsorption and saturation loading of H₂O (about 50 kJ mol⁻¹ the former, between 12 and 14 mol kg⁻¹ the latter) result much higher than those of CO₂, which is the most strongly adsorbed component.

Table 6. Sips and Langmuir adsorption parameters of H₂O in 4A zeolite. T₀=273 K.

<i>Parameter</i>	<i>Sips value</i>	<i>Confidence interval</i>	<i>Units</i>
C _{μs0}	13.7	± 1.4	mol·kg ⁻¹
χ	0.10	± 0.36	-
b ₀	1.08	± 0.50	Pa ⁻¹
Q _{Adsorption}	55.1	± 4.9	kJ·mol ⁻¹
n ₀	1.85	± 0.22	-
α	0.20	± 0.32	-
<i>Parameter</i>	<i>Langmuir value</i>	<i>Confidence interval</i>	<i>Units</i>
C _{μs0}	11.7	± 0.90	mol·kg ⁻¹
χ	0.55	± 0.19	-
b ₀	2 · 10 ⁻⁸	± 2 · 10 ⁻⁸	K ^{0.5} · Pa ⁻¹
Q _{Adsorption}	47.8	± 2.2	kJ·mol ⁻¹

3.2 Evaluation of diffusivity

The mass transport model requires the diffusivity of all the species for both surface and gas translation contributions. For this purpose, experimental single gas permeance values as a function of temperature are needed. However, the procedure used here for estimation of diffusivity depends on the species investigated. In case of strongly adsorbed species as CO₂, permeance values at a low temperature are used for the estimation of surface diffusion contribution, supposing the absence of gas translation. The knowledge of the experimental permeance and weight of surface diffusion at a fixed high temperature allow to obtain diffusivity by gas translation. In case of weakly adsorbed species such as H₂, the reverse procedure is applied. First, the high temperature permeance values are

used for the estimation of the gas translation diffusivity (no surface diffusion), then the low temperature ones for diffusivity related to surface diffusion.

In case of species presenting a moderate adsorption (e.g., CH₄), some hypotheses about the weight of the two mechanisms under certain temperature conditions are made and verified.

Below, the cases of DD3R, SAPO-34, NaY and 4A are presented.

3.2.1 DD3R membrane

The single gas permeance values of H₂, He, CO₂ and CO as a function of temperature measured by Kanezashi *et al.* [93] are considered for the estimation of the geometrical parameters of the specific DD3R membrane (DDR structure is shown in Figure 2) and the surface and gas translation contributions. The authors synthesized DDR membranes by secondary growth method on porous alumina disk, obtaining a zeolite layer of about 10 μm. This membrane has a good quality as reveals the very small permeance of SF₆ (kinetic diameter of 0.55 nm, DD3R pore size of about 0.4 nm), which is lower than 10⁻¹¹ mol m⁻² s⁻¹ Pa⁻¹ [93].

The ratio of nominal porosity over tortuosity (ε_0/τ_0) and activation energy for gas translation are evaluated using the experimental permeances of H₂ and He, which are weakly adsorbing components, at a high temperature. This is based on the assumption that, at a sufficiently high temperature, permeance is only attributed to gas translation diffusion. By collecting all the constant parameters in a factor β , permeance can be written as expressed by Eqs. 63-64:

$$Permeance_{GTD} = \frac{\varepsilon_0}{\tau_0} \frac{1}{RT\delta_{zeolite}} \frac{\lambda}{\zeta} \sqrt{\frac{8RT}{\pi MW}} e^{-\frac{E_{GT}}{RT}} = \beta \frac{\varepsilon_0}{\tau_0} e^{-\frac{E_{GT}}{RT}} \quad (63)$$

$$\beta = \frac{1}{RT\delta_{zeolite}} \frac{\lambda}{\zeta} \sqrt{\frac{8RT}{\pi MW}} \quad (64)$$

The activation energy for gas translation of helium is estimated from the experimental permeance obtained at 673 and 773 K (Eq. 65) by Kanezashi et al. [93] (points A and B of Figure 28):

$$E_{GT} = R \frac{\ln\left(\frac{\beta_{773}}{\beta_{673}}\right) - \ln\left(\frac{Permeance_{773}}{Permeance_{673}}\right)}{\left(\frac{1}{773} - \frac{1}{673}\right)} \quad (65)$$

Nominal tortuosity is evaluated by Eq. 66:

$$\frac{\varepsilon_0}{\tau_0} = \frac{Permeance}{\beta e^{-\frac{E_{GT}}{RT}}} \quad (66)$$

From Eq.58, it is obtained a $\varepsilon_0/\tau_0=0.036$, which corresponds to a $\tau_0=7.2$, considering a nominal porosity of 0.26, evaluated from the apparent density and the void volume [94]. This value of nominal tortuosity is in the reasonable range indicated in [95]. Surface diffusion parameters of He are assumed equal to those of H₂, since the Langmuir and Sips adsorption properties of He are not available. The validity of our assumptions is eventually verified by simulating the permeation through the zeolite in a wide temperature range from 273 to 773 K.

Activation energy of gas translation for diffusion H₂ and CO is evaluated by imposing the experimental available permeance at the highest temperature (773 K) only to gas translation diffusion (Eq. 63). Permeance attributed to surface diffusion (Eq. 67, in case of strong confinement scenario and Langmuir model) is evaluated in a different way for CO and H₂ with respect to CO₂. In the former case, parameters of both the species (i.e., D⁰_{SD} and E_{SD}) are then calculated from the two experimental permeances of Kanezashi *et al.* [93] at the lowest temperatures (298 and 373 K), by subtracting the gas translation contribution to the overall permeance. Regarding CO₂, only surface diffusion is supposed at 298 and 373 K. Thus, this contribution is subtracted to the global experimental permeance at the highest temperature to estimate the gas translation permeance and its activation energy E_{GT} .

$$\text{Permeance}_{SD} = \frac{\frac{\varepsilon \rho C_{\mu s} D_{SD}^0 e^{-\frac{E_{SD}}{RT}}}{\delta}}{(1+bP_{feed})+(1+bP_{permeate})} \quad (67)$$

The hypothesis to have only gas translation at 773 K is eventually verified simulating the permeation through the zeolite in the whole temperature range. Concerning H₂, this hypothesis results to be correct. Differently, surface diffusion of CO is still present at high temperatures; therefore, the estimated activation energy for gas translation diffusion is considered slightly higher. Table 7 reports all the estimated parameters, considering the strong confinement scenario for surface diffusion, i.e., diffusivity is a linear decreasing function of coverage. Since the diffusivity owed to surface diffusion is obtained from permeance values in single gas, it included the geometrical characteristics of the material, as porosity and tortuosity. Thus, it is expressed as an effective diffusivity, which is related to the surface diffusion one as follows (Eq. 68):

$$D_{SD,Effective}^0 = \frac{\varepsilon}{\tau} D_{SD}^0 \quad (68)$$

Hence, the gas translation and surface diffusion parameters are estimated from the values A and C-D of Figure 28. The others experimental values are used for model validation.

Table 7. Surface and gas translation diffusion parameters estimated for light gases in DD3R. Reprinted from Journal of Membrane Science, 564, P.F. Zito, A. Caravella, A. Brunetti, E. Drioli, G. Barbieri, Discrimination among gas translation, surface and Knudsen diffusion in permeation through zeolite membranes, 166-173, Copyright (2018), Elsevier.

Species	γ -	Gas Translation Diffusion		Surface Diffusion	
		$E_{GT}, J mol^{-1}$	$D_{SD, Effective}^0 m^2 s^{-1}$	$E_{SD}, J mol^{-1}$	
He	0.65	8233	-	-	
H ₂	0.73	9968	8.50E-9	4586	
CO ₂	0.83	16330	1.22E-9	6507	
CO	0.94	18900	2.94E-9	11989	

The model well describes the experimental behavior in the whole temperature range (Figure 28). It can be observed that H₂ permeation at 298 K takes place only by surface diffusion, which drastically tends to decrease with increasing temperature. On the other hand, gas translation becomes important with increasing temperature, being the only mechanism above 673 K. The intersection between the two contributions occurs at *ca.* 410 K, stating that gas translation becomes the dominant mechanism above this temperature. The estimated minimum is found at *ca.* 440 K. Permeation of He is similar to that of H₂. Only surface diffusion is present at 298 K, drastically decreasing with increasing temperature. Gas translation contribution of He is slightly greater than that of H₂, also owing to the smaller E_{GT} estimated for He (Table 7). Therefore, the intersection between surface and gas translation diffusion occurs at a lower temperature than in the H₂ case (i.e., at *ca.* 400 K). However, a minimum is estimated at *ca.* 450 K, since the gas translation contribution of He increases with increasing temperature less than that of H₂. The model predicts that CO₂ permeation is determined by surface diffusion up to a relatively high temperature. The line cross between the two contributions is observed at *ca.* 640 K and the minimum of permeance is found between the experimental values at 673 and 773 K (at *ca.* 690 K). In fact, a change in the temperature dependence of

permeance is clearly observed at high temperature. Specifically, the two experimental values at 673 and 773 K seem to be almost independent of temperature; this states a transition from surface to gas translation diffusion. On the contrary, Kanezashi *et al.* [93] considered CO₂ permeation owing only to surface diffusion, even at a high temperature. CO permeation at low temperatures occurs only by surface diffusion, whereas gas translation becomes significant above 450 K. The intersection between the two contributions is found at *ca.* 610 K. Differently from H₂ and CO₂, CO shows the minimum at a lower temperature (i.e., *ca.* 480 K) than that at the intersection between surface and gas translation diffusion, in the region where surface diffusion is the most important mechanism. This occurs since the reduction of CO surface diffusion permeance with increasing temperature is lower than that of the other species.

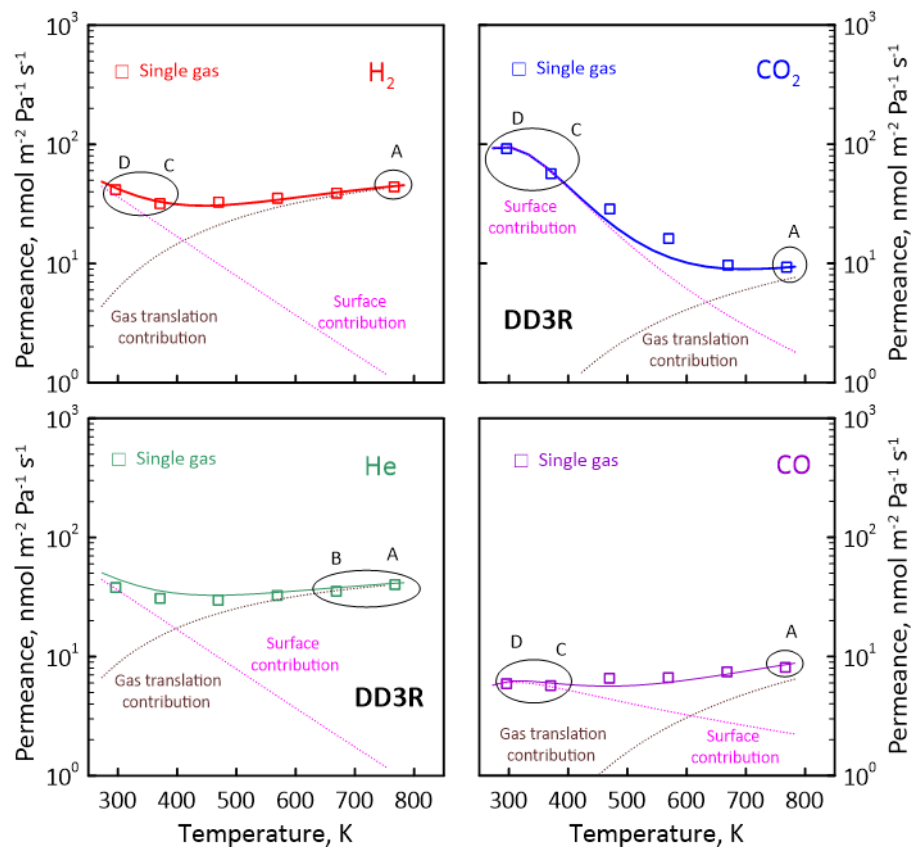


Figure 28. H₂, CO₂, CO and He permeance as a function of temperature through a DD3R membrane: experimental values (open symbols) of [93], overall permeance (solid lines), surface diffusion contribution (magenta dotted lines), gas translation diffusion contribution (brown dotted lines). Reprinted from Journal of Membrane Science, 564, P.F. Zito, A. Caravella, A. Brunetti, E. Drioli, G. Barbieri, Discrimination among gas translation, surface and Knudsen diffusion in permeation through zeolite membranes, 166-173, Copyright (2018), Elsevier.

3.2.2 SAPO-34 membrane

Surface and gas translation diffusion parameters (Table 8) are estimated from the experimental measurements of Li *et al.* [42], who provide the single gas permeance of CO₂, CH₄, N₂ and H₂ as a function of temperature. The authors prepared SAPO-34 membranes by in situ crystallization onto α -Al₂O₃ and stainless steel tubular supports [42]. The membrane considered in this work is the sample M1, having an area of about 5.1 cm². The good quality of this membrane is confirmed by the permeance of n-C₄H₁₀ (kinetic diameter of 0.43 nm, SAPO-34 pore size of about 0.38 nm), which is below the detection limit (9.6 x 10⁻¹¹ mol m⁻² s⁻¹ Pa⁻¹) [42]. For this membrane, it is estimated a zeolite layer of about 19 μ m, based on the thickness of membrane M2 (i.e., 25 μ m) and the permeance of both M1 and M2. In particular, thickness is estimated considering the same CO₂ permeability of both membranes (Eq. 69):

$$Permeance_{M1} \delta_{M1} = Permeance_{M2} \delta_{M2} \Rightarrow \delta_{M1} = \frac{\delta_{M2} Permeance_{M2}}{Permeance_{M1}} \quad (69)$$

The values of H₂ permeance at highest temperatures (i.e., 150 and 200°C of Figure 29) are here used for the estimation of nominal tortuosity and activation energy for gas translation diffusion, supposing that the weight of H₂ surface and gas translation diffusion in SAPO-34 are similar to those obtained in DD3R (see section 3.2.1), since H₂ is weakly adsorbed even at lower temperatures. In fact, a comparison between the saturation loadings as a function of temperature confirm the similar behaviour of the two zeolites. Moreover, also the two values of H₂ heats of adsorption in SAPO-34 and DD3R are similar (i.e., 4.2 and 3.2 kJ mol⁻¹, respectively). Once calculated τ_0 and E_{GT} , the surface diffusion parameters are estimated from the experimental permeances at the lowest temperatures. Concerning CO₂, it is reasonable to consider only the presence of surface diffusion at 24 and 100°C, since CO₂ is the most strongly adsorbing species. The value of E_{GT} is then calculated using the experimental permeance at 200°C, by subtracting the estimated surface diffusion permeance to the experimental one and attributing the resulting value to gas translation diffusion. The CH₄ is located in between CO₂ and H₂: it

is adsorbed more than H₂ and less than CO₂. The weight of gas translation diffusion on H₂ and CO₂ overall permeance is 90 and 30% at 200°C, respectively. Therefore, it is supposed a weight of 60% for CH₄ translation contribution on the overall permeance at 200°C. The experimental decreasing trend of N₂ permeance suggests the presence of only surface diffusion especially at a low temperature.

It is obtained a $\tau_0=2.64$, considering a nominal porosity of 0.236. This nominal porosity is estimated from the solid density (i.e., 1340 kg m⁻³ [79]) and the micropore volume of the zeolite (i.e., 0.23 [42]). A diffusional length and a coordination number of 1 nm and 5 are considered, as reported by Krishna and van Baten for materials belonging to CHA-type [96].

Table 8. Surface and gas translation diffusion parameters of H₂, CH₄, CO₂ and N₂. Reprinted from Journal of Membrane Science, 595, P.F. Zito, A. Brunetti, A. Caravella, E. Drioli, G. Barbieri. Mutual influence in permeation of CO₂-containing mixtures through a SAPO-34 membrane, 117534, Copyright (2020), Elsevier.

<i>Species</i>	<i>Gas Translation Diffusion</i>	<i>Surface Diffusion</i>	
	$E_{GT}, J mol^{-1}$	$D_{SD, Effective}^0 m^2 s^{-1}$	$E_{SD}, J mol^{-1}$
H ₂	10981	2.32E-8	7197
N ₂	30030	2.83E-9	6875
CO ₂	20432	2.89E-9	7818
CH ₄	15800	2.74E-10	6459

Permeance of CO₂, CH₄, N₂ and H₂ as a function of temperature in terms of surface and gas translation contribution is, therefore, showed (Figure 29) to appreciate the weight of each transport mechanism to the overall permeation. The CO₂ permeation takes place only with surface diffusion in the whole temperature range considered. In fact, the intersection between surface and gas translation diffusion occurs at temperatures higher than 530°C without the presence of a minimum. Permeation of CH₄ takes place only with surface diffusion at a low temperature, whereas the intersection occurs at about 140°C.

Li *et al.* [42] found an experimental minimum at 100°C, which agrees with this simulated one, confirming the validity of the hypothesis to have 60% of gas translation diffusion at 200°C. Nitrogen follows only surface diffusion in the temperature range investigated. Specifically, permeance decreases with increasing temperature since the reduction of adsorption prevails on the increment of diffusivity. However, the presence of a minimum at about 300°C is predicted, even though gas translation diffusion is still quite lower than surface diffusion. This minimum is owed to the slight temperature dependence of surface diffusion paired to the high increment of gas translation diffusion with increasing temperature.

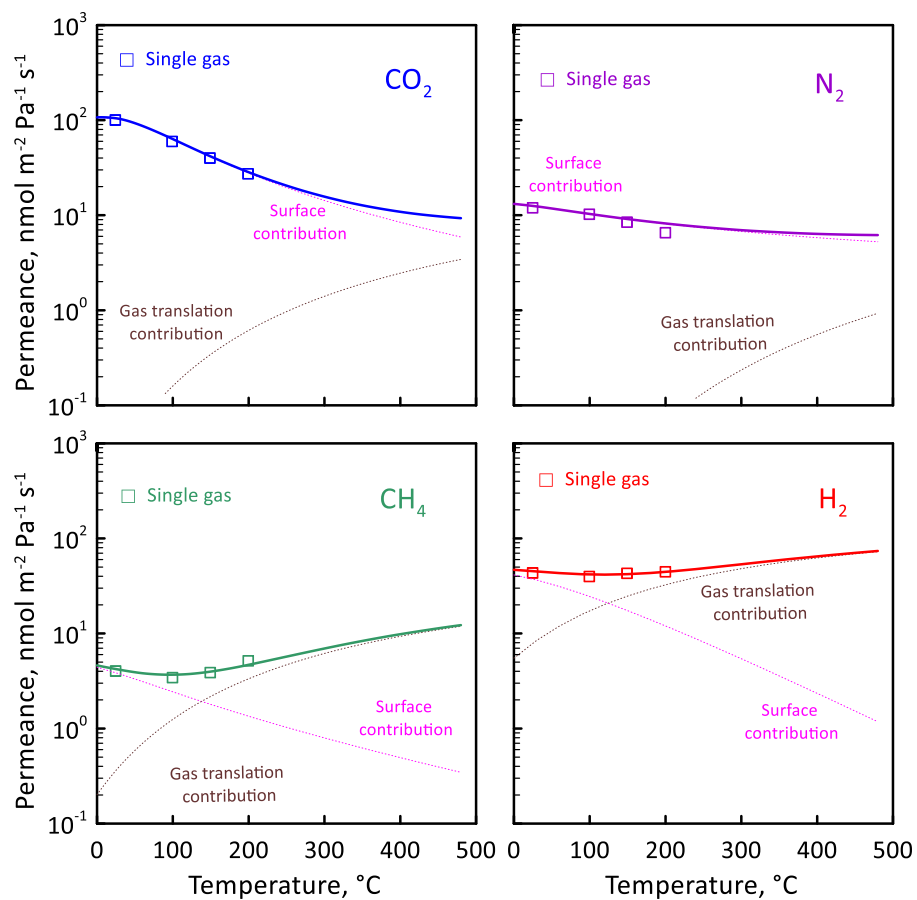


Figure 29. CO₂, CH₄, N₂ and H₂ permeance as a function of temperature through a SAPO-34 membrane: experimental values (open symbol) of [42], surface diffusion contribution (magenta dotted lines), gas translation diffusion contribution (brown dotted lines) and overall permeance (solid lines). Reprinted from Journal of Membrane Science, 595, P.F. Zito, A. Brunetti, A. Caravella, E. Drioli, G. Barbieri. Mutual influence in permeation of CO₂-containing mixtures through a SAPO-34 membrane, 117534, Copyright (2020), Elsevier.

3.2.3 4A membrane

As in the previous sections, the contributions to mass transport of H₂O, CO, CH₄ and H₂ in 4A membrane are evaluated using experimental single gas permeance values as a function of temperature taken from the literature [30]. In particular, Zhu *et al.* [30] synthesized a high quality zeolite 4A on a supporting disk consisting of TRUMEM™ TiO₂-coated stainless steel porous support with a diameter of 2.5 cm. Membrane layer had cubic crystals with a thickness of about 3.5 μm.

Surface diffusion parameters of H₂O, CO, CH₄ are here estimated from the experimental values at the lowest temperatures, supposing the absence of gas translation diffusion. Then, activation energy of gas translation is evaluated in the same way as for the other zeolites. Differently, it is not possible to preliminary assume only surface diffusion for H₂; thus, the evaluation of gas translation activation energy as first step is more appropriate. Nevertheless, experimental data at a sufficiently high temperature are not present to allow only the presence of gas translation diffusion to be supposed. A possible way to get a reasonable first estimation of E_{GT} is based on the approach of Xiao and Wei [59]. The authors showed that the activation energy for gas translation diffusion on ZSM-5 is a function of the ratio of pore size over kinetic diameter. The H₂ value of activation energy are 5275, 9968 and 10981 J mol⁻¹ for NaY, DD3R and SAPO-34, respectively [60, 69]. Thus, the E_{GT} of 4A is extrapolated, by plotting the activation energy values as a function of the ratios of pore size over kinetic diameter, which are 0.39, 0.72 and 0.76 for NaY, DD3R and SAPO-34, respectively (Table 9). A value of 9745 J mol⁻¹ is obtained for 4A (pore size over kinetic diameter of *ca.* 0.70).

Table 9. Activation energy for gas translation diffusion of NaY, DD3R and SAPO-34

<i>Zeolite</i>	$\frac{d_k}{d_{pore}}, -$	$E_{GT}, J mol^{-1}$
NaY	0.39	5275
4A	0.70	-
DD3R	0.72	9968
SAPO-34	0.76	10981

A Nominal tortuosity of 5 is considered for zeolite 4A [97], whereas nominal porosity is estimated to be 0.358, using the zeolite density (1990 kg m^{-3} [98]) and micropore volume ($0.28 \text{ cm}^3 \text{ g}^{-1}$ [99]). The diffusional length and coordination number of 4A are considered similar to those of 5A, which are 1.2 nm and 6, respectively [59]. The value of 9745 J mol^{-1} represents a first indication of the activation energy for gas translation diffusion. As it will be shown in chapter 4, a higher value 13000 J mol^{-1} allows a well reproduction of the experimental trend in mixture. Table 10 summarizes the mass transport parameters estimated in single gas and used for simulations in mixture.

Table 10. Surface and gas translation diffusion parameters estimated for H₂O, H₂, CO and CH₄ in 4A. Reprinted from Journal of Membrane Science, 574, P.F. Zito, A. Brunetti, A. Caravella, E. Drioli, G. Barbieri, Water vapor permeation and its influence on gases through a zeolite-4A membrane, 154-163, Copyright (2019), Elsevier.

<i>Species</i>	<i>Gas Translation Diffusion</i>		<i>Surface Diffusion</i>	
	$E_{GT}, J mol^{-1}$	$D_{SD, Effective}^0 m^2 s^{-1}$	$E_{SD}, J mol^{-1}$	
H ₂ O	3720	8.65E-12	7441	
H ₂	13000	1.81E-6	18494	
CO	8000	22.88E-6	35490	
CH ₄	13500	0.102E-6	19811	

Figure 30 shows both the overall permeance and the surface and gas translation contributions of H₂O, CO, CH₄ and H₂ as a function of temperature between 273 and 700 K. A surface diffusion much higher than gas translation is predicted for all the species.

A maximum in H₂O permeance can be observed at about 363 K owing to the opposite effects of increment of diffusivity and reduction of coverage. Above this temperature, the overall permeance decreases since the reduction of water coverage prevails on the increment of diffusivity. Thus, surface diffusion contribution decreases with temperature, whereas the gas translation one increases, this provoking an intersection between the two mechanisms at about 550 K.

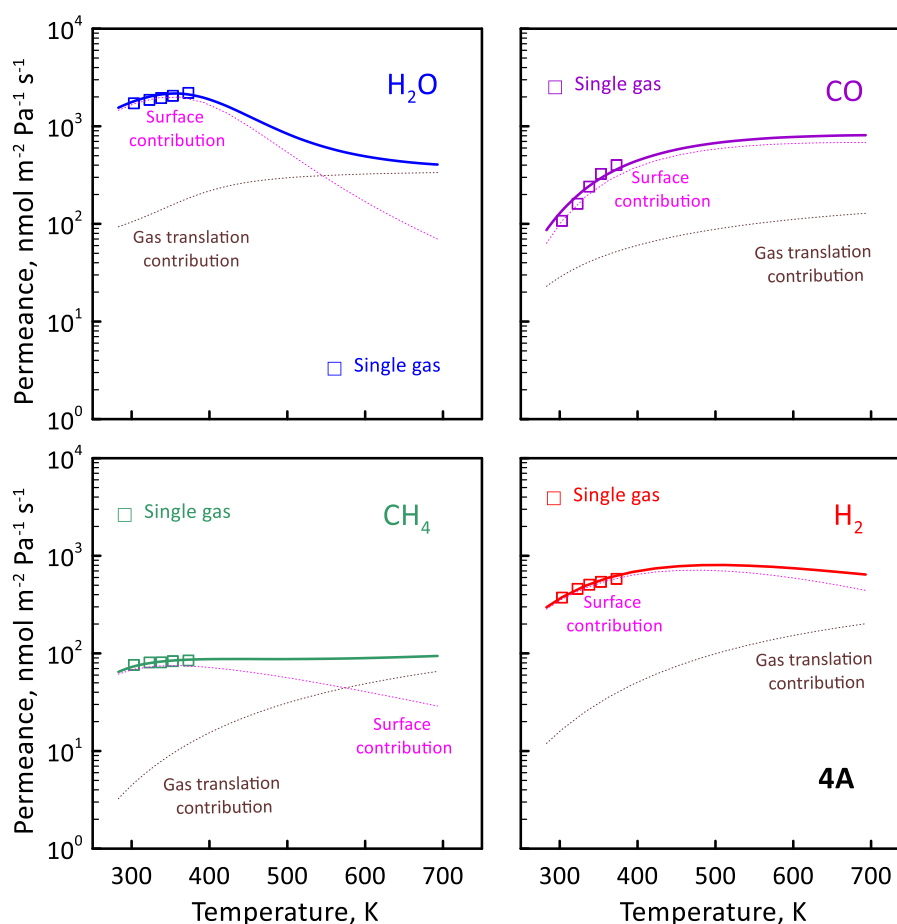


Figure 30. Permeance of H₂O, CH₄, CO and H₂ as a function of temperature through a 4A membrane: experimental values of [30] (open symbol) and (solid lines) calculated values of the overall permeance, surface diffusion contribution (magenta dotted lines) and gas translation diffusion contribution (brown dotted lines). Reprinted from Journal of Membrane Science, 574, P.F. Zito, A. Brunetti, A. Caravella, E. Drioli, G. Barbieri, Water vapor permeation and its influence on gases through a zeolite-4A membrane, 154-163, Copyright (2019), Elsevier.

Differently, CO shows an increasing permeance with temperature in the whole temperature range investigated. This trend occurs because surface diffusion increases in the whole temperature range without achieving any maximum. This phenomenon can be explained considering that CO saturation loading is found to be temperature-independent, since the empirical parameter χ estimated with the Sips' law is zero. Thus, reduction of coverage with temperature never becomes more important than increment of diffusivity. In addition, gas translation diffusion never exceeds surface diffusion of CO, remaining significantly lower in the whole temperature range investigated. Permeation of CH₄

increases at a low temperature, whereas it remains almost constant above 400 K, since the reduction of surface diffusion is balanced by the increment of gas translation contribution. Surface diffusion prevails on gas translation also in H₂ permeation up to 700 K. In fact, H₂ diffuses very fast owing to the smaller kinetic diameter compared to the other species. The high diffusivity is able to compensate the low coverage. Moreover, the coverage estimated by the Sips law's shows a slight decrease with increasing temperature, whereas diffusivity continuously increases. Differently, the relatively high activation energy for gas translation diffusion (13000 J mol⁻¹) is responsible of the small gas translation contribution. The simulated permeance of all the species (H₂O, CO, CH₄ and H₂) well agrees with the experimental values and trends measured by Zhu *et al.* [30].

3.2.4 NaY membrane

The presented model is also used for describing H₂ permeation through a NaY membrane (FAU structure as shown in Figure 3) experimentally measured by Hasegawa *et al.* [49], who prepared the zeolite layer on the inner surface of α -Al₂O₃ support tube having a length of 200 mm, internal and external diameters of 1.7 and 2.1 mm and a void fraction of 0.39. The authors measured very small permeances of n-C₄H₁₀ and i-C₄H₁₀, (kinetic diameter of 0.43 and 0.50 nm respectively, NaY pore size of 0.74 nm), which are 0.5 - 0.7 x 10⁻⁷ mol m⁻² s⁻¹ Pa⁻¹, suggesting the absence of serious defects inside the membrane.

The experimental permeation was previously modelled using the competition between surface and Knudsen diffusion [50] presenting some discrepancies at a low temperature. Activation energy for H₂ gas translation diffusion and the ratio of nominal porosity over nominal tortuosity ε_0/τ_0 are here estimated from the experimental values of permeance at 623 and 673 K (see, points A and B of Figure 31). Specifically, the surface diffusion contribution estimated in the work of Caravella *et al.* [50] is here used as first attempt and subtracted from the overall permeance at these two temperatures, allowing the estimation of permeance attributed to gas translation diffusion. Thus, Eqs. 65-66 are used for the estimation of the gas translation activation energy and the ratio ε_0/τ_0 . The new surface diffusion parameters are then calculated using the experimental permeances of Hasegawa

et al. [49] at the lowest temperatures (i.e., 308 and 338 K). A τ_0 of 1.5 is calculated fixing $\varepsilon_0=0.161$.

Table 11 reports the estimated parameters for H₂ compared to those obtained from the literature [50]. In particular, E_{GT} is different from zero, stating that gas translation diffusion is present for H₂. As a result, the weight of surface and gaseous diffusion to permeation is here modified and the surface diffusion parameters result different from those evaluated in the previous paper [50]. *Vice versa*, permeation of other components, such as CO₂ and N₂, neither exhibit the presence of a minimum nor any change in the experimental permeance slope at a high temperature [49]. Therefore, the activation energy for gas translation diffusion (E_{GT}) can be considered to be zero for these two species (i.e., Knudsen diffusion).

Table 11. Surface and gas translation diffusion parameters estimated for H₂ in NaY. Reprinted from Journal of Membrane Science, 564, P. F. Zito, A. Caravella, A. Brunetti, E. Drioli, G. Barbieri, Discrimination among gas translation, surface and Knudsen diffusion in permeation through zeolite membranes, 166-173, Copyright (2018) Elsevier.

Species	Gas Translation Diffusion		Surface Diffusion		Reference
	$E_{GT}, J mol^{-1}$	$D_{SD, Effective}^0 m^2 s^{-1}$	$E_{SD}, J mol^{-1}$		
H ₂	5275	1.39E-6	15708		This work
	-	2.40E-6	20636		[50]

Figure 31 shows the surface, gas translation and overall permeance H₂ as a function of temperature. The competition between surface and gas translation diffusion (red solid line) describes the experimental behavior of H₂ much better than the previous model, which took into account surface and Knudsen diffusion (black solid line). In fact, the present model is able to predict the H₂ increasing trend at low temperatures owing to surface diffusion. Specifically, the presence of gas translation instead of Knudsen increases the surface diffusion influence on the overall permeance at a low temperature with respect to that predicted by Caravella *et al.* [50]. Therefore, the maximum of permeance is found at *ca.* 450 K, whereas gas translation becomes more significant than

surface diffusion above 520 K. The presence of a minimum is not observed in the temperature range investigated. Nevertheless, permeance reduction is very small above 750 K, this indicating that H₂ is approaching to a minimum. The previous model [50] does not exhibit any maximum for H₂. In fact, H₂ permeance decreases in the whole temperature range considered, since Knudsen diffusion is the dominant mechanism even at low temperatures. That result caused a discrepancy of about 30% with the experimental values at a low temperature, whereas the present model correctly reproduces the behavior in such a low temperature range.

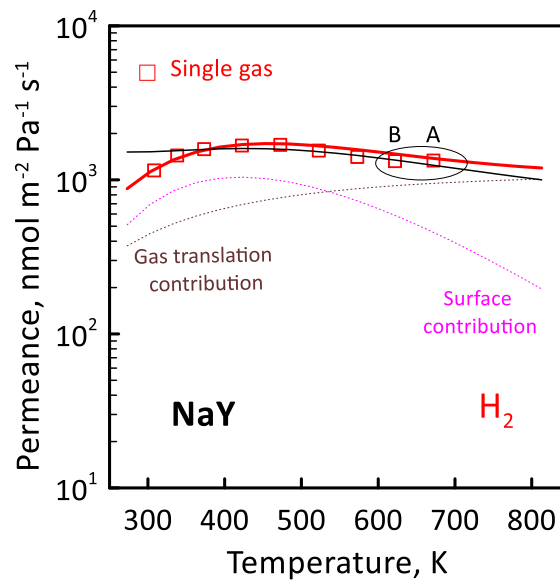


Figure 31. Single-gas permeance of H₂ as function of temperature through a NaY membrane: experimental data of [49] (symbols), overall permeance considering surface and gas translation diffusion (red solid lines), surface diffusion contribution (magenta dotted lines), gas translation contribution (brown dotted lines), H₂ overall permeances of [50] (black thin line). Reprinted from Journal of Membrane Science, 564, P.F. Zito, A. Caravella, A. Brunetti, E. Drioli, G. Barbieri, Discrimination among gas translation, surface and Knudsen diffusion in permeation through zeolite membranes, 166-173, Copyright (2018), Elsevier.

A further proof of the goodness of this model is given by comparing the estimated CO₂/H₂ selectivity value (i.e., the CO₂/H₂ permeance ratio in the mixture) to the experimental value of Kusakabe *et al.* [39], who measured a CO₂/H₂ selectivity of 27.8 at 308 K feeding an equimolar CO₂:H₂ mixture. The same value of 28 is here evaluated at 303 K, considering the competition between surface and gas translation diffusion. Differently, a lower selectivity of about 20 is obtained using the previous model, which considers Knudsen instead of gas translation. Therefore, the presence of gas translation well describes the CO₂:H₂ mixture permeation, much better than Knudsen diffusion.

In the next Chapter, surface and gas translation diffusion are used for the prediction of multicomponent permeation through SAPO-34, DD3R and 4A membranes.

4. Permeation of gas mixtures through zeolite membranes

In this chapter, the multicomponent gas permeation through the zeolite membranes presented in chapter 3 is investigated by a modelling analysis. The main results are presented in terms of permeance (Eq. 70) and selectivity (Eq. 71) of several gas mixtures changing temperature, pressure and feed composition.

$$Permeance_i = \frac{N_i}{\Delta P_i} \quad (70)$$

$$Selectivity_{i,j} = \frac{Permeance_i}{Permeance_j} \quad (71)$$

Dry and wet mixtures are analyzed, focusing on the mutual interaction among the permeating species. A particular attention is given to the hindering effect of the strongly adsorbed species on the permeation of the weakly adsorbed ones. Specifically, when molecules like CO₂ or H₂O are adsorbed into the zeolite surface, they represent a physical obstacle to both the adsorption and the “free” permeation of the remaining components, as H₂, CH₄, CO and N₂. For these species, a significant surface diffusion reduction is observed in mixture, since the adsorption sites are not accessible anymore. Differently, gas translation contribution results hindered only at a low temperature, consequently to a variation of the effective porosity and tortuosity in presence of adsorption. However, also the weakly adsorbed species like H₂ can have an important impact on the mixture

permeation. In fact, it is found and discussed that they provide a “promoting effect” on CO₂ with respect to the diffusion in single gas condition. Unexpectedly, CO₂ permeation in mixture results favoured in presence of fast components.

The hindering and, in some cases, the promoting effects imply good membrane performance in mixture. In fact, selectivity results much higher than the single gas one, making zeolite membranes good candidate for gas separation.

The single gas adsorption and diffusion properties previously evaluated in Chapter 3 are here used for prediction of multicomponent permeation

The results of this section are based on two published paper in international journals [69, 70].

4.1 Dry mixtures: the effect of CO₂

4.1.1 SAPO-34 membrane

The adsorption and diffusion properties estimated in single gas condition (Chapter 3) allow the prediction of multicomponent permeation through the M1 membrane synthesized by Li *et al.* [42], for which the characteristics are described in section 3.2.2. However, model needs a preliminary validation in mixture condition. For this purpose, the experimental measurements concerning an equimolar CO₂:CH₄ mixture as a function of temperature and feed pressure [42] are used (Figure 32). CO₂ permeance (blue solid line) shows the same decreasing trend with increasing temperature as in single gas condition (blue dotted line) since the reduction of coverage prevails on the increment of diffusivity. Moreover, carbon dioxide is not affected by the presence of methane, maintaining the same values of permeance than in single gas, with a slight increment at the lowest temperature (i.e., 25°C). Differently, CH₄ is hindered by the adsorbed CO₂ at a low temperature, presenting a significant drop in permeance (green solid line) with respect to that in single gas (green dotted line). This drop is attributed to the carbon dioxide adsorbed phase that does not allow methane adsorption. In fact, CH₄ coverage in mixture (Eq. 72) is expressed by the Langmuir law (Eq.7):

$$\theta_{CH_4} = \frac{(b_{CH_4} P_{CH_4})}{1 + (b_{CH_4} P_{CH_4}) + (b_{CO_2} P_{CO_2})} \quad (72)$$

Being the affinity constant of CO₂ ($b_{CO_2} = 8.2 \cdot 10^{-6} \text{ Pa}^{-1}$ at 25°C) higher than that of CH₄ ($b_{CH_4} = 2.1 \cdot 10^{-6} \text{ Pa}^{-1}$), methane coverage results much lower in mixture ($\theta_{CH_4} = 0.11$ in equimolar mixture with CO₂) than in single gas ($\theta_{CH_4} = 0.32$ as single gas at 222 kPa of feed pressure). Thus, its surface diffusion contribution is lower. Moreover, the presence of adsorbed CO₂ provokes an increase in the effective tortuosity and a reduction in the effective porosity during methane permeation (Eqs. 52-58 in Chapter 2). Thus, CH₄ gas translation contribution is reduced in mixture too.

Concerning the molar fluxes as a function of driving force (right side of Figure 32), an almost linear increment occurs especially at a low partial pressure difference, stating that the saturation condition of adsorption sites and the pore clogging are not achieved. In addition, CH₄ permeance results constant with driving force at about $3 \text{ nmol m}^{-2} \text{ s}^{-1} \text{ Pa}^{-1}$, the flux (Eq. 73) being almost linear with pressure difference in the whole ΔP_i considered. Differently, two different regions can be distinguished in case of CO₂: the low-pressure region (up to 100 kPa of driving force) where its permeance assumes the value of about $10 \text{ nmol m}^{-2} \text{ s}^{-1} \text{ Pa}^{-1}$; the high pressure one ($> 100 \text{ kPa}$) in which a lower slope for the line of flux versus ΔP_i is observed, being $8 \text{ nmol m}^{-2} \text{ s}^{-1} \text{ Pa}^{-1}$. This states CO₂ permeance is disadvantaged by the high pressure.

$$N_i = \text{Permeance}_i \Delta P_i \quad (73)$$

Both binary permeances and fluxes of CO₂ and CH₄ as functions of temperature and driving force (solid lines of Figure 29) are in a good agreement with the experimental values of Li *et al.* [42] (full symbols). Therefore, the model works very well in a wide range of feed pressure (100 - 600 kPa) and temperature (0 – 150°C).

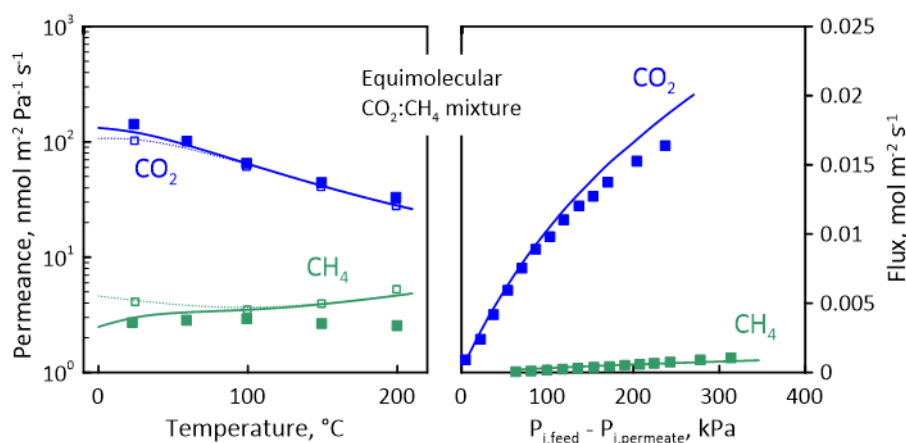


Figure 32. Permeance of CO₂ and CH₄ as a function of temperature through a SAPO-34 membrane (left side): experimental values of [42] in single gas (open symbols) and mixture (full symbol), estimated overall permeance in single gas (dotted lines) and mixture (solid lines). Flux of CO₂ and CH₄ as a function of feed pressure in binary mixture (right side): experimental values of [41] (full symbol), estimated fluxes in mixture (solid lines). Reprinted from Journal of Membrane Science, 595, P.F. Zito, A. Brunetti, A. Caravella, E. Drioli, G. Barbieri. Mutual influence in permeation of CO₂-containing mixtures through a SAPO-34 membrane, 117534, Copyright (2020), Elsevier.

In terms of mass transport mechanisms (Figure 33), surface diffusion gives the main contribution to CH₄ permeation in mixture, even if it is reduced by the presence of adsorbed CO₂. The intersection between the two surface and gas translation diffusion of methane occurs at about 150°C, close to the minimum observed in single gas. Differently from methane, CO₂ permeates only by surface diffusion in the whole temperature range investigated as a consequence of its strong adsorption on SAPO-34.

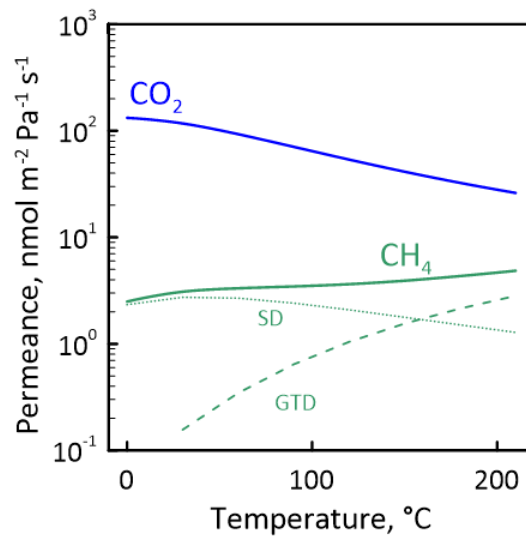


Figure 33. CO₂ and CH₄ permeance contributions in binary mixture as a function of temperature: overall permeance (solid lines), CO₂ surface diffusion (blue dotted lines), CH₄ surface diffusion (green dotted lines), CH₄ gas translation diffusion (green dashed lines).

The effect of temperature on the permeation of each species is investigated considering three equimolar mixtures containing CO₂ with H₂, N₂ and CH₄ (Figure 34). For a fixed temperature and total feed pressure, CO₂ permeance is favored by the presence of another species with respect to the single gas condition, since the reduction of driving force prevails on that of its permeating flux. In particular, the highest permeance is estimated in presence of H₂, followed by N₂ and CH₄, probably because H₂ is the weakest adsorbing species among those investigated and, thus, does not compete with CO₂ in adsorption. This causes a larger CO₂ flux when mixed with H₂ (or a lower reduction with respect to the single gas condition), resulting in a higher permeance. Unlike CO₂, the other species present a lower permeance in mixture compared to the single gas condition especially at a low temperature, where the CO₂ adsorption is higher. Hydrogen is the most negatively affected by the presence of carbon dioxide, presenting the strong deviation from the single gas behaviour. However, permeance of all the species increases with increasing temperature since the CO₂ hindering effect is lower.

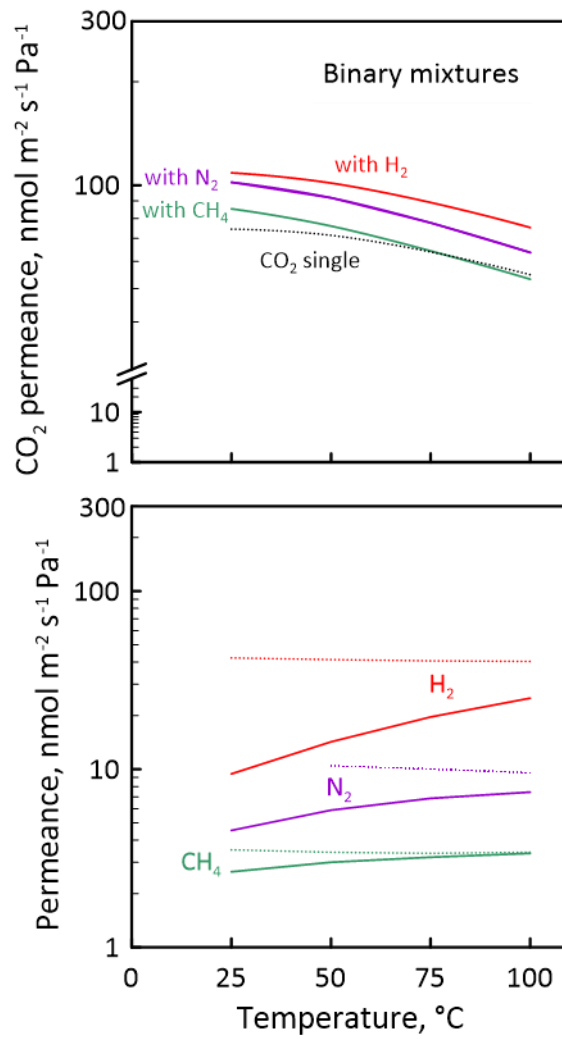


Figure 34. CO₂, H₂ and N₂ permeance as a function of temperature for equimolar CO₂:H₂, CO₂:N₂ and CO₂:CH₄ mixtures (solid lines) and single gases (dotted lines) at a feed pressure of 500 kPa. Permeate pressure = 101 kPa. Reprinted from Journal of Membrane Science, 595, P.F. Zito, A. Brunetti, A. Caravella, E. Drioli, G. Barbieri. Mutual influence in permeation of CO₂-containing mixtures through a SAPO-34 membrane, 117534, Copyright (2020), Elsevier.

In terms of separation performance, all the CO₂-containing mixtures present a selectivity (Eq. 74) much higher than the single gas one at the low temperatures (Figure 35).

$$Selectivity = \frac{Permeance_{CO_2}}{Permeance_{CH_4, N_2, H_2}} \quad (74)$$

Specifically, values of 32, 22 and 12 are estimated for CO₂/CH₄, CO₂/N₂ and CO₂/H₂ respectively at 25°C. The increment of temperature strongly reduces the selectivity values, which tend to the single gas ones. Selectivity of all the three mixtures are much higher than the Knudsen values, which are lower than 1 (i.e., 0.21, 0.80 and 0.60 for CO₂/H₂, CO₂/N₂ and CO₂/CH₄). This occurs for two different reasons: the presence of an adsorbed phase (i.e., surface diffusion mechanism) and a pore size that approaches the dimension of the species causing a non-null activation energy for gas translation diffusion.

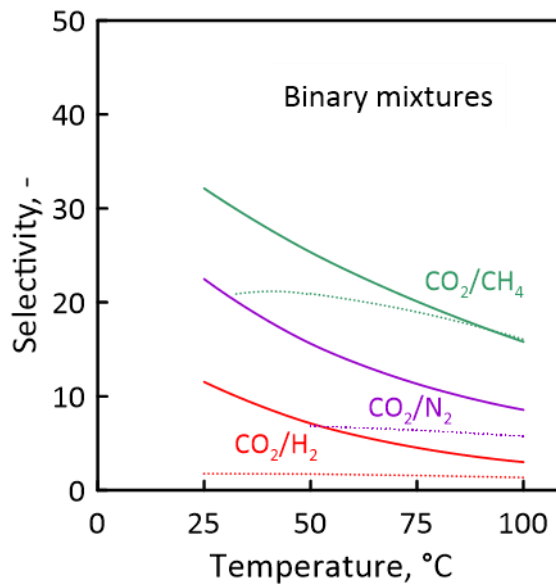


Figure 35. CO₂/H₂, CO₂/N₂ and CO₂/CH₄ selectivity values as functions of temperature for binary mixtures at a feed pressure of 500 kPa. Permeate pressure of 101 kPa. Single gas selectivity (dotted lines). Reprinted from Journal of Membrane Science, 595, P.F. Zito, A. Brunetti, A. Caravella, E. Drioli, G. Barbieri. Mutual influence in permeation of CO₂-containing mixtures through a SAPO-34 membrane, 117534, Copyright (2020), Elsevier.

Feed pressure has also a negative effect on permeance of all the components (Figure 36) since the chemical potential gradient of the adsorbed species decreases for coverages close to the saturation values [42]. CO₂ permeance is the most affected, being the most strongly adsorbed species among those investigated. As already observed for temperature, CO₂ permeance in mixture results higher than in single gas at the same total feed pressure.

On the contrary, the other components show a weak dependence on pressure since their diffusion partially takes place with gas translation diffusion, which is pressure-independent.

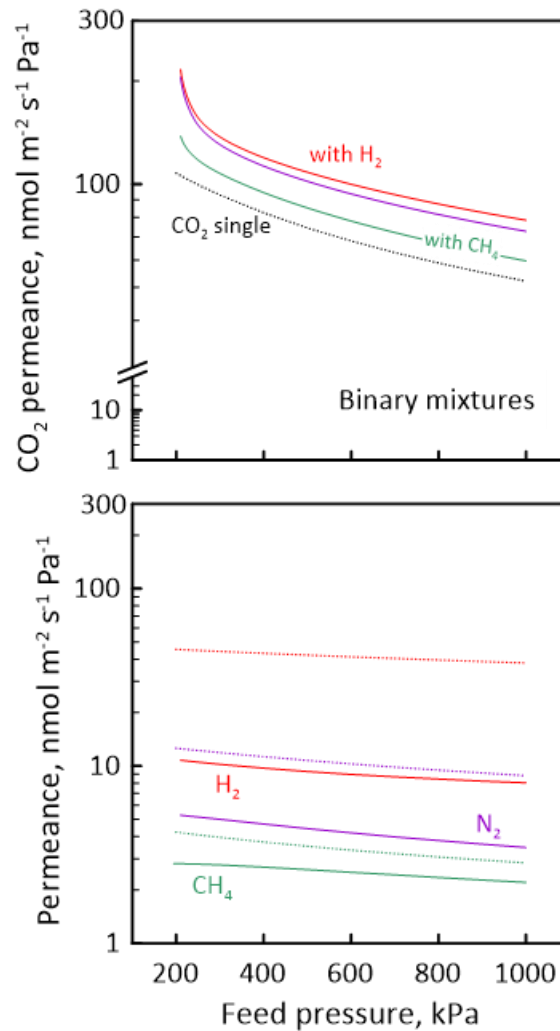


Figure 36. CO₂, H₂ and N₂ permeance as a function of feed pressure for equimolar CO₂:H₂, CO₂:N₂ and CO₂:CH₄ mixtures (solid lines) and single gases (dotted lines) at 25°C. Permeate pressure = 101 kPa. Reprinted from Journal of Membrane Science, 595, P.F. Zito, A. Brunetti, A. Caravella, E. Drioli, G. Barbieri. Mutual influence in permeation of CO₂-containing mixtures through a SAPO-34 membrane, 117534, Copyright (2020), Elsevier.

The dependence of permeance on mixture composition is also investigated using the permeance ratio, defined as the permeance of each component in mixture over that in single gas (Eq. (75)).

$$\text{Permeance ratio} = \frac{\text{Permeance}_i^{\text{Mixed gas}}}{\text{Permeance}_i^{\text{Single gas}}}, - \quad (75)$$

CO₂ permeance ratio increases with increasing composition of the other species, especially in presence of H₂, followed by N₂ and CH₄ (Figure 37). In particular, a CO₂ permeance 5 times greater than single gas is estimated for a mixture consisting of 95% of H₂. As aforementioned, this increment occurs because the reduction of driving force prevails on that of molar flux for a fixed feed pressure. Differently, the higher CO₂ permeance in mixture cannot be ascribable to the reduction of diffusivity with coverage, since Maxwell-Stefan diffusivity is assumed coverage-independent (i.e., weak confinement scenario). Unlike carbon dioxide, H₂, N₂ and CH₄ in mixture show a permeance lower than in single gas and reduced by the increasing CO₂ composition. However, above 0.2, permeance ratio becomes almost constant with increasing CO₂ feed molar fraction, probably because carbon dioxide coverage is close to the saturation condition.

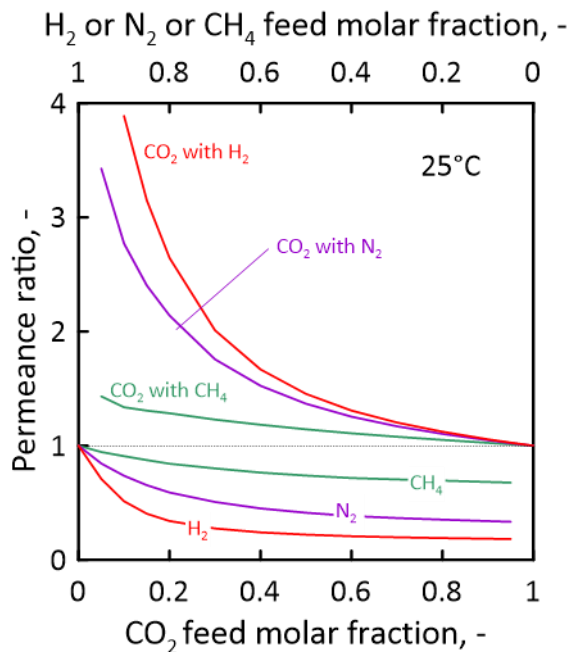


Figure 37. CO₂, CH₄, N₂ and H₂ permeance ratios as a function of CO₂ feed molar fraction for binary mixtures at a feed pressure of 500 kPa and 25°C. Reprinted from Journal of Membrane Science, 595, P.F. Zito, A. Brunetti, A. Caravella, E. Drioli, G. Barbieri. Mutual influence in permeation of CO₂-containing mixtures through a SAPO-34 membrane, 117534, Copyright (2020), Elsevier.

Selectivity is weakly affected by a change in feed composition (Figure 38). In particular, CO_2/H_2 selectivity shows a maximum of about 14 corresponding to the 15% of CO_2 in the feed stream. Below this maximum, H_2 permeance decreases more than the CO_2 one owing to the CO_2 hindering effect, whereas, above it, the adsorbed CO_2 does not increase significantly since the saturation condition of adsorption sites is approached. Thus, H_2 permeance decreases less than the CO_2 one. This maximum is also found by Hong *et al.* [35] for a feed concentration of about 45% of CO_2 at different operating condition (-20°C and 1.16 MPa). The greater CO_2 feed concentration of maximum found by Hong *et al.* [35] can be attributed to the much lower temperature (-20°C instead of 25°C), which moves the saturation condition of adsorption sites at higher CO_2 loading. CO_2/N_2 selectivity is the most influenced by the feed composition, varying from about 28 to 21 when CO_2 concentration in the feed stream passes from 0.05 to 0.95. Regarding the mixture $\text{CO}_2:\text{CH}_4$, selectivity assumes an oscillating trend around a value of 32, thus it can be considered independent of feed molar fraction.

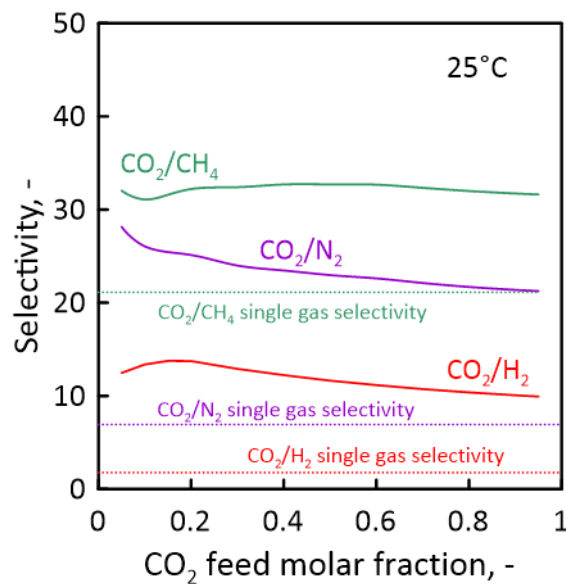


Figure 38. CO_2/H_2 , CO_2/N_2 and CO_2/CH_4 selectivity values as functions of CO_2 feed molar fraction for binary mixtures at a feed pressure of 500 kPa and 25°C . Reprinted from Journal of Membrane Science, 595, P.F. Zito, A. Brunetti, A. Caravella, E. Drioli, G. Barbieri. Mutual influence in permeation of CO_2 -containing mixtures through a SAPO-34 membrane, 117534, Copyright (2020), Elsevier.

The crucial properties that significantly affects the CO₂ permeation in mixture is the Maxwell-Stefan binary diffusivity $D_{SD,ij}$ (Eq. 38), expressed by Eq.76 in case of mixture CO₂-H₂:

$$D_{SD,CO_2,H_2} = D_{SD,CO_2}^{\frac{\theta_{CO_2}}{\theta_{CO_2} + \theta_{H_2}}} D_{SD,H_2}^{\frac{\theta_{H_2}}{\theta_{CO_2} + \theta_{H_2}}} \quad (76)$$

As can be observed in Figure 39, H₂ has the highest value of diffusivity D_{SD} , this causing a promoting effect on the binary diffusivity when mixed with CO₂. In fact, the binary CO₂:H₂ diffusivity increases from $1.2 \cdot 10^{-10}$ (value of CO₂ single diffusivity) to $1.3 \cdot 10^{-9}$ m² s⁻¹ (value of single H₂ diffusivity) as the hydrogen molar fraction ranges 0 to 1, showing a steep slope in the region of low CO₂ feed concentration. Nitrogen presents a lower positive effect on D_{ij} , since its single gas diffusivity (i.e., $1.8 \cdot 10^{-10}$ m² s⁻¹) is similar to that of CO₂. Methane ($D_i = 2.0 \cdot 10^{-11}$ m² s⁻¹ at 25°C) diffuses slower than carbon dioxide, causing a lower CO₂/CH₄ binary diffusivity than that of single CO₂.

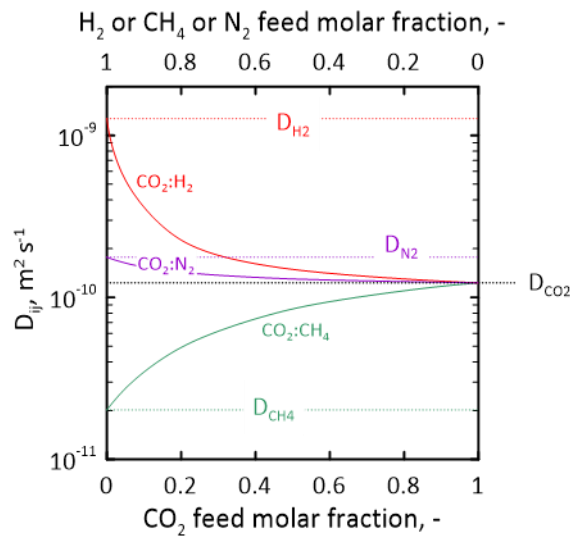


Figure 39. Maxwell-Stefan binary diffusivity as a function of CO₂ feed molar fraction for binary mixtures at 25°C. Value of single gas diffusivity for each gas (dotted lines). Reprinted from Journal of Membrane Science, 595, P.F. Zito, A. Brunetti, A. Caravella, E. Drioli, G. Barbieri. Mutual influence in permeation of CO₂-containing mixtures through a SAPO-34 membrane, 117534, Copyright (2020), Elsevier.

Although the slowing effect of CH₄, CO₂ permeance in mixture results higher than the single gas value for a fixed temperature and total feed pressure, as the permeance ratio previously revealed (Figure 37). This phenomenon occurs since CO₂ pressure difference corresponds to the overall one in single gas condition, whereas it is lower in mixture causing an increment in permeance (Eq. 70), since the reduction of driving force is more important than that of permeating flux. Thus, a more proper comparison between mixture and single gas can be done analyzing the behavior of flux and permeance when the same pressure difference is imposed (Figure 40). Fixing the same CO₂ driving force, which states a higher overall feed pressure in mixture than in single gas, CO₂ flux in mixture depends on the other component. Specifically, flux can be much higher, similar and much lower in the presence of H₂, N₂ and CH₄, respectively for a CO₂ feed composition of 0.20. The mixture fluxes approach the single gas value feeding a mixture containing 90% of CO₂. For all the mixture compositions, CO₂ flux increases with increasing pressure difference, showing a greater dependence at the lower driving force, being far from the saturation condition of adsorption sites and from the pores clogging by gas molecules. Permeance shows the opposite dependence on pressure difference, i.e., it decreases with increasing CO₂ driving force. However, it presents the same composition-dependence on flux. Thus, H₂ provides a real accelerating effect on CO₂ permeation, whereas CH₄ slows down its diffusion. On the other hand, N₂ less influence CO₂ flux and permeance with respect to the single gas values. These behaviors reflect the $D_{SD,ij}$ trends previously estimated (Figure 39). Therefore, the influence of another species on CO₂ permeation is not univocal, but depends on the diffusivity of this species compared to that of CO₂.

In the case of an equimolar CO₂:H₂:CH₄ mixture, the promoting and slowing effects are almost perfectly balanced (Figure 41). Therefore, CO₂ flux and permeance assumed almost the same values as in single gas, stating that the H₂ and CH₄ provide an equal and opposite effect on carbon dioxide permeation.

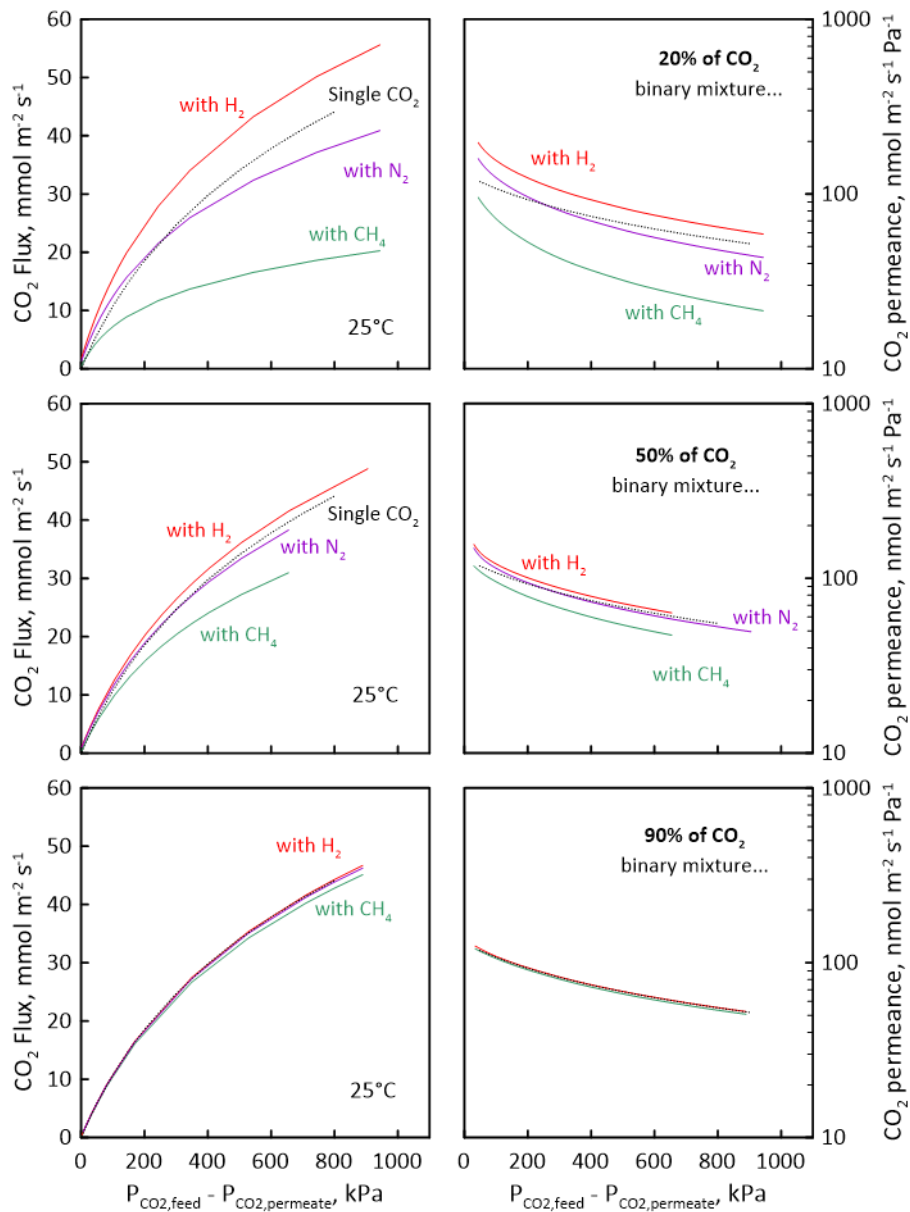


Figure 40. CO₂ molar flux and permeance as a function of CO₂ driving force for mixtures (solid lines) and single gas (dotted line). Reprinted from Journal of Membrane Science, 595, P.F. Zito, A. Brunetti, A. Caravella, E. Drioli, G. Barbieri. Mutual influence in permeation of CO₂-containing mixtures through a SAPO-34 membrane, 117534, Copyright (2020), Elsevier.

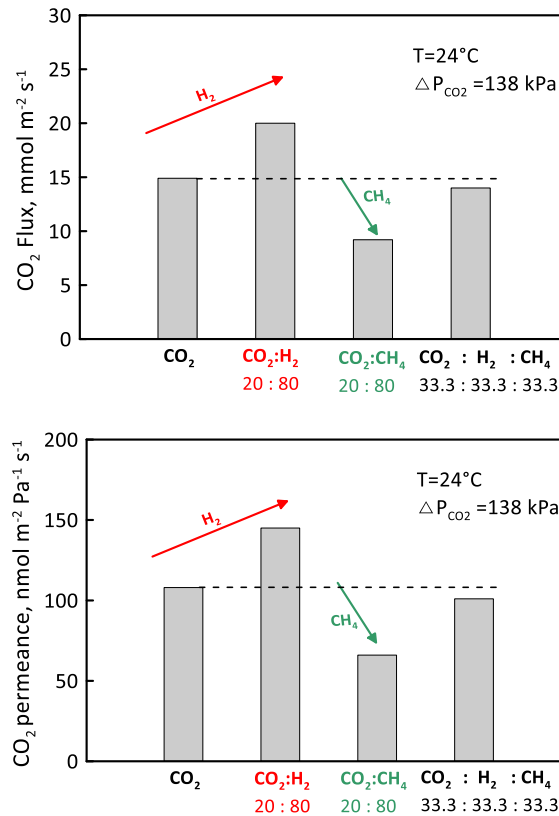


Figure 41. CO₂ molar flux and permeance values in mixture and single gas through a SAPO-34 membrane.

4.2 Humid mixtures: the effect of water vapor

4.2.1 4A membrane

The performance of SAPO-34 is investigated in dry condition. However, several industrial streams are water saturated and the presence of water vapor can significantly reduce the permeation of other gases (i.e., H₂, CO and CH₄) much more than CO₂, especially in hydrophilic materials such as 4A zeolite. In this thesis, this aspect is analyzed predicting the permeation through a 4A membrane prepared by Zhu *et al.* [30] as reported in section 3.2.3. At my knowledge, there are not models able to predict with a good accuracy the behavior of mixture consisting of water vapor and permanent gases. The adsorption and diffusion properties evaluated in the previous chapter are here used for validation and prediction of mixture permeation.

Permeance of H₂O and H₂ as a function of temperature in binary mixture conditions (H₂:H₂O=0.978:0.022) shows a strong hindering effect (Figure 42). A good agreement

between the experimental [30] and predicted permeation is obtained. A reduction of H₂ permeance of almost two orders compared to the single gas value was obtained at 303 K (e.g., from about 380 to 8 nmol m⁻² s⁻¹ Pa⁻¹). Permeance of H₂ increases with increasing temperature because of the reduction of H₂O adsorption and the consequent lower hindering effect. Moreover, differently from what occurred to CO₂ in SAPO-34, here water vapor in the mixture is not accelerated by hydrogen, maintaining the same permeance as in single gas. This can be attributed to the much higher adsorption of water vapor with respect to carbon dioxide, which reduces too much the amount of adsorbed H₂ that cannot provide any promoting effect. The increment of H₂ permeance paired to the reduction of that of H₂O with increasing temperature leads to an intersection between two permeance profiles at about 720 K (Figure 42). Therefore, membrane becomes H₂ selective at very high temperatures.

Another important aspect is that the dominant transport mechanism of H₂ changes from surface to gas translation diffusion from single gas to mixture (Figure 43). In fact, the adsorbed water vapor impedes the H₂ adsorption and, hence, its surface diffusion, which drastically falls down from about 360 (that is the single gas value) to 0.02 nmol m⁻² s⁻¹ Pa⁻¹ at 303 K. Differently, gas translation contribution is halved, passing from about 17 to 8 nmol m⁻² s⁻¹ Pa⁻¹ at a low temperature, consequently to the increment of the effective tortuosity and the reduction of effective porosity. The overall permeance passes from about 380 to 8 nmol m⁻² s⁻¹ Pa⁻¹, approaching the single gas values only above 700 K. The same phenomenon is observed for CH₄ and CO, which also shift their dominant mechanism from surface to gas translation diffusion under the influence of water vapor.

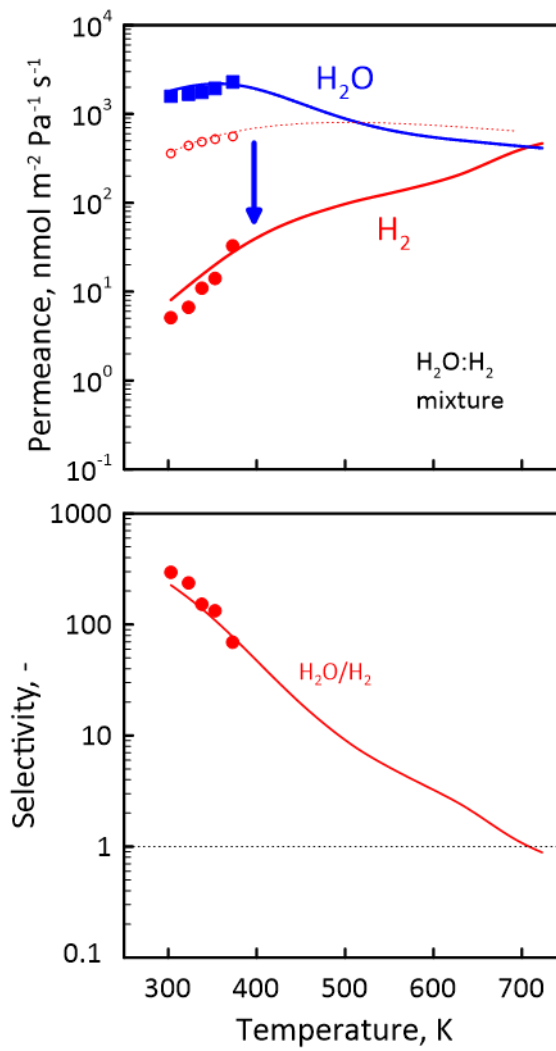


Figure 42. Permeance of H_2O and H_2 and $\text{H}_2\text{O}/\text{H}_2$ selectivity as functions of temperature for $\text{H}_2\text{O}:\text{H}_2=0.022:0.978$ mixture at 101 kPa of feed pressure. Experimental measurements of Zhu *et al.* [30] in single gas (open symbols) and mixture (full symbols), modelling results in single gas (dotted lines) and mixture (solid lines). Reprinted from Journal of Membrane Science, 574, P.F. Zito, A. Brunetti, A. Caravella, E. Drioli, G. Barbieri, Water vapor permeation and its influence on gases through a zeolite-4A membrane, 154-163, Copyright (2019), Elsevier.

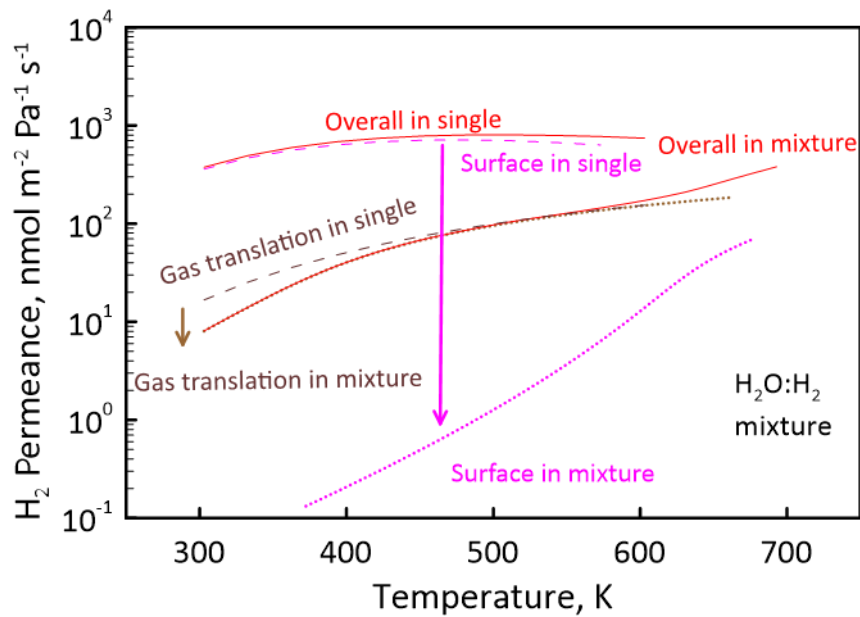


Figure 43. H_2 permeance contributions in single gas and in mixture with H_2O as a function of temperature: single surface diffusion contribution (magenta dashed line), binary surface diffusion contribution (magenta dotted line), single gas translation diffusion contribution (brown dashed line), binary gas translation contribution (brown dotted line), overall single permeance (red dashed line), overall mixture permeance (red solid line). Reprinted from Journal of Membrane Science, 574, P.F. Zito, A. Brunetti, A. Caravella, E. Drioli, G. Barbieri, Water vapor permeation and its influence on gases through a zeolite-4A membrane, 154-163, Copyright (2019), Elsevier.

The results in case of a mixture consisting of 0.978 of CH_4 and 0.022 of H_2O confirm the ability of the model to reproduce quite well the experimental trend and values of both the species in the whole temperature range considered and, especially, the drastic reduction of methane permeance in mixture (Figure 44). In fact, CH_4 permeance drops from about 70 in single gas to $2.4 \text{ nmol m}^{-2} \text{ s}^{-1} \text{ Pa}^{-1}$ in mixture at 303 K since surface diffusion is blocked (as for water vapor mixed with H_2). Thus, CH_4 in mixture permeates through gas translation diffusion. Permeance of CH_4 increases with temperature owing to the decreasing of H_2O adsorption, which reduces its hindering effect.

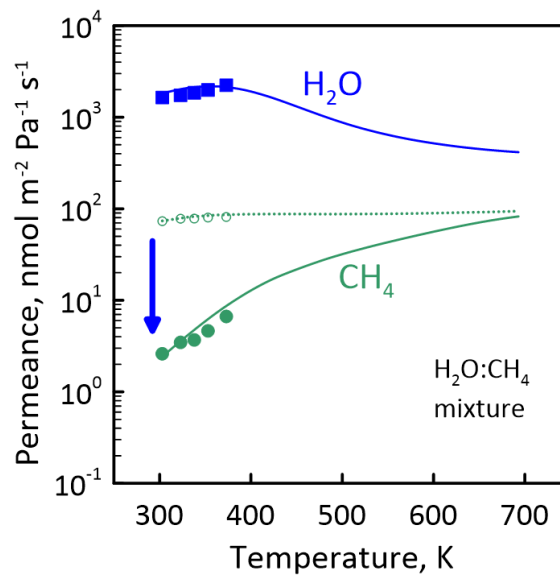


Figure 44. Permeance of H₂O and CH₄ as a function of temperature for H₂O: CH₄=0.022:0.978 mixture at 101 kPa of feed pressure. Experimental measurements of Zhu *et al.* [30] in single gas (open symbols) and mixture (full symbols), modelling results in single gas (dotted lines) and mixture (solid lines). Reprinted from Journal of Membrane Science, 574, P.F. Zito, A. Brunetti, A. Caravella, E. Drioli, G. Barbieri, Water vapor permeation and its influence on gases through a zeolite-4A membrane, 154-163, Copyright (2019), Elsevier.

The results of a H₂O:CO binary mixture (CO:H₂O=0.978:0.022) show a slight model deviation from the experimental values of CO (Figure 45). In particular, model predicts a lesser temperature dependence of permeance, which could be attributed to some discrepancies in coverage or activation energy for surface diffusion with respect to the experimental behavior. At high temperatures, H₂O and CO present an almost constant permeance. Even if CO is more strongly adsorbed than H₂ and CH₄, its presence does not affect the H₂O permeation in the mixture. The increment of CO permeance with increasing temperature occurs because of the reduction of H₂O coverage.

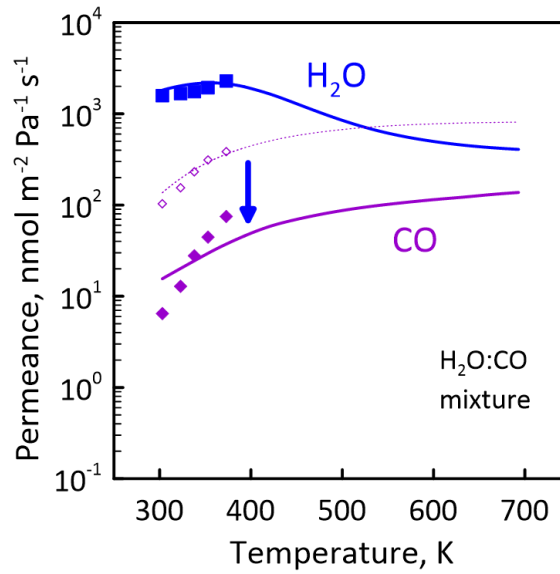


Figure 45. Permeance of H₂O and CO as a function of temperature for H₂O: CO=0.022:0.978 mixture at 101 kPa of feed pressure. Experimental measurements of Zhu *et al.* [30] in single gas (open symbols) and mixture (full symbols), modelling results in single gas (dotted lines) and mixture (solid lines). Reprinted from Journal of Membrane Science, 574, P.F. Zito, A. Brunetti, A. Caravella, E. Drioli, G. Barbieri, Water vapor permeation and its influence on gases through a zeolite-4A membrane, 154-163, Copyright (2019), Elsevier.

As mentioned before, the reduction of surface diffusion occurs because of the significant coverage reduction of each species when mixed with water vapor (Eq. 77 in case of CH₄ expressed by the Sips model), especially at low temperatures (Figure 46).

$$\theta_{CH_4} = \frac{(b_{CH_4} P_{CH_4})^{\frac{1}{n_{CH_4}}}}{1 + (b_{CH_4} P_{CH_4})^{\frac{1}{n_{CH_4}}} + (b_{H_2O} P_{H_2O})^{\frac{1}{n_{H_2O}}}} \quad (77)$$

A drastic drop is observed up to about 450 K, in the region where the adsorption of water vapor is strong. Mixture coverage of H₂, CH₄ and CO presents a maximum at about 480, 390 and 360 K, respectively, following the reverse of the adsorption strength: the more a species is adsorbed, the lower the temperature of this maximum results. Below this maximum, the reduced H₂O hindering effect with temperature prevails on the decreasing of coverage; above, the opposite phenomenon occurs. Above 500 K, coverage in mixture approaches that in single gas, since the H₂O leaves many adsorption sites available,

allowing the adsorption of the other components. Unlike other species, coverage of water vapor does not change from single gas to mixture.

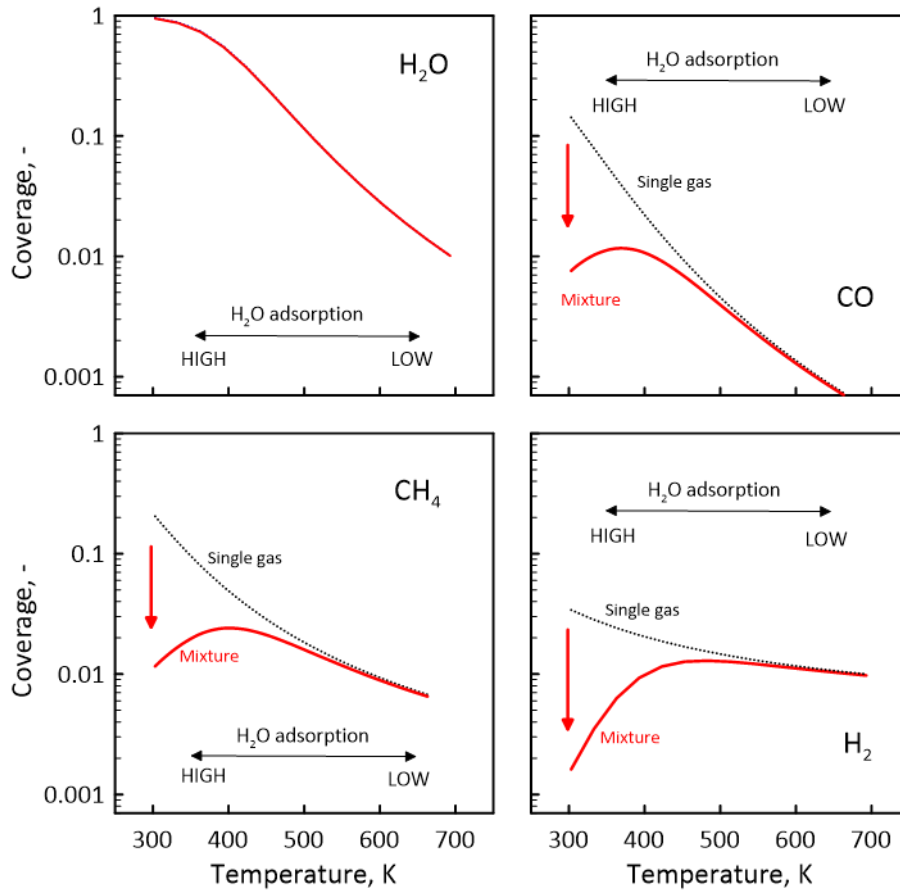


Figure 46. H₂O, CO, CH₄ and H₂ surface coverage of the feed side in single gas (back dotted lines) and binary mixture (red solid lines). Reprinted from Journal of Membrane Science, 574, P.F. Zito, A. Brunetti, A. Caravella, E. Drioli, G. Barbieri, Water vapor permeation and its influence on gases through a zeolite-4A membrane, 154-163, Copyright (2019), Elsevier.

Despite the adsorbed water vapor essentially impedes surface diffusion of the other species, this hindering effect is partially exerted on gas translation diffusion too, as previously observed in case of H₂ (Figure 43). From the physical point of view, this phenomenon occurs since the adsorbed molecules affect the effective porosity and tortuosity (Eqs.78-79 in case of H₂), which change with respect to the geometrical nominal values ε_0 and τ_0 and the single gas ones (dotted lines of Figure 47).

$$\varepsilon_{H_2} = \varepsilon_0 - \rho(1 - \varepsilon_0) + N_{Av} (d_{k,H_2O}^3 C_{\mu,H_2O} + d_{k,H_2}^3 C_{\mu,H_2}) \quad (78)$$

$$\tau_{H_2} = \tau_0 + \frac{\gamma_{H_2} \sigma_{H_2} (1 - \sigma_{H_2})}{\varepsilon_{H_2} \gamma_{H_2}} \quad (79)$$

It can be observed that the single gas ε and τ correspond to the nominal ones for H_2 , which is weakly adsorbed on the zeolite surface. Only a slight deviation is estimated at the low temperatures for CO and CH_4 , especially in effective porosity, being the volume available for diffusion partially occupied by the adsorbed molecules. A different situation is obtained in presence of water vapor; in fact, effective porosity of all the species is halved, being about 0.17 at 303 K. The nominal value (i.e., $\varepsilon_0=0.358$) is obtained only above 650 K. The presence of H_2O increases the effective tortuosity to about 5.4 for all the species at 303 K, which decreases with increasing temperature and approaches the nominal value at 500 K.

The selectivity of each binary mixture (solid lines in Figure 48) compared to the single gas one (dotted lines) points out the important effect of water vapor on the separation performance of 4A membrane. Zeolite membrane is selective towards H_2O also in single gas, except above 500 K, where CO and H_2 permeates as water vapor. In particular, single gas selectivity values of H_2O/CH_4 , H_2O/CO and H_2O/H_2 are about 25, 13 and 5 at 303 K, which decreases to 4, 0.5 and 0.6 at 700 K. At about 500 K, H_2O/CO selectivity achieves the Knudsen value (i.e., 1.25), becoming lower as temperature increases. On the other hand, Knudsen selectivity values are never achieved for H_2O/CH_4 and H_2O/H_2 , being 0.94 and 0.33, respectively. The separation performance highly improves in mixture; in fact, it is estimated an increment of selectivity of about 30 times in case of for H_2O/CH_4 , passing from 25 to 750. This improvement disappears at 700 K. In case of H_2O/CO , the presence of adsorbed water vapor enhances the selectivity from 13 to 120 at 303 K, whereas the highest increment is observed for the H_2 -containing wet mixture, for which selectivity passes from 5 to 225. However, H_2O/H_2 presents the greater temperature dependence, since its selectivity drops from 225 to 1 when temperature increases from 303 to 700 K. This phenomenon takes place because, in absence of adsorbed water vapor as at a high temperature, H_2 comes back to be the faster diffusing species inside the membrane, achieving the permeance values of H_2O .

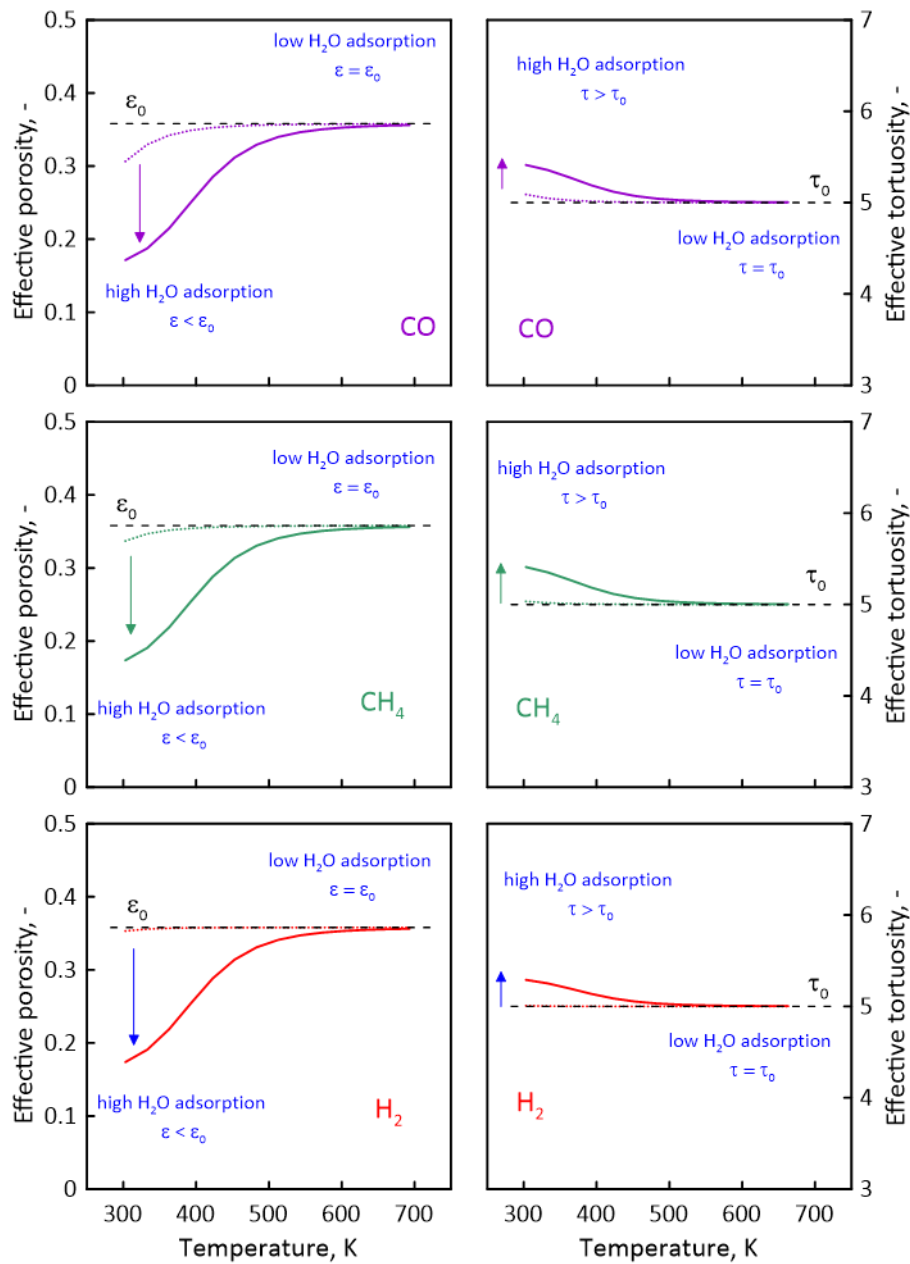


Figure 47. Effective porosity and tortuosity as a function of temperature during the permeation of CO, CH₄ and H₂ as single gas (dotted lines) and in mixture with H₂O (solid lines). Nominal porosity and tortuosity of the zeolite (black dashed lines). Reprinted from Journal of Membrane Science, 574, P.F. Zito, A. Brunetti, A. Caravella, E. Drioli, G. Barbieri, Water vapor permeation and its influence on gases through a zeolite-4A membrane, 154-163, Copyright (2019), Elsevier.

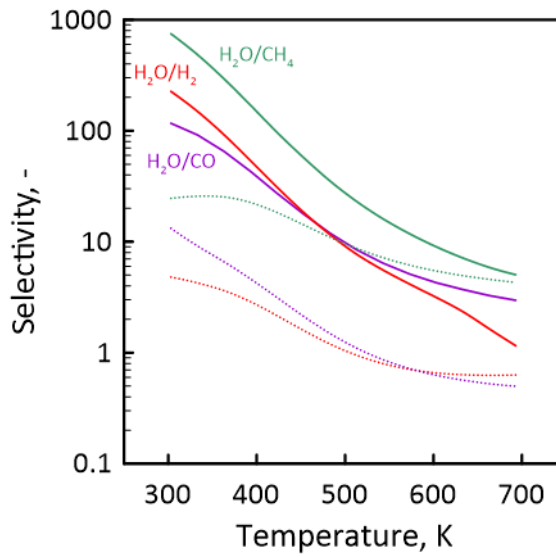


Figure 48. H₂O/CH₄, H₂O/H₂ and H₂O/CO selectivity as a function of temperature in binary mixture (solid lines) and single gas (dotted lines). Reprinted from Journal of Membrane Science, 574, P.F. Zito, A. Brunetti, A. Caravella, E. Drioli, G. Barbieri, Water vapor permeation and its influence on gases through a zeolite-4A membrane, 154-163, Copyright (2019), Elsevier.

Therefore, operating at moderate temperature enables the removal of small amount of water vapor (e.g., 0.022 mol%) from multicomponent gas mixtures to be achieved, allowing the water vapor to be collected as pure stream on the permeate side.

5. Experimental analysis

This Chapter deals with the experimental measurements of CO₂, H₂, CH₄ and N₂ permeation through a DDR membrane. This experimental campaign intends to investigate the mutual influence of gases in mixture on the permeation through the membrane and the variations of separation properties with respect to those measured in single gas. Moreover, it is used to support and validate the modelling analysis. Three CO₂-containing mixtures (CO₂:N₂, CO₂:H₂, CO₂:CH₄) at different compositions are considered, analyzing the effect of temperature (25-75°C) and feed pressure (300-700 kPa) on the separation properties of a membrane, which was kindly supplied by the team of Prof. Xuehong Gu at the Nanjing Tech University (China). The DDR membrane was synthesized by secondary growth on the outer surface of α -alumina four channel hollow fiber support [27]. The tubular membrane presents an area of 5.8 cm² and a zeolite thickness of about 5 μ m (Figure 49).

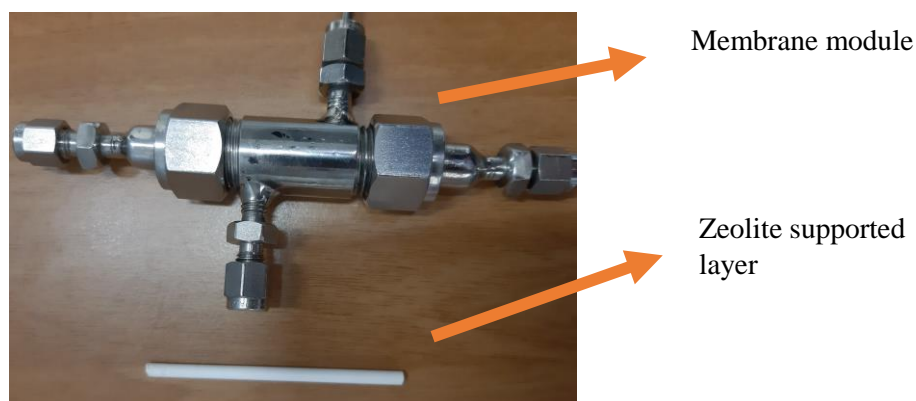


Figure 49. Zeolite membrane used for permeation measurements.

In the last part of this chapter, the experimental and modelling results in terms of CO₂ permeance and selectivity are compared to those summarized in the Robeson's diagrams [5].

Some results described in this chapter are also reported in a recent publication [100].

5.1 Permeation through a DDR membrane

Permeation of gas mixtures and single gas is experimentally measured using the apparatus described in Chapter 2 (Figure 12).

The separation performance of the membrane module is evaluated in terms of permeance and selectivity of the gas mixture. Permeance is evaluated as the ratio of the measured permeating flux and the partial pressure differences between the two membrane sides (Eq. 70). Selectivity is defined as the ratio between the membrane permeance of two gases (Eq. 71). The negligibility of partial pressure profiles along the membrane module length is assured, operating with a stage cut lower than 1%. This hypothesis is verified by comparing the mixture compositions of feed and retentate streams, which result quite similar. Experimental data are periodically verified to check their reproducibility. The standard deviation is below 6%.

The single gas permeation experiments as a function of temperature are carried out between 25 and 75°C, operating at 500 kPa of feed pressure and atmospheric permeate pressure (Figure 50). In the temperature range investigated, CO₂ results the most permeable gas, followed by H₂, N₂ and CH₄. All the gases show a temperature dependence, ascribable to the mass transport mechanisms governing their permeation. CO₂ permeance slightly decreases with the temperature, this decreasing trend is ascribable to the reduction of the adsorbed phase. Differently, N₂ and less CH₄ present a maximum around 50°C, which can be attributed to a competition between the adsorption reduction and diffusion increase. H₂ permeance, instead, presents a minimum at 50°C. It is a very weakly adsorbed gas and its coverage is very low even at moderate temperatures. This minimum represents the transition point from surface to gas translation diffusion, as it is discussed in the modelling analysis.

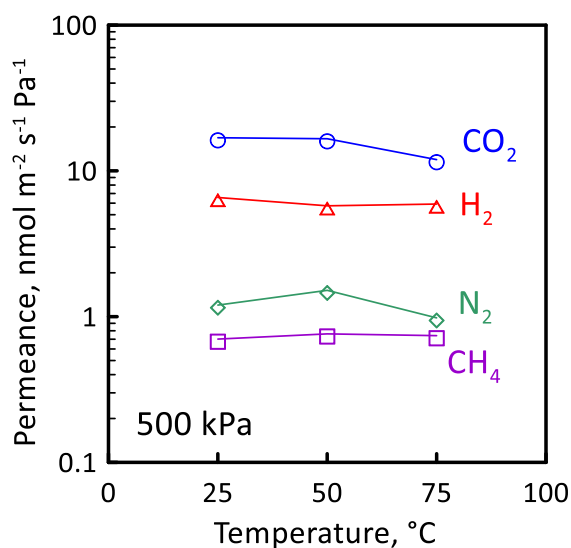


Figure 50. Single gas permeance of CO₂, CH₄, H₂ and N₂ as a function of temperature at 500 kPa of feed pressure. Reprinted with permission from P.F. Zito, A. Brunetti, E. Drioli, G. Barbieri, CO₂ separation via a DDR membrane: mutual influence of mixed gas permeation, *Ind. Eng. Chem. Res.* **2019**. Copyright (2019) American Chemical Society.

The separation performance of a DDR membrane is analyzed by experimental measurements on various CO₂ containing mixtures. The first mixture investigated is CO₂:H₂=40.1:59.9 changing temperature and feed pressure (Figure 51). It can be observed that CO₂ permeance decreases with increasing temperature, as also estimated by the modelling analysis on SAPO-34, being the reduction of adsorption more important than the increment of diffusivity with temperature. On the contrary, H₂ permeance is favored by the increasing temperature since the hindering effect of the adsorbed CO₂ becomes less important. For a fixed temperature, feed pressure reduces the CO₂ permeance, which takes place by surface diffusion (pressure disadvantaged), whereas it does not affect the H₂ one, since hydrogen permeates especially following gas translation diffusion (pressure independent). A CO₂ permeance increment with respect to the single gas value is measured at 300 kPa owing to the presence of H₂, whereas this promoting effect tends to vanish at high feed pressure, probably because the increased coverage of CO₂ makes the adsorbed amount of H₂ too low to affect the binary diffusivity $D_{SD,ij}$. Selectivity of mixture results much higher than the single gas one at 25°C and 300 kPa,

being about 17 instead of 2, whereas feed pressure and temperature abate the gap, which disappear at 75°C and 700 kPa.

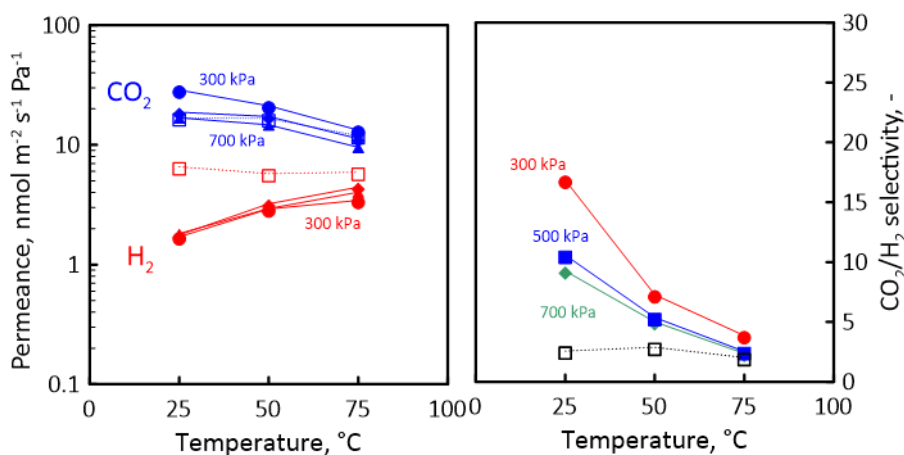


Figure 51. CO₂ and H₂ permeance and CO₂/H₂ selectivity as a function of temperature for CO₂:H₂=40.1:59.9 mixture at 300, 500 and 700 kPa (full symbols) and single gas (open symbols). Reprinted with permission from P.F. Zito, A. Brunetti, E. Drioli, G. Barbieri, CO₂ separation via a DDR membrane: mutual influence of mixed gas permeation, *Ind. Eng. Chem. Res.* **2019**. Copyright (2019) American Chemical Society.

Carbon dioxide shows the same trend when mixed with N₂ (Figure 52). In particular, its permeance decreases with temperature and feed pressure, but, contrarily to what observed in presence of H₂, it is found to be similar to that measured with single gas at 300 kPa and lower for the higher feed pressures. N₂ permeance slightly depends on temperature, most likely because the reduction of both nitrogen sorption and hindering effect played by CO₂ are balanced by the increment of diffusivity, resulting in a quite constant trend of permeance. It can be observed that nitrogen does not provide any promoting effect on CO₂ permeance, probably because its diffusivity is similar to that of carbon dioxide. Thus, the binary diffusivity is not enhanced for this mixture. As observed for CO₂:H₂ mixture, the permeance of the less permeable gas, in this case N₂, is lower than that measured in single gas condition, even though by a less extend with respect to that observed for H₂. In any case, it reflects on a higher CO₂/N₂ selectivity with respect to single gas one. CO₂/N₂ selectivity increases from about 13 to 28 when temperature

decreases from 75 to 25°C at 300 kPa. A mixture selectivity lower than the single gas value is measured at 75°C, imposing a feed pressure of 500 or 700 kPa.

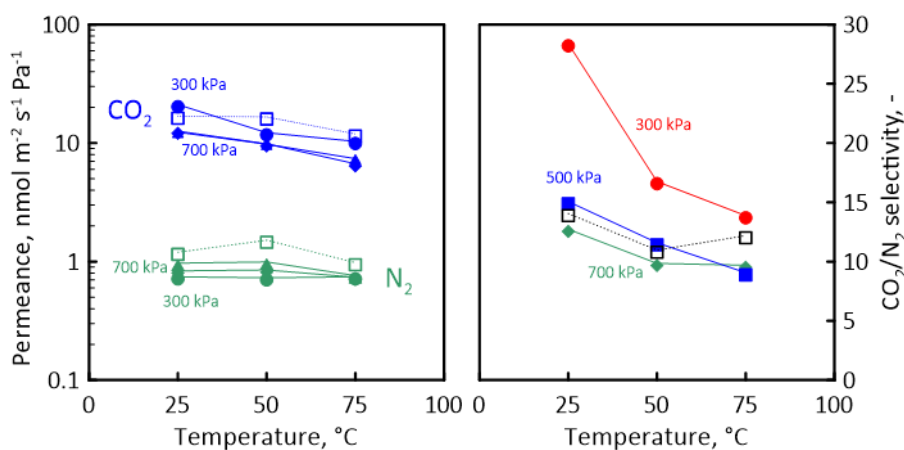


Figure 52. CO₂ and N₂ permeance and CO₂/N₂ selectivity as a function of temperature for CO₂:H₂=40.4:59.6 mixture at 300, 500 and 700 kPa (full symbols) and single gas (open symbols). Reprinted with permission from P.F. Zito, A. Brunetti, E. Drioli, G. Barbieri, CO₂ separation via a DDR membrane: mutual influence of mixed gas permeation, *Ind. Eng. Chem. Res.* **2019**. Copyright (2019) American Chemical Society.

Both CO₂-containing mixtures exhibit similar trends of permeance as a function of feed pressure (Figure 53). The highest deviation with respect to the single gas behavior is measured for H₂, whose permeance slightly increases owing to the increment of its driving force. The same considerations can be done for N₂. Differently, the decreasing trend of CO₂ permeance with feed pressure can be explained considering that CO₂ is the strongest adsorbing species among those investigated, approaching the saturation loading as pressure increases and this causes a reduction of chemical potential gradient of the adsorbed phase, with consequent permeance reduction. Thus, selectivity is disadvantaged by a high feed pressure, therefore, the low pressure (300 kPa) enhances the separation capability of the membrane. In fact, CO₂/N₂ and CO₂/H₂ selectivity values are two to five times greater than correspondent single gas ratio at 300 kPa, allowing to emphasize how most often the separation properties measured with single gas provide misleading information on the actual separation capability of membranes.

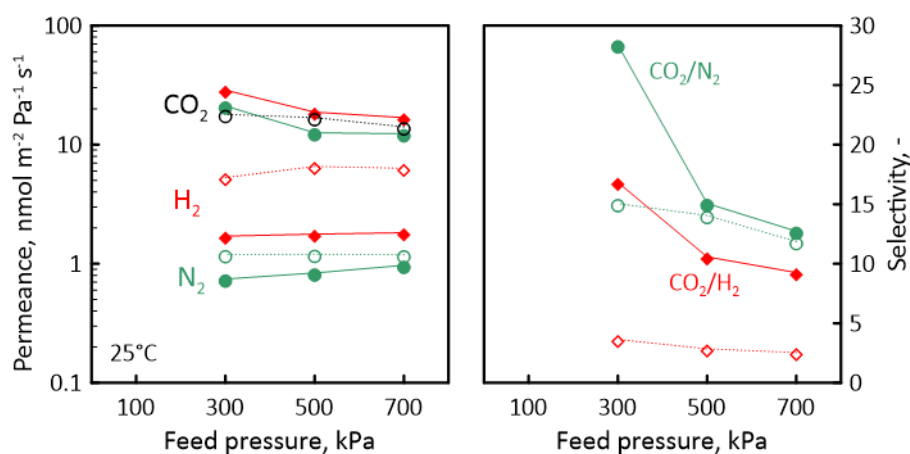


Figure 53. CO₂, H₂ and N₂ permeance and selectivity as a function of feed pressure for CO₂:N₂=40.4:59.6 and CO₂:H₂=40.1:59.9 mixtures (full symbols) and single gas (open symbols). Reprinted with permission from P.F. Zito, A. Brunetti, E. Drioli, G. Barbieri, CO₂ separation via a DDR membrane: mutual influence of mixed gas permeation, *Ind. Eng. Chem. Res.* **2019**. Copyright (2019) American Chemical Society.

In terms of permeance ratio (Eq. 75), CO₂ permeance is found to be proportional to the composition of the other species (Figure 54), as also estimated for SAPO-34. In the previous section, this behavior is explained as a reduction of driving force more important than that of flux for a fixed total feed pressure. Moreover, in case of DD3R, a further possible explanation of this trend is that CO₂ could follow the strong confinement scenario (i.e., linear reduction of diffusivity with coverage) and, in this case, its diffusivity would be higher in mixture, being coverage lower than in case of single CO₂. Carbon dioxide permeance is found higher in presence of H₂, since hydrogen is the species with the fastest diffusivity and lowest adsorption. Specifically, a permeance ratio of about 2.5 is measured for a mixture containing 95% of H₂. Unlike CO₂, H₂ and N₂ permeance are reduced by the increment of carbon dioxide concentration, this hindering effect being stronger on H₂.

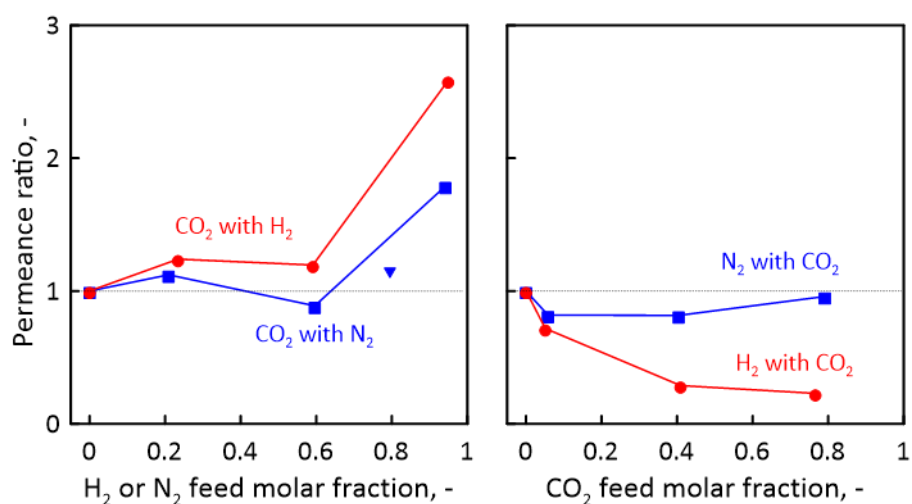


Figure 54. CO₂, H₂ and N₂ permeance ratio (full symbols) as a function of feed molar fraction for CO₂:H₂ and CO₂:N₂ mixtures at 25°C and 700 kPa of feed pressure. CO₂ permeance for mixture CO₂:N₂:O₂=15:80:5 (full triangle). Reprinted with permission from P.F. Zito, A. Brunetti, E. Drioli, G. Barbieri, CO₂ separation via a DDR membrane: mutual influence of mixed gas permeation, *Ind. Eng. Chem. Res.* **2019**. Copyright (2019) American Chemical Society.

The permeance variations with the mixture composition directly reflected on selectivity (Figure 55). In CO₂:H₂ mixtures, the prevailing reduction of H₂ permeance with respect to that of CO₂ induces an increment of selectivity with the increasing of CO₂ composition. Opposite trend is observed for CO₂/N₂ selectivity. At a CO₂ concentration below 40% (i.e., above 60% of N₂), N₂ permeance change is relatively limited with respect to that of CO₂. As the concentration of CO₂ increased, both species exhibit a similar permeance trend, implying a constant selectivity, close to that of single gases and, thus, independent of the feed mixture composition.

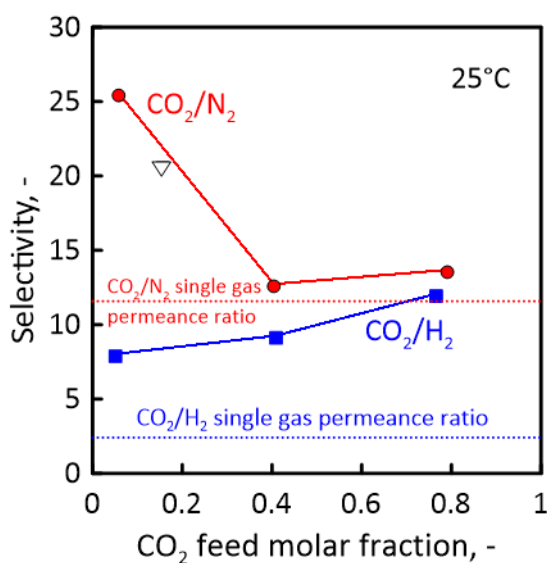


Figure 55. CO₂/H₂ and CO₂/N₂ selectivity values as functions of CO₂ feed molar fraction CO₂:H₂ and CO₂:N₂ mixtures at a feed pressure of 700 kPa. Selectivity and permeate molar fraction for mixture CO₂:N₂:O₂=15:80:5 (open triangles). Reprinted with permission from P.F. Zito, A. Brunetti, E. Drioli, G. Barbieri, CO₂ separation via a DDR membrane: mutual influence of mixed gas permeation, *Ind. Eng. Chem. Res.* **2019**. Copyright (2019) American Chemical Society.

Figure 56 shows the permeance ratio (Eq. 75) for the binary mixtures containing about 40% of CO₂ at 25°C. A significant reduction of H₂, N₂ and CH₄ permeance in mixture is observed at 300 kPa (Figure 56-left side), in particular CH₄ and H₂ are more affected than N₂. CH₄ is the most strongly adsorbed species after CO₂; therefore, when mixed with CO₂, its adsorbed amount is reduced in comparison to the single gas, owing to the competitive sorption with CO₂. This effect, added to the hindering effect exerted by adsorbed CO₂, which reduces gas translation diffusion, induces an overall permeance reduction. Differently, H₂ is a weakly adsorbent species but has a very fast diffusion, which is hindered in mixture by the presence of CO₂. The permeance ratio is 1/3 at 300 kPa, afterwards its reduction is very little constant as the pressure increases. N₂ is in the intermediate condition between CH₄ and H₂: it is moderately adsorbed and diffuses inside the pores up to three order of magnitude faster than CH₄ but about 100 times slower than H₂ (Table 12). Hence, the presence of CO₂ has a minor effect on its diffusion and its permeance.

CO₂, indeed, is positively affected by the presence of the other species for a fixed total feed pressure. In all the explored mixtures, CO₂ permeance is, in fact, at 300 kPa always higher than that measured in single gas (Figure 56, right side). This positive variation strictly depends on the other species in mixture. When mixed with N₂ or CH₄, CO₂ permeance (about 21 nmol m⁻² Pa⁻¹ s⁻¹) has almost the same value, which is about 1.2 higher than that in single gas. In presence of H₂, CO₂ permeance passes from about 18 to 29 nmol m⁻² Pa⁻¹ s⁻¹. As aforementioned, these different behaviors can be attributed to the promoting effect exerted by the faster H₂. In addition, when mixed with another gas, the total adsorbed amount is less (in particular, for CO₂:H₂ mixtures) and CO₂ diffusion can be higher (e.g., strong confinement scenario) [96, 101, 102, 103]. Since H₂ is the less adsorbing species, CO₂ permeance assumes the highest value when mixed with it. When mixed with N₂ and CH₄ it tends to fall down at the higher feed pressures, becoming less than the single gas value at 700 kPa. Likely, the slowing effect on CO₂ provoked by both the bulky molecules (N₂ and CH₄) and the reduction of CO₂ diffusivity is not fully balanced by the increment of its adsorbed coverage. In addition, as the pressure increases, a clogging of pore can be approached, and this can contribute to the permeance reduction since the permeating flux increases by a lesser extent.

Table 12. Estimated mixture loading [67] and single gas diffusivity [28, 47] at 25°C. Reprinted with permission from P.F. Zito, A. Brunetti, E. Drioli, G. Barbieri, CO₂ separation via a DDR membrane: mutual influence of mixed gas permeation, *Ind. Eng. Chem. Res.* **2019**. Copyright (2019) American Chemical Society.

<i>Species</i>	<i>Loading at 300 kPa, mol kg⁻¹</i>			<i>Diffusivity, m² s⁻¹</i>
	CO ₂ :CH ₄	CO ₂ :N ₂	CO ₂ :H ₂	
CO ₂	1.8	1.5	2.1	1.6·10 ⁻¹¹
CH ₄	0.3	-	-	7.7·10 ⁻¹⁴
N ₂	-	0.1	-	3.1·10 ⁻¹¹
H ₂	-	-	0.01	5.0·10 ⁻⁹

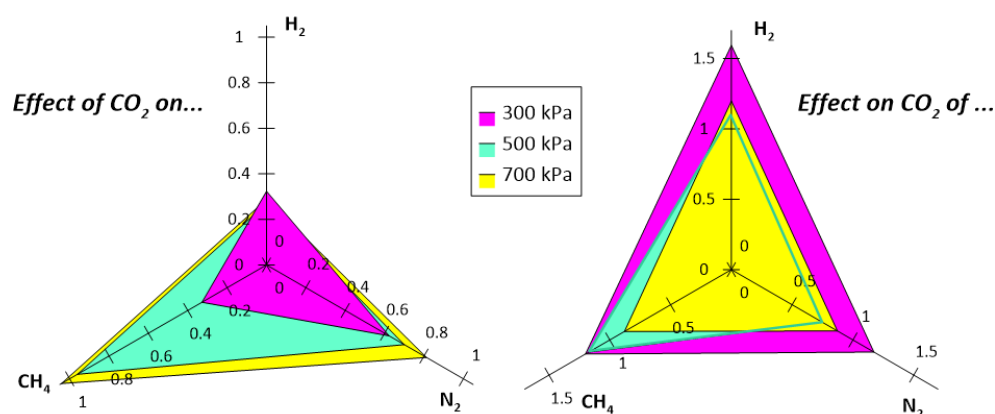


Figure 56. Permeance ratio for binary mixtures containing 40% of CO₂ at three feed pressures- Effect of (left side) CO₂ on H₂, N₂ and CH₄ permeance; (right side) H₂, N₂ and CH₄ on CO₂ permeance at 25°C. Reprinted with permission from P.F. Zito, A. Brunetti, E. Drioli, G. Barbieri, CO₂ separation via a DDR membrane: mutual influence of mixed gas permeation, *Ind. Eng. Chem. Res.* **2019**. Copyright (2019) American Chemical Society.

5.2 Comparison with the modelling results

The experimental measurements are also compared to the simulation results using the surface and gas translation diffusivity values estimated in the modelling analysis (section 3.2.1 of Chapter 3). Concerning the single CO₂ and H₂ permeation (Figure 57), a perfect agreement between model and experimental results is obtained by multiplying the experimental permeances by a constant factor of 7. This factor contains the differences in membrane thickness, operating conditions (e.g., feed pressure, use of sweep gas), synthesis processes, geometrical characteristics (e.g., porosity and tortuosity) and silicon/aluminum ratio. Specifically, the diffusion properties (i.e., activation energy and pre-exponential factor for surface diffusion) used for simulation are estimated from experimental measurements carried out using a sweep gas on the permeate side [93], whereas an atmospheric permeate pressure was fixed in the home-made experiments. It is well-known that the presence of sweep provokes an increment of flux and, therefore, permeance, since the driving force increases. Thus, the simulation considering 1 atm on the permeate side could overestimate the permeance with respect to the no-sweep condition. Moreover, the diffusion properties are estimated on a DD3R membrane different [93] from that used for the experimental tests. Thus, the two DDR membranes

can present some geometrical differences (e.g., porosity and tortuosity) and a different Si/Al ratio, which strongly affects the CO₂ adsorption. All these differences can be collected in the constant factor of 7.

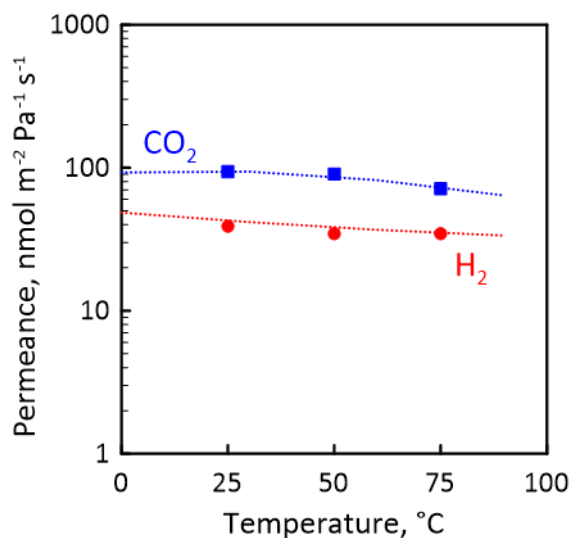


Figure 57. Single gas permeance of CO₂ and H₂ as a function of temperature: experimental measurements multiplied by 7 (full symbols), modelling results (dotted lines). Adapted with permission from P.F. Zito, A. Brunetti, E. Drioli, G. Barbieri, CO₂ separation via a DDR membrane: mutual influence of mixed gas permeation, *Ind. Eng. Chem. Res.* **2019**. Copyright (2019) American Chemical Society.

The same constant factor of 7 is applied in the comparison with the mixture measurements in order to verify if it is maintained also in this case (Figure 58). It can be observed that the experimental drop of H₂ permeance is perfectly described as well as its increment with increasing temperature. On the contrary, some discrepancies are observed for CO₂: the experimental value (multiplied by 7) coincides with the model only at 25°C, whereas model slightly overestimated the CO₂ diffusion at the higher temperatures. This causes some differences in selectivity values that, however, are close to the experimental ones, providing a further validation of the modelling analysis and a good capacity of the model to predict the experimental behavior, especially in terms of selectivity.

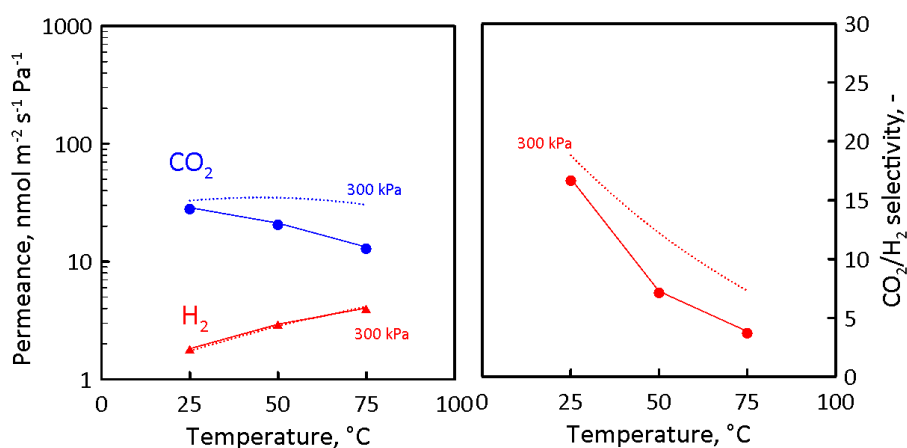


Figure 58. Permeance of CO₂ and H₂ as a function of temperature for CO₂:H₂=40.4:59.6 mixture at 300 kPa. Experimental measurements multiplied by 7 (full symbols), modelling results (dotted lines).

Model is therefore used for prediction of permeance and selectivity trends as functions of temperature for a mixture of industrial interest, such as the syngas (i.e., CO₂: H₂: CO = 0.05:0.5:0.45 as in [104]) in a DD3R membrane (Figure 59) using the diffusion parameters evaluated in Chapter 3 (Table 7). As expected, carbon dioxide is the most permeating species at low temperatures, since it adsorbs stronger than the remaining species do. Its permeance in the mixture (blue solid line) is higher than that in single gas condition (blue dotted line) at low temperatures. The increment is owed to surface diffusion that increases in the mixture and tends to vanish above 150°C. Furthermore, the small amount of CO₂ present in mixture is able to reduce the H₂ permeance from *ca.* 50 to 8 nmol m⁻² s⁻¹ Pa⁻¹ at 0°C, which changes its temperature dependence from single gas (red dotted line) to mixture (red solid line). Differently, CO is not affected by the presence of the small amount of CO₂, owing to its stronger adsorption with respect to H₂. For all the species, the effect of gas translation contribution can be appreciated at high temperatures, where the permeance increases with increasing temperature. Permeances of CO₂ and CO present a minimum at *ca.* 420 and 210°C respectively, as in single gas (section 3.2.1). On the other hand, H₂ permeance continuously increases with increasing temperature because of the lower CO₂ hindering effect paired to the increasing gas translation contribution. The CO₂/CO and CO₂/H₂ selectivity values at 30°C are estimated to be 36 and 18, showing a decreasing trend with temperature because of the CO₂

adsorption reduction. Furthermore, a reverse CO_2/H_2 selectivity is found above 180°C , tending to 5 at higher temperatures; on the other hand, CO_2/CO selectivity tends to 1.

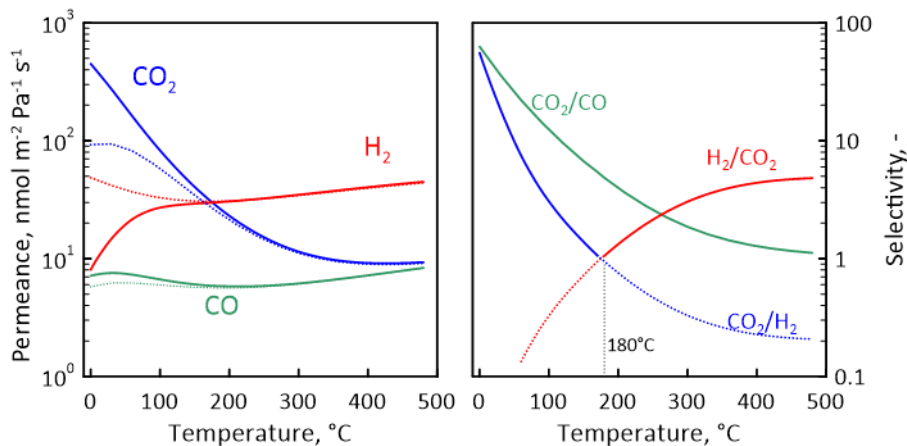


Figure 59. Permeance and selectivity values as a function of temperature for a syngas mixture $\text{CO}_2:\text{CO}:\text{H}_2 = 0.05:0.45:0.50$ in a $10\ \mu\text{m}$ thick DD3R membrane. Feed and permeate pressure are 300 and 101 kPa, respectively. Permeance in single gas (dotted lines), permeance in mixture (solid lines). Adapted from Journal of Membrane Science, 564, P.F. Zito, A. Caravella, A. Brunetti, E. Drioli, G. Barbieri, Discrimination among gas translation, surface and Knudsen diffusion in permeation through zeolite membranes, 166-173, Copyright (2018), Elsevier.

The effect of feed pressure on permeance and selectivity is also estimated at 25°C (Figure 60). Permeance of CO_2 and CO decreases with increasing feed pressure since both the species permeate only with surface diffusion under this operating condition. Therefore, the increment of feed pressure approaches the adsorbed phase to the saturation condition. Differently, gas translation diffusion also contributes to the overall permeance of H_2 . However, this contribution, which is pressure-independent, is not sufficient to compensate the reduction of surface diffusion. Hence, H_2 overall permeance also decreases. The CO_2/CO selectivity is slightly disadvantaged by feed pressure, decreasing from 42 to 33. On the contrary, CO_2/H_2 selectivity is almost pressure independent, remaining almost constant around a value of 20, with a maximum of 23 at 500 kPa.

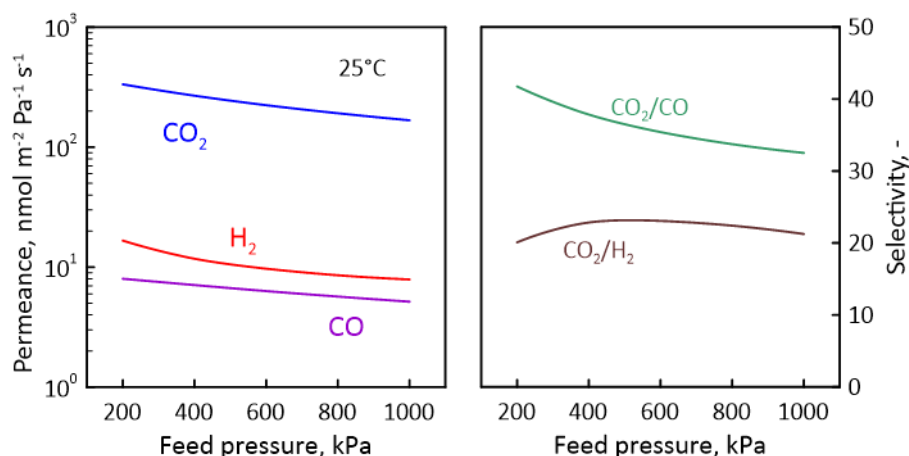


Figure 60. Permeance and selectivity values as a function of feed pressure for a syngas mixture CO₂:CO:H₂ = 0.05:0.45:0.50 in a 10 μm thick DD3R membrane at 25°C and a permeate pressure of 101 kPa. Adapted from Journal of Membrane Science, 564, P.F. Zito, A. Caravella, A. Brunetti, E. Drioli, G. Barbieri, Discrimination among gas translation, surface and Knudsen diffusion in permeation through zeolite membranes, 166-173, Copyright (2018), Elsevier.

The selectivity versus permeability values obtained from both modelling and experimental analysis are compared using the upper bound [5, 105] for different pairs of gases. The first mixture investigated is CO₂-H₂, for which the performance of three different zeolite membranes (i.e., DD3R, SAPO-34 and NaY) are reported (Figure 61). It can be observed that the trade-off between permeability and selectivity is always below the upper bound [105] in single gas condition (open symbol). Furthermore, CO₂ permeates more than H₂ through SAPO-34 and DD3R, as reveals the single CO₂/H₂ selectivity higher than 1, whereas the opposite behavior is found in NaY, which has larger pore size (i.e., 0.74 nm). A significant increment of selectivity towards carbon dioxide is estimated in mixture (CO₂:H₂ = 40:60), since the strong CO₂ adsorption hinders the H₂ diffusion. Thus, the pair permeability-selectivity is able to overcome the upper bound for DD3R (CO₂ permeability of 429 barrers and CO₂/H₂ of 17) and NaY (CO₂ permeability of about 3800 barrers and CO₂/H₂ of 62). Particular is the case of NaY, for which the greatest increment of selectivity compared to the single gas one is found. Specifically, CO₂/H₂ selectivity passes from 0.15 to 62, stating that the CO₂ hindering effect in this zeolite is much more important than in the other ones. In fact, the analysis of the adsorption properties reveals that NaY adsorbs CO₂ much more (e.g., saturation loading of 7.6 mol kg⁻¹ at 25°C [60]) than DD3R (2.9 mol kg⁻¹) and SAPO-34 (4.4 mol kg⁻¹).

Moreover, a higher CO₂ permeability in mixture than in single gas is observed for all the three materials, as revealed by the positive slope of each line connecting single gas and mixture values. This phenomenon is also observed for CO₂-N₂ (Figure 62) and CO₂-CH₄ (Figure 63). Another important aspect is that the boost in permeability does not follow that of pore size, being SAPO-34 (pore dimension of 0.38 nm) more permeable to CO₂ than NaY (pore dimension 0.74 nm). A possible explanation to the lower permeability of NaY is its higher activation energy for surface diffusion (i.e., about 18800 J mol⁻¹) than SAPO-34 (i.e., about 7800 J mol⁻¹), stating that this mechanism is easier in the latter case.

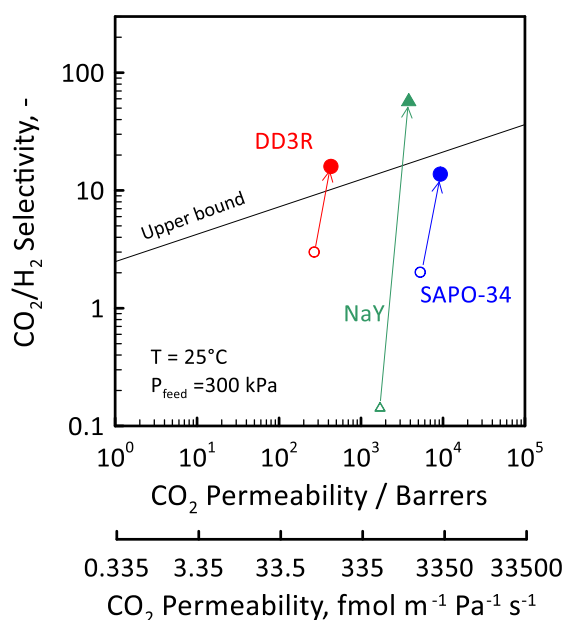


Figure 61. CO₂/H₂ selectivity as a function of CO₂ permeability through DD3R, NaY and SAPO-34 in binary mixture (full symbols) and single gas (open symbols). Upper bound [105] (black solid line).

Concerning the pairs CO₂-N₂ (Figure 62) and CO₂-CH₄ (Figure 63). Robeson's upper bound shows a negative slope, since selectivity decreases with increasing CO₂ permeability. Moreover, CO₂ permeability is always higher in SAPO-34, since this material adsorbs more CO₂ than DD3R. Regarding the mixture carbon dioxide – nitrogen, Robeson's upper bound is overcome only using SAPO-34, which provides a CO₂ permeability and a CO₂/N₂ selectivity of 8400 barrers and 27, respectively, in mixture. Therefore, the increment of selectivity owing to presence of adsorbed CO₂ is less

significant than in case of CO₂:H₂, since N₂ competes more in adsorption with carbon dioxide. Concerning the CO₂:CH₄ pair, the upper bound is exceeded using both DD3R and SAPO-34 in mixture. DD3R presents higher selectivity (i.e., 106) but lower permeability (330 barrers) than SAPO-34 (selectivity of 40 and CO₂ permeability of 6500 barrers).

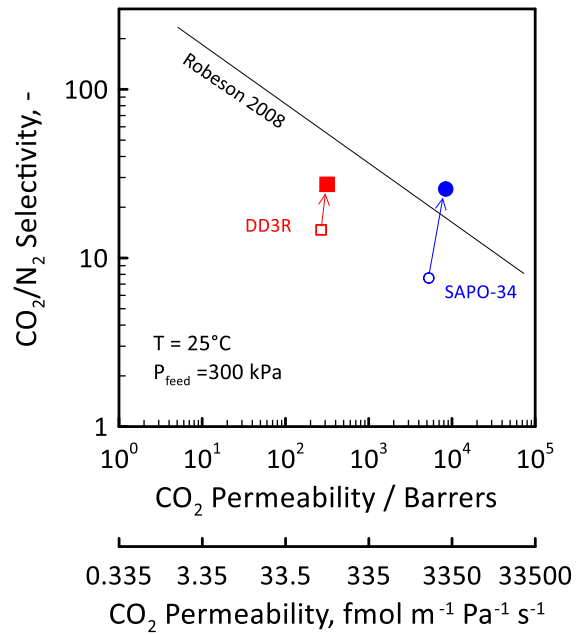


Figure 62. CO₂/N₂ selectivity as a function of CO₂ permeability through DD3R and SAPO-34 in binary mixture (full symbols) and single gas (open symbols). Robeson upper bound [5] (black solid line).

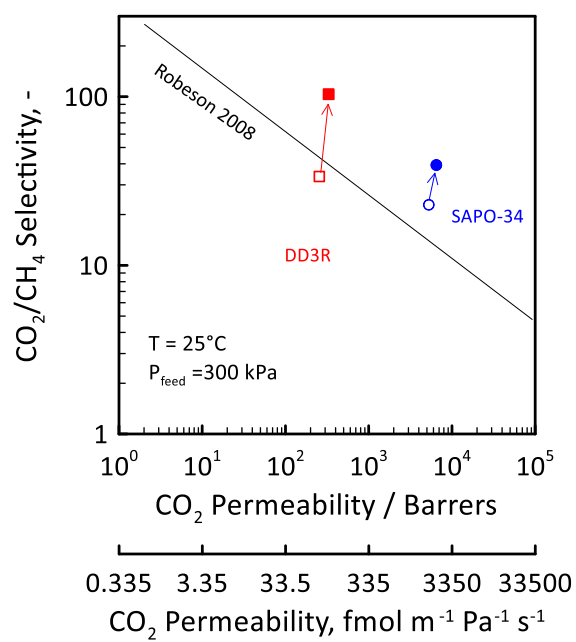


Figure 63. CO₂/CH₄ selectivity as a function of CO₂ permeability through DD3R and SAPO-34 in binary mixture (full symbols) and single gas (open symbols). Robeson upper bound [5] (black solid line).

Conclusions

In this thesis, the gas permeation and separation through different zeolite membranes (i.e., SAPO-34, DD3R, 4A and NaY) were analyzed by a modelling and experimental analysis (in case of DDR), which were also focused on the evaluation of the contributions to mass transport through zeolite pores. In particular, it was considered a model taking into account the competition between surface and gas translation diffusion, where surface diffusion of a strongly adsorbed species exerts a hindering effect on the permeation of other components (more weakly adsorbed) changing the effective porosity and tortuosity of the membrane, in addition to the well-known effect of reducing coverage in mixture.

The proposed model successfully described the mass transport of mixtures containing CO₂ and permanent gases (i.e., H₂, N₂, CH₄ and CO) through zeolite membranes under dry and moist conditions. Unexpectedly, gas translation affected the overall permeation also at a low temperature, as in the case of H₂ permeation through NaY, allowing to reproduce very well the increasing permeance if paired to surface diffusion. On the contrary, the previous model, which considered Knudsen diffusion instead of gas translation, overestimated the H₂ permeation of about 30%.

Among the main results, permeation of CO₂ in mixture was found to differ from the single gas because of the influence exerted by the other diffusing species. Specifically, for a fixed driving force, CO₂ flux and permeance were higher, similar or lower than those in single gas in presence H₂, N₂ and CH₄, respectively. The promoting or slowing effects were attributed to the increase or reduction of the Maxwell-Stefan binary diffusivity, which directly affects surface diffusion. The fast H₂ improved the CO₂ diffusion, whereas the slow CH₄ reduced it. Differently, N₂ did not significantly affect the CO₂ permeation, since the two components showed a similar diffusivity. In addition, the adsorbed CO₂

hindered the diffusion of H₂, N₂ or CH₄, causing a reduction of their permeance and a consequent increment of selectivity with respect to the single gas values.

In SAPO-34, the estimated CO₂/H₂ selectivity (about 12 at room temperature) increased by six times, still being double at 100°C. Concerning CO₂/N₂ and CO₂/CH₄, the increments in mixture were about 3 times (from 7 to 22) and 1.5 (from 21 to 32), respectively, feeding equimolar mixtures.

The experimental analysis on a DDR membrane provided selectivity values of 28, 17 and 106 when CO₂ was mixed with N₂, H₂ and CH₄, whereas the CO₂ permeance exceed 1.5 times the single gas value. The increase of mixture selectivity was significant in presence of H₂ (up to 5 times more).

SAPO-34 was predicted to exceed the permeability/selectivity upper bound for CO₂/CH₄ and CO₂/N₂, whereas the highest CO₂/H₂ selectivity was estimated using a NaY membrane, owing to its higher capacity to adsorb CO₂. Experimental measurements showed that DDR exceeds the upper bound for CO₂/CH₄ and CO₂/H₂.

Permeation of gas mixtures containing water vapor and other permanent gases through a 4A membrane was well described by this model (for the first time). Water vapour induced a stronger permeance reduction on permanent gases than CO₂ (especially in terms of surface diffusion), owed to its very high adsorption. Differently, permeation of H₂O was not promoted/slowed by the presence of the other species, since their amount adsorbed was too low to give any contribution to the Maxwell-Stefan binary diffusivity.

The hindering effect exerted by the adsorbed CO₂ and H₂O paired to the promoting one attributed to H₂ made zeolite membranes very selective, in particular at the moderate temperatures.

The present analysis well explained and clarified the permeation of CO₂ and other gases as well as the high CO₂/gas or H₂O/gas selectivity through zeolite membranes, based on the elementary steps of mass transport such as Langmuir/Sips adsorption, Maxwell-Stefan surface diffusion, gas translation diffusion.

This model, being validated for several mixtures and membranes, contributes to a better understanding of the multicomponent permeation through zeolite pores. Therefore, it can be used as first step for predicting the separation performance of various zeolite membranes. In particular, the evaluation of permeance and selectivity in mixture and their

dependence on temperature, pressure and composition provide an indication of the appropriate operating conditions to be fixed for the selective removal of key components as CO₂ and water vapor from multicomponent feed streams. This deep knowledge of permeation in mixture is crucial in the design of separation units.

Notation

B	Inverted diffusivity matrix in the Maxwell-Stefan model, $s\ m^{-2}$
B_{ii}	Element of matrix [B], defined by Eq. 42, $s\ m^{-2}$
B_{ij}	Element of matrix [B], defined by Eq. 43, $s\ m^{-2}$
b_0	Langmuir or Sips affinity constant at the reference temperature, Pa^{-1}
b	Langmuir or Sips affinity constant, $Pa^{-1/n}$
b_∞	Sips affinity constant at infinite temperature, $Pa^{-1/n}$
C_μ	Molecular loading, $mol \cdot kg^{-1}$
$C_{\mu s}$	Saturation molecular loading, $mol \cdot kg^{-1}$
$C_{\mu s 0}$	Saturation loading of component i at the reference temperature, $mol \cdot kg^{-1}$
D^0_{SD}	Pre-exponential factor for surface diffusivity, $m^2\ s^{-1}$
$D^0_{SD,Effective}$	Effective surface diffusion diffusivity, $m^2\ s^{-1}$
D_{SD}	Maxwell-Stefan diffusivity for surface diffusion, $m^2\ s^{-1}$
$D_{SD,ii}$	Self-exchange diffusivity of component i , $m^2\ s^{-1}$
$D_{SD,ij}$	Maxwell-Stefan binary diffusivity of surface diffusion, $m^2\ s^{-1}$
$D_{SD,jj}$	Self-exchange diffusivity of component j , $m^2\ s^{-1}$
d_k	Kinetic diameter of the molecules, m
$d_{pore,0}$	Mean pore diameter at zero-loading conditions, m
E_{GT}	Activation energy for gas translation diffusion, $J\ mol^{-1}$
E_{SD}	Activation energy for surface diffusion, $J\ mol^{-1}$
f	Fugacity, Pa
$k_{adsorption}$	Kinetic constant for adsorption reaction
$k_{desorption}$	Kinetic constant for desorption reaction
$m_{adsorbed}$	Absolute amount adsorbed, $kg\ kg^{-1}$
m_{excess}	Excess amount adsorbed, $kg\ kg^{-1}$

M	Molar mass, kg mol^{-1}
n	Pressure exponent in the Sips model, -
n_0	Empirical exponent in the Sips model at the reference temperature, -
$n_{absolute}$	Absolute amount adsorbed, mol kg^{-1}
n_{excess}	Excess amount adsorbed, mol kg^{-1}
N	Molar flux, $\text{mol s}^{-1} \text{m}^{-2}$
N_{Av}	Avogadro's number, mol^{-1}
P	Pressure, Pa
$Q_{Adsorption}$	Langmuir or Sips heat of adsorption, $\text{kJ}\cdot\text{mol}^{-1}$
r	Membrane radial coordinate, m
$r_{adsorption}$	Rate of adsorption, mol s^{-1}
$r_{desorption}$	Rate of desorption, mol s^{-1}
R	Gas constant, $8.314 \text{ J}\cdot\text{mol}^{-1}\cdot\text{K}^{-1}$
R_1	Membrane inner radius, m
R_2	External radius of zeolite layer, m
$S_{g,0}$	Zero-loading specific area, $\text{m}^2 \text{kg}^{-1}$
T	Temperature, K
T_0	Reference temperature, K
u	Velocity of the adsorbed species, m s^{-1}
$V_{adsorbed}$	Volume of the adsorbed phase, $\text{m}^3 \text{kg}^{-1}$
V	Volume of the gas phase, $\text{m}^3 \text{kg}^{-1}$
z	Membrane space coordinate, m

Greek letters

α	Empirical parameter for temperature dependence of n , -
β	Parameter defined by Eq.64, $\text{mol m}^{-2} \text{s}^{-1} \text{Pa}^{-1}$
Γ	Thermodynamic factor, -
γ	Parameter described by Eq.56, -
∇	Gradient operator, m^{-1}
δ	Membrane thickness, m
$\delta_{zeolite}$	Zeolite layer thickness, m
ε_0	Porosity at zero-loading conditions, -
ε	Effective porosity, -

ζ	Coordination number, -
λ	Diffusional length, m
μ	Chemical potential, J mol ⁻¹
θ	Loading degree, -
ρ	Zeolite density, kg m ⁻³
$\rho_{adsorbed}$	Density of the adsorbed phase, kg m ⁻³
ρ_{bulk}	Density of the gas phase, kg m ⁻³
σ	Covered surface fraction, -
τ_0	Tortuosity at zero-loading conditions, -
τ	Effective tortuosity, -
χ	Empirical parameter for temperature dependence of saturation loading -

Subscripts / Superscripts

i,j	Generic <i>i-th</i> and <i>j-th</i> species
<i>GTD</i>	Gas translation diffusion
<i>SD</i>	Surface diffusion

References

- [1] E. Drioli, A. Brunetti, G. Di Profio, G. Barbieri, Process Intensification strategies and membrane engineering, *Green Chem.* **2012**, *14*, 1561-1572.
- [2] N. Kosinov, J. Gascon, F. Kapteijn, E.J.M. Hensen, Recent developments in zeolite membranes for gas separation, *J. Membr. Sci.* **2016**, *499*, 65-79.
- [3] L.J. Lozano, C. Godínez, A.P. de los Ríos, F.J. Hernández-Fernández, S. Sánchez-Segado, F.J. Alguacil, Recent advances in supported ionic liquid membrane technology, *J. Membr. Sci.* **2011**, *376*, 1-14.
- [4] M. Hasib-ur-Rahman, M. Siaj, F. Larachi, Ionic-liquids for CO₂ capture- Developments and progress, *Chem. Eng. Process.* **2010**, *49*, 313-322.
- [5] L.M. Robeson, The upper bound revisited, *J. Membr. Sci.* **2008**, *320*, 390-400.
- [6] T.A. Peters, M. Stange, H. Klette, R. Bredesen, High-pressure performance of thin Pd-23% Ag/stainless steel composite membranes in water gas shift mixtures; influence of dilution, mass transfer and surface effects on the hydrogen flux, *J. Membr. Sci.* **2008**, *316*, 119-127.
- [7] A. Caravella, F. Scura, G. Barbieri, E. Drioli, Inhibition by CO polarization in Pd-based membranes: a novel permeation reduction coefficient, *J. Phys. Chem. B* **2010**, *114*, 12264-12276.
- [8] S. Hara, K. Sakaki, N. Itoh, Decline in hydrogen permeation due to concentration polarization and CO hindrance in a palladium membrane reactor, *Ind. Eng. Chem. Res.* **1999**, *38*, 4913-4918.
- [9] G. Barbieri, F. Scura, F. Lentini, G. De Luca, E. Drioli, A novel model equation for the permeation of hydrogen in mixture with carbon monoxide through Pd-Ag membranes, *Sep. Purif. Technol.* **2008**, *61*, 217-224.
- [10] F. Scura, G. Barbieri, G. De Luca, E. Drioli, The influence of the CO inhibition effect on the estimation of the H₂ purification unit surface, *Int. J. Hydrogen Energy* **2008**, *33*, 4183-4192.
- [11] A. Tavolaro, E. Drioli, Zeolite membranes, *Adv. Mater.* **1999**, *11*, 975-996.

-
- [12] K.S. Walton, M.B. Abney, M.D. LeVan, CO₂ adsorption in Y and X zeolites modified by alkali metal cation exchange, *Micropor. Mesopor. Mater.* **2006**, *91*, 78-84.
- [13] K. Makrodimitris, G.K. Papadopoulos, D.N. Theodorou, Prediction of permeation properties of CO₂ and N₂ through silicalite via molecular simulations, *J. Phys. Chem. B* **2001**, *105*, 777-788.
- [14] Ch. Baerlocher, L.B. McCusker, D.H. Olson, Atlas of zeolite framework types, Sixth revised Edition, *Elsevier*, Amsterdam, **2007**.
- [15] P.R. Van Tassel, H. Ted Davis, A.V. McCormick, Adsorption simulations of small molecules and their mixtures in a zeolite micropore, *Langmuir* **1994**, *10*, 1257-1267.
- [16] A.R. Loiola, J.C.R.A. Andrade, J.M. Sasaki, L.R.D. da Silva, Structural analysis of zeolite NaA synthesized by a cost-effective hydrothermal method using kaolin and its use as water softener, *J. Colloid Interf. Sci.* **2012**, *367*, 34-39.
- [17] F. Darkrim, A. Aoufi, P. Malbrunot, Hydrogen adsorption in the NaA zeolite: A comparison between numerical simulations and experiments, *J. Chem. Phys.* **2000**, *112*, 5991-5999.
- [18] E. Jaramillo, M. Chandross, Adsorption of small molecules in LTA zeolites. 1. NH₃, CO₂, and H₂O in zeolite 4A, *J. Phys. Chem. B* **2004**, *108*, 20155-20159.
- [19] E. García-Pérez, D. Dubbeldam, T.L.M. Maesen, S. Calero, Influence of cation Na/Ca ratio on adsorption in LTA 5A: a systematic molecular simulation study of alkane chain length, *J. Phys. Chem. B* **2006**, *110*, 23968-23976.
- [20] M.-H. Simonot-Grange, A. Waldeck, D. Barthomeuf, G. Weber, Contribution to the study of framework modification of SAPO-34 and SAPO-37 upon water adsorption by thermogravimetry, *Thermochim. Acta* **1999**, *329*, 77-82.
- [21] S. Himeno, M. Takenaka, S. Shimura, Light gas adsorption of all-silica DDR- and MFI-type zeolite: computational and experimental investigation, *Mol. Simul.* **2008**, *34*, 1329-1336.
- [22] A. Ghoufi, L. Gaberova, J. Rouquerol, D. Vincent, P.L. Llewellyn, G. Maurin, Adsorption of CO₂ and CH₄ and their binary mixture in Faujasite NaY: A combination of molecular simulations with gravimetry-nanometry and microcalorimetry measurements, *Micropor. Mesopor. Mater.* **2009**, *119*, 117-128.

-
- [23] G. Maurin, P.L. Llewellyn, R.G. Bell, Adsorption Mechanism of Carbon Dioxide in Faujasites: Grand Canonical Monte Carlo Simulations and Microcalorimetry Measurements. *J. Phys. Chem. B* **2005**, *109*, 16084-16091.
- [24] P. Demontis, H. Jobic, M.A. Gonzalez, G.B. Suffritti, Diffusion of Water in Zeolites NaX and NaY Studied by Quasi-Elastic Neutron Scattering and Computer Simulation. *J. Phys. Chem. C* **2009**, *113*, 12373-12379.
- [25] Y. Cui, H. Kita, K. Okamoto, Preparation and gas separation performance of zeolite T membrane, *J. Mater. Chem.* **2004**, *14*, 924-932.
- [26] S. Khajavi, J.C. Jansen, F. Kapteijn, Production of ultra pure water by desalination of seawater using a hydroxy sodalite membrane, *J. Membr. Sci.* **2010**, *356*, 52-57.
- [27] L. Wang, C. Zhang, X. Gao, L. Peng, J. Jiang, X. Gu, Preparation of defect-free DDR zeolite membranes by eliminating template with ozone at low temperature, , *J. Membr. Sci.* **2017**, *539*, 152-160.
- [28] J. van den Bergh, W. Zhu, J. Gascon, J.A. Moulijn, F. Kapteijn, Separation and permeation characteristics of a DD3R zeolite membrane, *J. Membr. Sci.* **2008**, *316*, 35-45.
- [29] X. Xu, W. Yang, J. Liu, X. Chen, L. Lin, N. Stroh, H. Brunner, Synthesis and gas permeation properties of an NaA zeolite membrane, *Chem. Commun.* **2000**, 603-604.
- [30] W. Zhu, L. Gora, A.W.C. van den Berg, F. Kapteijn, J.C. Jansen, J.A. Moulijn, Water vapour separation from permanent gases by a zeolite-4A membrane, *J. Membr. Sci.* **2005**, *253*, 57-66.
- [31] S.M. Lee, N. Xu, J.R. Grace, A. Li, C.J. Lim, S.S. Kim, F. Fotovat, A. Schaadt, R.J. Wite, Structure, stability and permeation properties of NaA zeolite membranes for H₂O/H₂ and CH₃OH/H₂ separations, *J. Eur. Ceram. Soc.* **2018**, *38*, 211-219.
- [32] B. Liu, C. Tang, X. Li, B. Wang, R. Zhou, High-performance SAPO-34 membranes for CO₂ separations from simulated flue gas, *Micropor. Mesopor. Mater.* **2020**, *292*, 109712.
- [33] S. Li, C.Q. Fan, High-flux SAPO-34 membrane for CO₂/N₂ separation, *Ind. Eng. Chem. Res.* **2010**, *49*, 4399-4404.
- [34] S. Li, J.L. Falconer, R.D. Noble, SAPO-34 membranes for CO₂/CH₄ separations: effect of Si/Al ratio, *Micropor. Mesopor. Mater.* **2008**, *110*, 310-317

-
- [35] M. Hong, S. Li, J.L. Falconer, R.D. Noble, Hydrogen purification using a SAPO-34 membrane, *J. Membr. Sci.* **2008**, *307*, 277-283.
- [36] W. Mei, Y. Du, T. Wu, F. Gao, B. Wang, J. Duan, J. Zhou, R. Zhou, High-flux CHA zeolite membranes for H₂ separations, *J. Membr. Sci.* **2018**, *565*, 358-369.
- [37] H. Guo, G. Zhu, H. Li, Z. Zou, X. Yin, W. Yang, S. Qiu, R. Xu, Hierarchical growth of large-scale ordered zeolite silicalite-1 membranes with high permeability and selectivity for recycling CO₂, *Angew. Chem.* **2006**, *118*, 7211-7214.
- [38] K. Kusakabe, T. Kuroda, A. Murata, S. Morooka, Formation of a Y-type zeolite membrane on a porous α -alumina tube for gas separation, *Ind. Eng. Chem. Res.* **1997**, *36*, 649-655.
- [39] K. Kusakabe, T. Kuroda, K. Uchino, Y. Hasegawa, S. Morooka, Gas permeation properties of ion-exchanged faujasite-type zeolite membranes, *AIChE J.* **1999**, *45*, 1220-1226.
- [40] J.C. White, P.K. Dutta, K. Shqau, H. Verweij, Synthesis of ultrathin zeolite Y membranes and their application for separation of carbon dioxide and nitrogen gases, *Langmuir* **2010**, *26*, 10287-10293.
- [41] X. Gu, J. Dong, T.M. Nenoff, Synthesis of defect-free FAU-type zeolite membranes and separation for dry and moist CO₂/N₂ mixtures, *Ind. Eng. Chem. Res.* **2005**, *44*, 937-944.
- [42] S. Li, J.L. Falconer, R.D. Noble, SAPO-34 membranes for CO₂/CH₄ separation, *J. Membr. Sci.* **2004**, *241*, 121-135.
- [43] J.C. Poshusta, V.A. Tuan, J.L. Falconer, R.D. Noble, Synthesis and permeation properties of SAPO-34 tubular membranes, *Ind. Eng. Chem. Res.* **1998**, *37*, 3924-3929.
- [44] T. Wu, B. Wang, Z. Lu, R. Zhou, X. Chen, Alumina-supported AIPO-18 membranes for CO₂/CH₄ separation, *J. Membr. Sci.* **2014**, *471*, 338-346.
- [45] W.J.W. Bakker, L.J.P. van den Broeke, F. Kapteijn, J.A. Moulijn, Temperature dependence of one-component permeation through a silicalite-1 membrane, *AIChE J.* **1997**, *43*, 2203-2214.
- [46] M. Kanezashi, Y.S. Lin, Gas permeation and diffusion characteristics of MFI-type zeolite membranes at high temperatures, *J. Phys. Chem. C* **2009**, *113*, 3767-3774.

-
- [47] J. van den Bergh, A. Tihaya, F. Kapteijn, High temperature permeation and separation characteristics of an all-silica DDR zeolite membranes, *Micropor. Mesopor. Mater.* **2010**, *132*, 137-147.
- [48] S. Miachon, P. Ciavarella, L. van Dyk, I. Kumakiri, K. Fiaty, Y. Schuurman, J.-A. Dalmon, Nanocomposite MFI-alumina membranes via pore-plugging synthesis: Specific transport and separation properties, *J. Membr. Sci.* **2007**, *298*, 71-79.
- [49] Y. Hasegawa, K. Kusakabe, S. Morooka, Effect of temperature on the gas permeation properties of NaY-type zeolite formed on the inner surface of a porous support tube, *Chem. Eng. Sci.* **2001**, *56*, 4273-4281.
- [50] A. Caravella, P.F. Zito, A. Brunetti, E. Drioli, G. Barbieri, A novel modelling approach to surface and Knudsen multicomponent diffusion through NaY zeolite membranes, *Micropor. Mesopor. Mater.* **2016**, *235*, 87-99.
- [51] P. F. Zito, A. Caravella, A. Brunetti, E. Drioli, G. Barbieri, Knudsen and surface diffusion competing for gas permeation inside silicalite membranes, *J. Membr. Sci.* **2017**, *523*, 456-469.
- [52] D.D. Do, Adsorption Analysis: Equilibria and Kinetics, Imperial College Press, London, 1998
- [53] R. Krishna, Multicomponent surface diffusion of adsorbed species. A description based on the generalized Maxwell-Stefan diffusion equations, *Chem. Eng. Sci.* **1990**, *45*, 1779-1791.
- [54] R. Krishna, A unified approach to the modelling of intraparticle diffusion in adsorption processes, *Gas Separ. Purif.* **1993**, *7*, 91-104.
- [55] R. Krishna, Problems of pitfalls in the use of the Fick formulation for intraparticle diffusion, *Chem. Eng. Sci.* **1993**, *48*, 845-861.
- [56] R. Krishna, , J.A. Wesselingh, The Maxwell-Stefan approach to mass transfer, *Chem. Eng. Sci.* **1997**, *52*, 861-911.
- [57] K. Malek, T.J.H. Vlugt, B. Smit, Adsorption and diffusion in porous systems, Chapter 14 in Computational methods in catalysis and material science: an introduction for scientists and engineers, Eds. R.A. Van Santen, P. Sautet, Wiley-VCH Verlag GmbH & Co. KGaA, 2009
- [58] D.A. Reed, G. Ehrlich, Surface diffusion, atomic jump rates and thermodynamics, *Surf. Sci.* 1981, *102*, 588-609.

-
- [59] J. Xiao, J. Wei. Diffusion mechanism of hydrocarbons in zeolites – I. Theory, *Chem. Eng. Sci.* **1992**, *47*, 1123-1141.
- [60] P.F. Zito, A. Caravella, A. Brunetti, E. Drioli, G. Barbieri, Discrimination among gas translation, surface and Knudsen diffusion in permeation through zeolite membranes, *J. Membr. Sci.* **2018**, *564*, 166-173.
- [61] F. Kapteijn, J.A. Moulijn, R. Krishna, The generalized Maxwell-Stefan model for diffusion in zeolites: sorbate molecules with different saturation loadings, *Chem. Eng. Sci.* **2000**, *55*, 2923-2930.
- [62] G.R. Gavalas, Diffusion in Microporous Membranes: Measurements and Modeling, *Ind. Eng. Chem. Res.* **2008**, *47*, 5797-5811.
- [63] P.J.A.M. Kerkhof, A modified Maxwell-Stefan model for transport through inert membranes: the binary friction model, *Chem. Eng. J.* **1996**, *64*, 319-343.
- [64] A. Vignes, Diffusion in binary solutions, *Ind. Eng. Chem. Fundam.* **1966**, *5*, 189–199.
- [65] A.I. Skoulidas, D.S. Sholl, R. Krishna, Correlation effects in diffusion of CH₄/CF₄ mixtures in MFI zeolite. A study linking MD simulations with the Maxwell-Stefan formulation, *Langmuir* **2003**, *19*, 7977-7988.
- [66] P.F. Zito, A. Caravella, A. Brunetti, E. Drioli, G. Barbieri, Estimation of Langmuir and Sips models adsorption parameters for NaX and NaY FAU zeolites, *J. Chem. Eng. Data* **2015**, *60*, 2858-2868.
- [67] A. Caravella, P.F. Zito, A. Brunetti, E. Drioli, G. Barbieri, Evaluation of pure-component adsorption properties of DD3R based on the Langmuir and Sips models, *J. Chem. Eng. Data* **2015**, *60*, 2343-2355.
- [68] P.F. Zito, A. Caravella, A. Brunetti, E. Drioli, G. Barbieri, Light gases saturation loading dependence on temperature in LTA 4A zeolite, *Micropor. Mesopor. Mater.* **2017**, *249*, 67-77.
- [69] P.F. Zito, A. Brunetti, A. Caravella, E. Drioli, G. Barbieri. Mutual influence in permeation of CO₂-containing mixtures through a SAPO-34 membrane, *J. Membr. Sci.* **2020**, *595*, 117534.
- [70] P.F. Zito A. Brunetti, A. Caravella, E. Drioli, G. Barbieri, Water vapor permeation and its influence on gases through a zeolite-4A membrane, *J. Membr. Sci.* **2019**, *574*, 154-163.

-
- [71] J. Moellmer, A. Moeller, F. Dreisbach, R. Glaeser, R. Staudt, High pressure adsorption of hydrogen, carbon dioxide and methane on the metal-organic framework HKUST-1, *Micropor. Mesopor. Mater.* **2011**, *138*, 140-148.
- [72] X.B. Zhao, B. Xiao, A.J. Fletcher, K.M. Thomas, Hydrogen adsorption on functionalized nanoporous activated carbons, *J. Phys. Chem. B* **2005**, *109*, 8880-8888.
- [73] K.M. Thomas, Hydrogen adsorption and storage on porous materials, *Catalysis Today* **2007**, *120*, 389-398.
- [74] M.-A. Richards, P. Bénard, R. Chahine, Gas adsorption process in activated carbon over a wide temperature range above the critical point. Part 1: modified Dubinin-Astakhov model, *Adsorption* **2009**, *15*, 43-51.
- [75] J. Dong, X. Wang, H. Xu, Q. Zhao, J. Li, Hydrogen storage in several microporous zeolites, *Int. J. Hydrogen Energy* **2007**, *32*, 4998-5004.
- [76] A.L. Myers, P.A. Monson, Adsorption in porous materials at high pressure: theory and experiment, *Langmuir* **2002**, *18*, 10261-10273.
- [77] R. Krishna, Adsorptive separation of CO₂/CH₄/CO gas mixtures at high pressure, *Micropor. Mesopor. Mater.* **2012**, *156*, 217-223.
- [78] P.S. Yaremov, V.G. Il'in, Features of the adsorption of hydrogen by various types of microporous materials, *Theor. Exp. Chem.* **2008**, *44*, 67-74.
- [79] A. Golmakani, S. Fatemi, J. Tamnanloo, CO₂ capture from the tail gas of hydrogen purification unit by vacuum swing adsorption process, using SAPO-34, *Ind. Eng. Chem. Res.* **2016**, *55*, 334-350.
- [80] S. Li, Z. Zong, S.J. Zhou, Y. Huang, Z. Song, X. Feng, R. Zhou, H.S. Meyer, M. Yu, M.A. Carreon, SAPO-34 membranes for N₂/CH₄ separation: preparation, characterization, separation performance and economic evaluation, *J. Membr. Sci.* **2015**, *487*, 141-151.
- [81] F. Stéphanie-Victoire, A.-M. Goulay, E. Cohen de Lara, Adsorption and coadsorption of molecular hydrogen isotopes in zeolites. 1. Isotherms of H₂, HD, and D₂ in NaA by thermomicrogravimetry, *Langmuir* **1998**, *14*, 7255-7259.
- [82] E.D. Akten, R. Siriwardane, D.S. Sholl, Monte Carlo Simulation of single- and binary-component adsorption of CO₂, N₂, and H₂ in zeolite Na-4A, *Energy Fuels* **2003**, *17*, 977-983.

-
- [83] N.K. Jensen, T.E. Rufford, G. Watson, D.K. Zhang, K. Ida Chan, E.F. May, Screening zeolites for gas separation applications involving methane, nitrogen, and carbon dioxide, *J. Chem. Eng. Data* **2012**, *57*, 106-113.
- [84] R.J. Mohr, D. Vorkapic, M.B. Rao, S. Sircar, Pure and binary gas adsorption equilibria and kinetics of methane and nitrogen on 4A zeolite by isotope exchange technique, *Adsorption* **1999**, *5*, 145-158.
- [85] D.V. Cao, R.J. Mohr, M.B. Rao, S. Sircar, Self-Diffusivities of N₂, CH₄, and Kr on 4A zeolite pellets by isotope exchange technique, *J. Phys. Chem. B* **2000**, *104*, 10498-10501.
- [86] R.T. Adams, J Suk Lee, T.-H. Bae, J.K. Ward, J.R. Johnson, C.W. Jones, S. Nair, W.J. Koros, CO₂-CH₄ permeation in high zeolite 4A loading mixed matrix membranes, *J. Membr. Sci.* **2011**, *367*, 197-203.
- [87] R.J. Harper, J.R. Stifel, R.B. Anderson, Adsorption of gases on 4A synthetic zeolite, *Can. J. Chem.* **1969**, *47*, 4661-4670.
- [88] E. Jaramillo, M. Chandross, Adsorption of small molecules in LTA zeolites. 1. NH₃, CO₂, and H₂O in zeolite 4A, *J. Phys. Chem. B* **2004**, *108*, 20155-20159.
- [89] J.D. Eagan, R.B. Anderson, Kinetic and equilibrium of adsorption on 4A zeolite, *C. J. Colloid Interf. Sci.* **1975**, *50*, 419-433.
- [90] H. Ahn, J.-H. Moon, S.-H. Hyun, C.-H. Lee, Diffusion mechanism of carbon dioxide in zeolite 4A and CaX pellets, *Adsorption* **2004**, *10*, 111-128.
- [91] A. Romero-Pérez, G. Aguilar-Armenta, Adsorption kinetics and equilibria of carbon dioxide, ethylene, and ethane on 4A(CECA) zeolite, *J. Chem. Eng. Data* **2010**, *55*, 3625-3630.
- [92] A. Gorbach, M. Stegmaier, G. Eigenberger, measurement and modeling of water vapor adsorption on zeolite 4A – Equilibria and kinetics, *Adsorption* **2004**, *10*, 29-46.
- [93] M. Kanezashi, J. O'Brien-Abraham, Y.S. Lin, Gas permeation through DDR-type zeolite membranes at high temperatures, *AIChE J.* **2008**, *54*, 1478-1486.
- [94] W. Zhu, F. Kapteijn, J.A. Moulijn, M.C. den Exter, J.C. Jansen, Shape selectivity in adsorption on the all-silica DD3R, *Langmuir* **2000**, *16*, 3322-3329.

-
- [95] X. Gao, J.C. Diniz da Costa, S.K. Bhatia, The transport of gases in a supported mesoporous silica membrane, *J. Membr. Sci.* **2013**, *438*, 90-104.
- [96] R. Krishna, J.M. van Baten, Insights into diffusion of gases in zeolites gained from molecular dynamic simulations, *Micropor. Mesopor. Mater.* **2008**, *109*, 91-108.
- [97] D.M. Ruthven, Principles of Adsorption and Adsorption Processes, Wiley, New York, 1984.
- [98] K.F. Loughlin, Water isotherm models for 4A (NaA) zeolite, *Adsorption* **2009**, *15*, 337-353.
- [99] M. Palomino, A. Corma, F. Rey, S. Valencia, New insight on CO₂ – methane separation using LTA zeolites with different Si/Al ratios and a first comparison with MOFs, *Langmuir* **2010**, *26*, 1910-1917.
- [100] P.F. Zito A. Brunetti, E. Drioli, G. Barbieri, CO₂ separation via a DDR membrane: mutual influence of mixed gas permeation, *Ind. Eng. Chem. Res.* **2019**.
- [101] R. Krishna, J.M. van Baten, Onsager coefficients for binary mixture diffusion in nanopores. *Chem. Eng. Sci.* **2008**, *63*, 3120.
- [102] J. van den Bergh, S. Ban, T.J.H. Vlugt, F. Kapteijn, Modeling the loading dependency of diffusion in zeolites: the relevant site model. *J. Phys. Chem. C* **2009**, *113*, 17840.
- [103] J. van den Bergh, S. Ban, T.J.H. Vlugt, F. Kapteijn Modeling the loading dependency of diffusion in zeolites: the relevant site model extended to mixtures in DDR-type zeolite. *J. Phys. Chem. C* **2009**, *113*, 21856.
- [104] A. Brunetti, G. Barbieri, E. Drioli, Upgrading of a syngas mixture for pure hydrogen production in a Pd-Ag membrane reactor, *Chem. Eng. Sci.* **2009**, *64*, 3448-3454.
- [105] H.Q. Lin, E. Van Wagner, B.D. Freeman, L.G. Toy, R.P. Gupta, Plasticization-enhanced hydrogen purification using polymeric membranes, *Science* **2006**, *311*, 639.

Publications on international journals during the PhD

1. **P.F. Zito**, A. Caravella, A. Brunetti, E. Drioli, G. Barbieri, Light gases saturation loading dependence on temperature in LTA 4A zeolite, *Micropor. Mesopor. Mater.* **2017**, 249, 67-77. DOI: [10.1016/j.micromeso.2017.04.021](https://doi.org/10.1016/j.micromeso.2017.04.021)
2. **P.F. Zito**, A. Caravella, A. Brunetti, E. Drioli, G. Barbieri, CO₂/H₂ selectivity prediction of NaY, DD3R, and silicalite zeolite membranes, *Ind. Eng. Chem. Res.* **2018**, 57, 11431-11438. DOI: [10.1021/acs.iecr.8b02707](https://doi.org/10.1021/acs.iecr.8b02707)
3. **P.F. Zito**, A. Caravella, A. Brunetti, E. Drioli, G. Barbieri, Discrimination among gas translation, surface and Knudsen diffusion in permeation through zeolite membranes, *J. Membr. Sci.* **2018**, 564, 166-173. DOI: [10.1016/j.memsci.2018.07.023](https://doi.org/10.1016/j.memsci.2018.07.023)
4. **P.F. Zito**, A. Brunetti, A. Caravella, E. Drioli, G. Barbieri, Water vapor permeation and its influence on gases through a zeolite-4A membrane, *J. Membr. Sci.* **2019**, 574, 154-163. DOI: [10.1016/j.memsci.2018.12.065](https://doi.org/10.1016/j.memsci.2018.12.065)
5. **P.F. Zito**, A. Brunetti, E. Drioli, G. Barbieri, CO₂ separation via a DDR membrane: mutual influence of mixed gas permeation, *Ind. Eng. Chem. Res.* **2019**. DOI: [10.1021/acs.iecr.9b03029](https://doi.org/10.1021/acs.iecr.9b03029)
6. **P.F. Zito**, A. Brunetti, A. Caravella, E. Drioli, G. Barbieri. Mutual influence in permeation of CO₂-containing mixtures through a SAPO-34 membrane, *J. Membr. Sci.* **2020**, 595, 117534. DOI: [10.1016/j.memsci.2019.117534](https://doi.org/10.1016/j.memsci.2019.117534)

Publications on national journals during the PhD

1. **P.F. Zito**, A. Caravella, A. Brunetti, E. Drioli, G. Barbieri. Separazione di miscele di H₂ e CO₂ con membrane zeolitiche, *La Chimica e l'Industria*, anno II, n°1, gennaio/febbraio 2019.

Book chapters during the PhD

1. **P. F. Zito**, A. Brunetti, A. Caravella, E. Drioli, G. Barbieri. “Membranes based on MOFs”, Chapter 8 in “Metal Organic Frameworks. Applications in Separations and Catalysis”, pages 223 -250, Editors H. Garcia and S. Navalon. Wiley, 2018. [DOI:10.1002/9783527809097.ch8](https://doi.org/10.1002/9783527809097.ch8)
2. **P. F. Zito**, A. Caravella, A. Brunetti, E. Drioli, G. Barbieri G. “Mass transport in zeolite membranes for gas treatment: a new insight”, Chapter 7 in "Membrane engineering for the treatment of gases", Volume 1 "Gas-separation Problems Combined with Membrane Reactors", 2017, Eds. E. Drioli, G. Barbieri, A. Brunetti, The Royal Society of Chemistry, Cambridge, The United Kingdom. [DOI: 10.1039/9781788010436-00183](https://doi.org/10.1039/9781788010436-00183)

Presentations to international conferences during the PhD

1. **P. F. Zito**, A. Brunetti, A. Caravella, E. Drioli, G. Barbieri, PERMEA 2019, Membrane Conference of Visegrad Countries, August 26-29, 2019, Eötvös Lorand University, Budapest, Hungary – (oral presentation).
2. **P. F. Zito**, A. Caravella, A. Brunetti, E. Drioli, G. Barbieri, 4° EURO-ASIA ZEOLITE CONFERENCE, January 27-30, 2019, Hotel Villa Diodoro, Taormina (ME), Italy – (poster presentation).

Presentations to seminars during the PhD

1. **P. F. Zito**, A. Caravella, A. Brunetti, E. Drioli, G. Barbieri. “Knudsen and surface diffusion competing for gas permeation inside zeolite membranes”, ITM-CNR SEMINAR DAYS 2016 “The annual update of advances promoted at Institute on Membrane Technology, National Research Council (ITM-CNR)”, December 1th, 2016, UNICAL, Rende (CS), Italy – (oral presentation).

2. **P. F. Zito**, A. Caravella, A. Brunetti, E. Drioli, G. Barbieri. “CO₂/H₂ selectivity of NaY, DD3R and silicalite zeolite membranes”, ITM-CNR SEMINAR DAYS 2017 “The annual update of advances promoted at Institute on Membrane Technology, National Research Council (ITM-CNR)”, December 19th – 20th, 2017, UNICAL, Rende (CS), Italy – (oral presentation).

3. **P. F. Zito**, A. Caravella, A. Brunetti, E. Drioli, G. Barbieri. “Permeation of wet and dry gas mixtures through zeolite membranes”, ITM-CNR SEMINAR DAYS 2018 “The annual update of advances promoted at Institute on Membrane Technology, National Research Council (ITM-CNR)”, December 19th – 20th, 2018, UNICAL, Rende (CS), Italy – (oral presentation).

Teaching activity during the PhD

1. Tutor of Chemistry for the degree in Management Engineering, academic year 2017/18, Department of Mechanical, Energy and Management Engineering, University of Calabria.

2. Lecturer of Chemistry for the degree in Mechanical Engineering, academic year 2018/19, Department of Mechanical, Energy and Management Engineering, University of Calabria.

3. Tutor of Chemistry for the degree in Mechanical Engineering, academic year 2019/20, Department of Mechanical, Energy and Management Engineering, University of Calabria.